The Mechanism of Floc Formation by Hydrodynamic Cavitation and Its Application on Fine Particle Flotation

by

HAO HUANG

A thesis submitted in partial fulfillment of the requirements for the degree of

Master of Science

in

Chemical Engineering

Department of Chemical and Materials Engineering
University of Alberta

Abstract

In recent decades, hydrodynamic cavitation has been used to enhance fine particle flotation recovery in mineral engineering. Such an increase was mainly attributed to the generation of flocs/aggregates of fine particles during the hydrodynamic cavitation process. However, the mechanism of floc formation in hydrodynamic cavitation still remains unclear. This study aims to fill this knowledge gap regarding the agglomeration mechanism of fine particles in hydrodynamic cavitation.

Fine molybdenite particles with the diameters less than 37 μm were investigated with the cavitation system. The optimized geometry Venturi tube investigated in previous studies of our research group was applied in a hydrodynamic cavitation system for microbubble generation and floc formation. Floc size was measured to study the relationship between the cavitation intensity and flotation efficiency. Under cavitation with inlet air injection, floc size increased to 140 μm efficiently. Microscope images of generated flocs were captured to examine the structure. It was found that cavitated bubbles acted as the bridges between particles in the floc structure. Zeta potential distribution was measured to investigate the interaction between microbubbles and fine particles. Strong attachment of microbubbles and particles were demonstrated in cavitation treatment.

Hydrodynamic cavitation was also applied in micro-flotation of fine particles to study the effect of flocs in the mineral flotation. An increase of 20% in recovery of fine molybdenite was achieved after cavitation with inlet air injection. Fine silica particles in the same size range were used as a comparison. No significant increase of fine silica recovery was found.

This observation indicates that cavitation predominantly affects hydrophobic particles based on contact angle results. At last, the flotation of the mixture of molybdenite and silica was investigated to demonstrate the selectivity of hydrodynamic cavitation in mineral processing.

Acknowledgements

I would like to thank my supervisor Dr. Qingxia Liu for his patient guidance and great support during my graduate studies. I am so grateful to be a member of his team. Not only for the fancy equipment and excellent working conditions he provided, but also for the knowledge, thoughts and enthusiasm he delivered.

I would like to thank Dr. Zhenghe Xu for his permission to use the equipment in his labs, which played a vital role in my research.

I would like to express my appreciation to my advisor Dr. Vu NT Truong, who guided my research plan, pushed my research schedule, gave me lots of suggestions and helped me with my thesis. I would also like to thank my first advisor Dr. Adrien Bussonnière who showed me the way to do research and the way of thinking. I am very glad to have had these two advisors during my graduate studies. Their enthusiasm and dedication to research set a very good example for me.

I would also like to a show my appreciation to Dr. Jing Liu, Angela Xue, Bo Liu, Chao Qi, Hanrui Zheng, Mingda Li, Vitalii Dodonov, and Yuran Chen for their help and suggestion in the experiment. I would also like to extend my appreciation to all my colleagues in the group for their kindly support and wonderful advice.

I would also like to thank to Carl Corbett, James Skwarok, Jie Ru, Nancy Zhang, and Mingli Cao to help me with my device setup and equipment training.

I would like to acknowledge the financial support from Natural Science and Engineering Research Council of Canada (NSERC), the Canadian Centre for Clean Coal/Carbon and

Mineral Processing Technologies (C5MPT) and Canadian Mining Industry Resource Organization (CAMIRO).

Finally, I would like to thank my parents for their support and encouragement in my life and research. I am also grateful to my family members and friends who have supported me over the years.

Table of Contents

List of Tables

List of Figures or Illustrations

List of Symbols

P	Pressure of the throat
V	Liquid throat velocity
ρ	Liquid density
γ_{SG}	Solid–gas interfacial tension
γ_{SL}	Solid–liquid interfacial tension
γ_{LG}	Liquid–gas interfacial tension
θ_{CB}	Apparent contact angle on the textured surface
θ_{C}	Equilibrium contact angle
θ_v	Contact angle of vapor
f_s	Area fractions of the solid on the surface
f_v	Area fractions of the vapor on the surface
θ_p	Apparent contact angle on the surface of pellet
θ_s	Intrinsic contact angle of the sample
θ_b	Intrinsic contact angle of boric acid

R	Flotation recovery
m_{feed}	Weight of feed
m_{conc}	Weight of concentrate
m_{tail}	Weight of tailing
G	Grade of valuable part in ore
$m_{conc,metal}$	Weight of valuable part in concentrate
$m_{conc,ore}$	Weight of concentrate.
R_{∞}	Ultimate recovery
k	First-order rate constant
ϕ	Time correction factor
R_a	Arithmetical mean deviation,
R_q	Root mean square deviation
R_t	Maximum peak-to-valley height

Abbreviations

DAF	Dissolved air flotation
HIA	High intensity agitation
HIC	High intensity condition
MIBC	4-Methyl-2-pentanol
XRF	X-ray fluorescence
XRD	X-ray diffraction
XPS	X-ray photoelectron spectroscopy
FTIR	Fourier transform infrared spectroscopy
NTU	Nephelometric turbidity unit
SCCM	Standard cubic centimeters per minute
HC	Hydrodynamic Cavitation
SEM	Scanning electron microscope
SLPM	Standard liter per minute
TCM	Total carbonaceous matters

Chapter 1 Introduction

1.1 Background

Mineral flotation has been widely used for the recovery of valuable minerals for more than 100 years, and is achieved by utilizing the differences of their physicochemical surface properties[1,2]. In the flotation process, hydrophobic particles attached to air bubbles are transported upwards to form a froth layer, while the hydrophilic particles are left in the slurry as the tailings[3]. Of special interest in recent decades for many studies in conventional mineral flotation is the low recovery of fine particles, which is mainly due to the low collision efficiency with conventional flotation bubbles[4,5]. Additionally, the kinetic energy of fine particles is insufficient to rupture the liquid film between particles and bubbles, which causes a low attachment efficiency[6–10]. To increase the particle-bubble collision and attachment efficiency, numerous innovative approaches have been developed, either by increasing particle size or by decreasing flotation bubble size[9,11–17]. To decrease bubble size, four different methods have been reported, including dissolved air flotation (DAF), electro-flotation, turbulent micro-flotation, and cavitation[15,18–25].

Dissolved air flotation can improve the floatability of fine particles with the dissolved air in the solution. The gas nuclei on the surface of fine particles can increase the attachment probability to conventional sized bubbles. In another words, the attachment of fine mineral particles with frosted tiny bubbles on the surface to a conventional sized bubble is more favored than the direct attachment of mineral particles and conventional bubbles[26].

Electro-flotation is widely used in the wastewater treatment industry, which uses electrolysis for the generation of tiny bubbles. Hydrogen bubbles, oxygen bubbles and chlorine bubbles generated by electrolyzing the aqueous medium can carry fine particles in the slurry to float together[22]. Compared to dissolved air flotation, it can not only generate much smaller bubbles, but also provide a good coverage of the whole surface area of the flotation tank.

Turbulent micro-flotation is based on pre-aggregation of fine particles to reach an aggregate size which is suitable for the attachment with flotation-sized bubbles. It is performed in a long and narrow channel with gas microbubbles in treated saturated mixture flows. The flow rate is adjusted to maintain a turbulent stream flow to ensure the aggregation of bubbles and particles.

Cavitation, as one of the most efficient ways to enhance flotation recovery, has also been commonly applied in the mineral flotation process. It can generate microbubbles due to the rupture of water surface, which is believed as a key role to enhance fine particles flotation. It can be classified into three types, acoustic cavitation, optical cavitation and hydrodynamic cavitation. The acoustic cavitation makes use of the high energy of ultrasonic to treat liquid. It can make the gas nuclei existing in liquid vibrate and grow to generate bubbles. As for the optical cavitation, laser is used to lower local pressure to vapor pressure which is beneficial to bubble formation. The hydrodynamic cavitation, as an economic and environmental friendly approach, has shown a significant improvement of fine particle flotation recovery[24,27]. Not only are the microbubbles generated in this process, but also the high shear force plays an important role to overcome the energy barrier between particles and bubbles, which makes them easy to attach.

In order to understand more comprehensively the role of hydrodynamic cavitation in floc formation and fine particle flotation, the Venturi tube, one of the most widely applied devices in hydrodynamic cavitation, was investigated in the study. In the hydrodynamic cavitation process, the microbubbles are generated by the rupture of a liquid-liquid or a liquid-solid interface of a high-speed fluid flow. When the local pressure at the throat falls below the liquid vapor pressure, a large number of bubbles are generated due to the cavities and gas nuclei in the liquid[28–30].

As for the mechanism of floc formation, there are two hypothesizes to illustrate the possible role of hydrodynamic cavitation in fine particle flotation[1,31]. One belief is that flocculation is achieved via the bubble-bridge in hydrodynamic cavitation. Another suggests that particles attached to tiny bubbles increase the attachment probability with flotation-sized bubbles. As a result, the formation of larger flocs improves the fine particle flotation recovery.

1.2 Aim and Objective

Although the effect of hydrodynamic cavitation in enhancing fine particle recovery has been proved by many experiments, the mechanism of floc generation in hydrodynamic cavitation still requires the further investigation. This study aims to provide an insight of the interaction among fine particles and bubbles and the process of floc formation in the hydrodynamic cavitation. The recovery of fine particle flotation is further investigated, and an enhancement of fine particle flotation is accounted to the formation of flocs in the hydrodynamic cavitation.

The main objectives of this study are as following:

1. To evaluate the microbubbles generated by hydrodynamic cavitation, Mastersizer was used for bubble size measurement and Turbidimeter was used to compare the quantity.
2. To investigate the flocs generation in hydrodynamic cavitation, the flocs sizes were measured by Mastersizer and their structures were observed and analyzed by Optical Microscope.
3. To study the bubble-particle interactions, zeta potential distribution analysis technique was applied.
4. To examine the effect of hydrodynamic cavitation at different studied conditions in the fine particle flotation, micro-flotation tests were carried out to study the recovery of fine particles. Fine silica particles were also introduced to further demonstrate the selectivity of hydrodynamic cavitation in valuable mineral flotation.

1.3 Thesis Outline

In Chapter 1, the background of hydrodynamic cavitation applied in mineral processing for fine particle flotation is introduced. In Chapter 2, current approaches to enhance fine particle flotation recovery, the effect of the Venturi tube in hydrodynamic cavitation and its application in fine particle flotation are reviewed. In Chapter 3, the characteristics of molybdenite and silica, the experimental techniques, and the specific procedures are described. In Chapter 4, the process of floc generation and the structure of flocs are investigated. In Chapter 5, the effects of hydrodynamic cavitation on fine particle flotation and selectivity are discussed. In Chapter 6, the effects of the optimized Venturi tube on column flotation are studied. In Chapter 7, the results obtained from the last three chapters are summarized. In Chapter 8, future work regarding the process of bubbles formed on particle surfaces and the relation of cavitation efficiency and particle surface roughness are proposed.

1.4 Reference

(1) Klassen, V.J., Mokrousov, V. A. *An Introduction to the Theory of Flotation*; Butterworths, London. **1963**.

(2) Farrokhpay, S. The Significance of Froth Stability in Mineral Flotation - A Review. *Adv. Colloid Interface Sci.* **2011**, *166* (1–2), 1–7.

(3) Sutherland, K. L. Physical Chemistry of Flotation. XI: Kinetics of the Flotation Process. *J. Phys. Colloid Chem.* **1948**, *52* (2), 394–425.

(4) Trahar, W. J.; Warren, L. J. The Flotability of Very Fine Particles - A Review. *Int. J. Miner. Process.* **1976**, *3* (2), 103–131.

(5) Sun, W.; Hu, Y.; Dai, J.; Liu, R. Observation of Fine Particle Aggregating Behavior Induced by High Intensity Conditioning Using High Speed CCD. *Trans. Nonferrous Met. Soc. China.* **2006**, *16* (1), 198–202.

(6) Miettinen, T.; Ralston, J.; Fornasiero, D. The Limits of Fine Particle Flotation. *Miner. Eng.* **2010**, *23* (5), 420–437.

(7) Nguyen Van, A.; Kmet', S. Collision Efficiency for Fine Mineral Particles with Single Bubble in a Countercurrent Flow Regime. *Int. J. Miner. Process.* **1992**, *35* (3–4), 205–223.

(8) Derjaguin, B. V.; Dukhin, S. S. Theory of Flotation of Small and Medium-Size

Particles. *Prog. Surf. Sci.* **1993**, *43* (1–4), 241–266.

(9) Nguyen, A. V.; George, P.; Jameson, G. J. Demonstration of a Minimum in the Recovery of Nanoparticles by Flotation: Theory and Experiment. *Chem. Eng. Sci.* **2006**, *61* (8), 2494–2509.

(10) Dai, Z.; Fornasiero, D.; Ralston, J. Particle-Bubble Collision Models--a Review. *Adv. Colloid Interface Sci.* **2000**, *85* (2–3), 231–256.

(11) Yoon, R. H.; Luttrell, G. H. The Effect of Bubble Size on Fine Particle Flotation. *Miner. Process. Extr. Metall. Rev.* **1989**, *5* (1–4), 101–122.

(12) Han, M.; Kim, T. Il; Kim, J. Effects of Floc and Bubble Size on the Efficiency of the Dissolved Air Flotation (DAF) Process. *Water Sci. Technol.* **2007**, *56* (10), 109–115.

(13) Cassell, E. A.; Kaufman, K. M.; Matuevic, E. The Effects of Bubble Size on Microflotation. *Water Res.* **1975**, *9* (12), 1017–1024.

(14) Calgaroto, S.; Azevedo, A.; Rubio, J. Flotation of Quartz Particles Assisted by Nanobubbles. *Int. J. Miner. Process.* **2015**, *137*, 64–70.

(15) Zhou, Z. a.; Xu, Z.; Finch, J. a.; Hu, H.; Rao, S. R. Role of Hydrodynamic Cavitation in Fine Particle Flotation. *Int. J. Miner. Process.* **1997**, *51* (1–4), 139–149.

(16) Collins, G. L.; Jameson, G. J. Experiments on the Flotation of Fine Particles the Influence of Particle Size and Charge. *Chem. Eng. Sci.* **1976**, *31*, 985–991.

(17) Yoon, R. H. Microbubble Flotation. *Miner. Eng.* **1993**, *6* (6), 619–630.

(18) Kitchener, J. A.; Gochin, R. J. The Mechanism of Dissolved Air Flotation for

Potable Water: Basic Analysis and a Proposal. *Water Res.* **1981**, *15* (5), 585–590.

(19) Matis, K. A.; Gallios, G. P.; Kydros, K. A. Separation of Fines by Flotation Techniques. *Sep. Technol.* **1993**, *3* (2), 76–90.

(20) Mishchuk, N.; Ralston, J.; Fornasiero, D. Influence of Dissolved Gas on van Der Waals Forces between Bubbles and Particles. *J. Phys. Chem. A.* **2002**, *106* (4), 689–696.

(21) Dai, Z.; Fornasiero, D.; Ralston, J. Influence of Dissolved Gas on Bubble-Particle Heterocoagulation. *J. Chem. Soc. - Faraday Trans.* **1998**, *94* (14), 1983–1987.

(22) Kyzas, G. Z.; Matis, K. A. Electroflotation Process: A Review. *J. Mol. Liq.* **2016**, *220*, 657–664.

(23) De Oliveira Da Mota, I.; De Castro, J. A.; De Góes Casqueira, R.; De Oliveira Junior, A. G. Study of Electroflotation Method for Treatment of Wastewater from Washing Soil Contaminated by Heavy Metals. *J. Mater. Res. Technol.* **2015**, *4* (2), 109–113.

(24) Zhou, W.; Chen, H.; Ou, L.; Shi, Q. Aggregation of Ultra-Fine Scheelite Particles Induced by Hydrodynamic Cavitation. *Int. J. Miner. Process.* **2016**, *157*, 236–240.

(25) Videla, A. R.; Morales, R.; Saint-Jean, T.; Gaete, L.; Vargas, Y.; Miller, J. D. Ultrasound Treatment on Tailings to Enhance Copper Flotation Recovery. *Miner. Eng.* **2016**, *99*, 89–95.

(26) Teixeira, M. R.; Rosa, M. J. Integration of Dissolved Gas Flotation and Nanofiltration for M. Aeruginosa and Associated Microcystins Removal. *Water Res.* **2006**, *40* (19), 3612–3620.

(27) Rahman, A.; Darban, K.; Mahmoud, A.; Maoming, F. Nano-Microbubble Flotation of Fine and Ultrafine Chalcopyrite Particles. *Int. J. Min. Sci. Technol.* **2014**, *24* (4), 559–566.

(28) Kumar, P. S.; Pandit, A. B. Modeling Hydrodynamic Cavitation. *Chem. Eng. Technol.* **1999**, *22* (12), 1017–1027.

(29) Hu, H.; Finch, J. a.; Zhou, Z.; Xu, Z. Numerical and Experimental Study of a Hydrodynamic Cavitation Tube. *Metall. Mater. Trans. B.* **1998**, *29* (4), 911–917.

(30) Arrojo, S.; Benito, Y. A Theoretical Study of Hydrodynamic Cavitation. *Ultrason. Sonochem.* **2008**, *15* (3), 203–211.

(31) Dziensiewicz, J., Pryor, E. J. An Investigation into the Action of Air in Froth Flotation. *Trans. IMM.* **1950**, *59*, 455–491.

Chapter 2 Literature Review

2.1 Introduction of Molybdenite

Molybdenite (MoS_2) is a mineral of molybdenum disulfide, which is a common and important source of molybdenum. About 80% of molybdenum produced is used in steel alloys, including high-strength alloys and superalloys, because it can form hard, stable carbides in alloys. There are two different geometries for molybdenite[1]. The main difference between them is the stacking layer. One is the trigonal form with three distinct layers, while the other is the hexagonal form with only two distinct layers. Each layer of the structure consists of two sheets of sulfur atoms and a single sheet of molybdenum atoms in the middle[2]. There is a strong covalent bond between Mo-S. However, the interaction between S-S is the weak van der Waals force. Because of the layer structure, the molybdenite particles show two types of surfaces: face and edge. The nonpolar face is hydrophobic resulting from the break of S-S bonds with an 80° contact angle, while the polar edge is hydrophilic due to the rupture of the strong covalent Mo-S bonds with a contact angle of 35°[3]. Therefore, the natural hydrophobicity of molybdenite depends on the particle face/edge aspect ratio. The fine molybdenite particles with a low face/edge aspect ratio have more hydrophilic edge parts exposed, causing a high detachment probability with bubbles during the flotation process[4]. In other words, fine particles with lower probability of bubble-particle collision exhibit a low flotation efficiency during the mineral flotation process[5–7].

2.2 The Limitation of Fine Particle Flotation

Froth flotation, as one of the most efficient ways for the separation of mineral particles, has been used in mineral processing plants for more than 100 years. Different minerals have their own unique physicochemical surface properties, such as contact angle, wettability, hydrophilicity, roughness and so on[8]. Essentially, the principle of mineral flotation is based on the differences of their surface properties. During the flotation process, mineral particles are floated to the surface of the slurry via the attachment with air bubbles, merging together to form the froth layer. It is believed that the main component of the froth are hydrophobic particles while the hydrophilic particles, which have less tendency to attach to air bubbles, remain in the slurry and are flushed away. These non-floatable mineral particles are known as tailings.

However, this conventional approach to separate valuable minerals was not as highly efficient as expected. It reported a low flotation rate and poor recovery of fine particles, which is mainly due to the low collision efficiency with conventional flotation bubbles[9–12]. Gaudin *et al.* first found this problem in sulfide mineral flotation 90 years ago[13]. It was noticed that the best recoveries of lead, zinc and copper sulfide minerals were obtained for the particle size range of 10 to 50 µm.

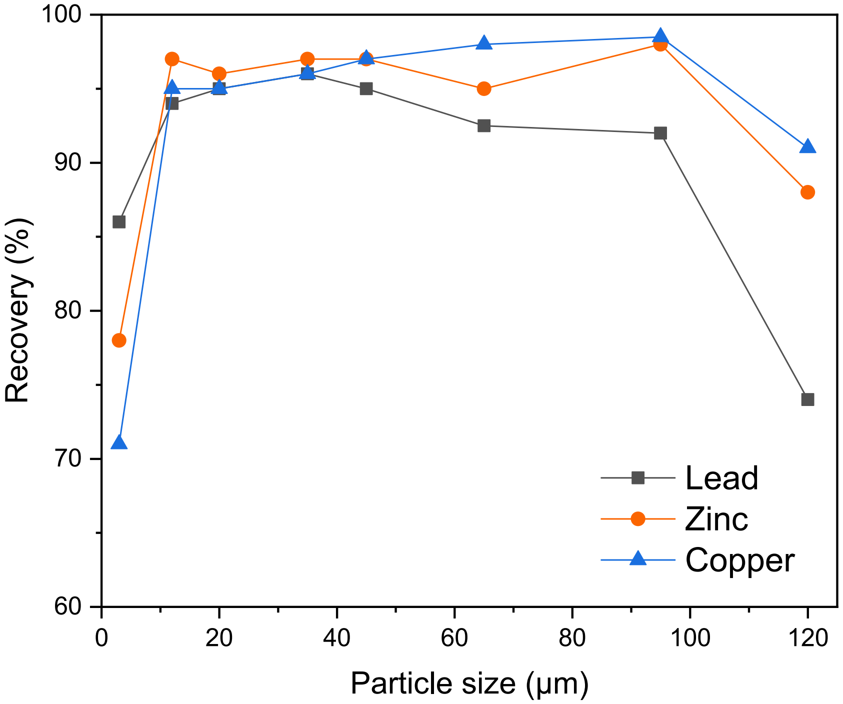

Figure 2-1 Recovery of different minerals with different particle sizes

(Data replotted from Gaudin et al., 1931.)[13]

In the later investigations from other researchers, it was found that neither fine particles (< 37 μm) nor coarse particles (> 100 μm) could achieve the best recovery (Figure 2-1). Conventional mineral flotation shows good performance just in the normal particle size range. The limitation of fine and coarse particle flotation, therefore, has been seriously studied in recent decades. To date, research scholars have found several alternative solutions. Of special interest in this thesis research is the flotation of fine particles, which will be discussed in more detail in the next section.

2.3 Approaches to Enhance Fine Particle Recovery

To increase the flotation rate and recovery of fine particles, many approaches have been developed[9,14–16]. Fundamentally, the flotation recovery of fine mineral particles potentially enhances with an increase of the particle-bubble collision and attachment, either by decreasing bubble size in flotation or increasing particle size.

Air distributors were first applied for the generation of smaller bubbles, which were initially used for water purification[17]. It was found that forcing dispersed air through a porous plate and mixing with it a small amount of ethanol in a distributor could greatly reduce the bubble size[18]. It was also proved that the generation of small bubbles resulted from the combination of a sparger with small porosity and the presence of surfactants[19]. Ham *et al.* investigated various types of flat glass plate distributors such as porous glass plates, single-hole, and multi-hole glass plates[20]. It was found that multi-hole distributors gave much better results compared to either porous or single-hole distributors in a flotation column.

Dissolved air flotation was also introduced as another unique technique to generate small bubbles. In dissolved air flotation procedure, small bubbles are produced by the pressure reduction of a water stream saturated with air[16]. The absorption of air nuclei on mineral particles is beneficial to the attachment of these particles to conventional flotation bubbles[21,22]. It was also noted that carbon dioxide and air played a significant role in enhancing particle-bubble collision[23].

In addition, electro-flotation was reported as an important approach in fine particle flotation. It can generate tiny bubbles of oxygen and hydrogen through the electrolytic process. Oxygen is formed at the anode while hydrogen is formed at the cathode.

These electrolytic bubbles, with an average diameter of 20 - 40 μm, are suitable for fine particle flotation[24]. They can increase up to 70% - 100% of the recovery depending on the type of minerals and their particle sizes[25]. Compared to dissolved air flotation, electro-flotation can not only generate much smaller bubbles, but also provide a good coverage of the whole surface area of the flotation cell.

Besides the approaches mentioned above, cavitation is also widely used in the mineral flotation process for the improvement of fine particle flotation. It can be classified into three types: acoustic cavitation, optical cavitation and hydrodynamic cavitation.

Lasers are commonly used in optical cavitation for bubble generation. The energy provided by the laser can create an overheated region at the focal point, causing an explosive liquid-vapor phase transition[26]. The superheated vapor can easily expand to form vapor bubbles and attach to the surfaces of particles. It was also found that the probability of laser cavitation of water confined between hydrophobic cuvette surfaces is enhanced as compared with the case of hydrophilic surfaces[27].

The main idea of acoustic cavitation is using ultrasonic energy to treat liquid. It can cause the gas nuclei which already exist in liquid to vibrate and grow to generate bubbles. Ultrasound was initially used for surface cleaning, and was then later applied to enhance coal flotation[28–30]. It was found that not only can it produce cavitation bubbles, but also it may clean the mineral particle surface via high energy transfer to the interface[31–34]. The clay on the coal surface is thus removed, exposing a new surface and making reagents easy to adsorb (Figure 2-2). Thus, the flotation recovery of coal is increased significantly.

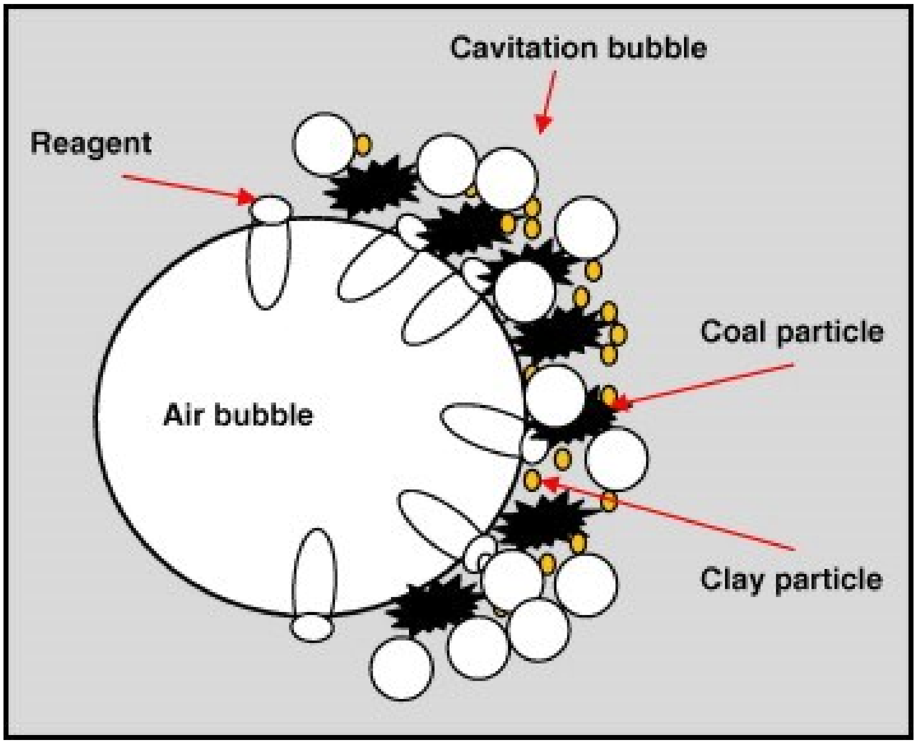

Figure 2-2 Mechanism of ultrasonically created cavitation bubbles on the coal flotation[34]

Ozkan *et al.* pretreated magnesite slimes with ultrasonic treatment to effectively achieve a higher recovery of < 38 µm magnesite wastes[35]. Videla *et al.* also used a similar kind of treatment to enhance copper flotation recovery, which achieved an increase of 3.1% in total recovery[36]. Although acoustic cavitation is considered as an effective way to enhance fine and ultrafine particles flotation, the high operational cost is still a limitation of this technology.

Hydrodynamic cavitation can be achieved with an orifice plate, the Venturi tube or a high intensity agitation (HIA) cell[37]. Theoretically, they can cause a relative lower local pressure compared to the vapor pressure. As the water surface is ruptured, many microbubbles will generate. The HIA cell, also called HIC (high intensity condition) cell, has been proven as a simple and convenient method for bubble generation with hydrodynamic cavitation in the industry[38,39]. It is a specially designed agitation tank with several flat blades on the wall. The impeller is aligned at the center of the tank[40,41]. During cavitation, many microbubbles will be created as the agitation speed increases.

Hydrodynamic cavitation, as an economic and environment-friendly approach, has shown a significant improvement in fine particle flotation recovery[42,43]. Not only are the microbubbles generated in this process, but also the high shear force plays as an important role in overcoming the energy barrier between particles and bubbles, allowing for easier attachment between the two[44].

2.4 Venturi Tube

The Venturi tube is one of the most widely-used devices in the hydrodynamic cavitation. In the hydrodynamic cavitation process, the microbubbles are generated by the rupture of a liquid-liquid or a liquid-solid interface of a high-speed fluid flow. When the liquid passes through the throat part of Venturi tube, the liquid flow rate increases with a higher kinetic and potential at the expense of the pressure[37]. As the local pressure at the throat falls below the liquid vapor pressure, a great number of bubbles are generated due to the cavities and gas nuclei in the liquid[45,46].

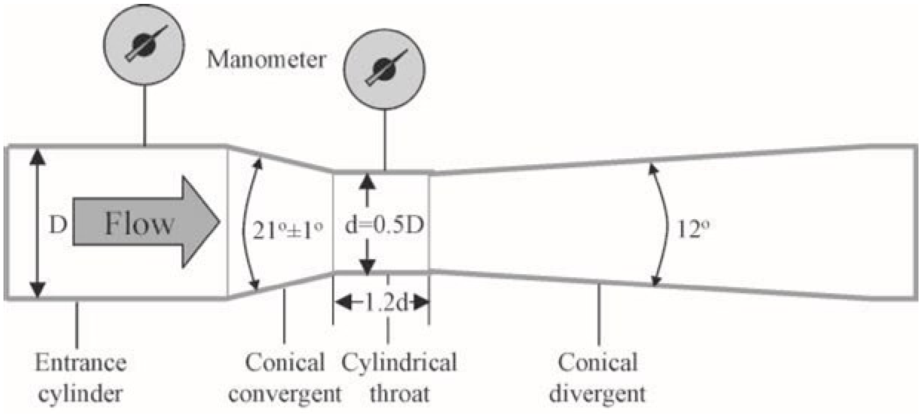

Figure 2-3 Schematic diagram of the Venturi tube[47]

To investigate the effect of the operating parameters, Gogate and Pandit built a model and found that inlet pressure through the tube, liquid properties, and tube geometry were the important parameters[37]. The increased inlet pressure should be kept below a certain optimum value to avoid super-cavitation phenomenon. A liquid with lower vapor pressure, viscosity and higher surface tension is recommended. Additionally, a smaller throat diameter can produce higher intensities, which is regarded as a desired beneficial effect.

Since the earlier model did not consider the interactions of the bubbles and the changes of the liquid flow, Moholkar and Pandit modified and improved the model for further study and found new discoveries[48]. The outlet pressure will increase as the inlet pressure increases, which may reduce bubble cluster life. The active volume of the Venturi tube can be increased while increasing the tube to pipe area ratio. The smaller initial size of the gas nuclei and bubbles makes much more contribution to bubble generation during cavitation as compared to the bigger size.

In addition, some other parameters which may affect the hydrodynamic cavitation were proven by Arrojo and Benito, who found that the time scales of rarefaction and pressure played a major role[49]. On the one hand, the large characteristic scale of rarefaction promotes bubble growth since it can lead to a higher collapse temperature and long rarefaction periods can decrease the cavitation threshold. On the other hand, excessive bubble densities may diminish the efficiency of bubble-bubble interactions. Similar affects were also investigated by Soyama and Hoshino[50]. It was revealed that the aggressive intensity could simply be increased by decreasing the tube to pipe area ratio without the need of extra power. Although the outlet pressure varied with inlet pressure, the cavitation number was constant. The same phenomenon was observed as the length of the cavitation region in the Venturi tube changed with time.

2.5 Fine Particle Flotation with Hydrodynamic Cavitation

Up to now, fine particle flotation has still been a critical problem in the mineral flotation industry. As mentioned before, the combination of microbubbles generated by the hydrodynamic cavitation and typical flotation sized bubbles can be a potential solution in the fine particle flotation process.

Many scholars have used the Venturi tube as a bubble generator in their studies. Zhou *et al.* found that the presence of surfactants and dissolved gas could enhance bubble formation[51]. In addition, Fang noticed that the cavitated nanobubbles would preferentially nucleate on the surface of hydrophobic particles[52]. It was also noticed that an increase of frother concentration can decrease the size of microbubbles, while increasing the dissolved oxygen or carbon dioxide concentration may cause an opposite effect. Similarly, Pourkarimi *et al.* also observed that microbubble size increases with an increase of the dissolved air flow rate, and a decrease of the pressure within the Venturi tube[53]. However, with a different opinion, Li *et al.* revealed that increasing the throat velocity and dissolved gas concentration had little effect on the size of cavitation bubbles[54]. Instead, the quantity of generated bubbles increased significantly.

The Venturi tube has been applied to different fine mineral particle flotations. Zhou *et al.* found that with hydrodynamic cavitation treatment, the recovery of ultrafine (< 10 μm) scheelite increased by about 20%[43]. It was discussed that the nanobubbles generated by hydrodynamic cavitation promoted the aggregation of hydrophobic scheelite particles in low NaOl conditions. Sobhy and Tao connected the Venturi tube to the flotation column to enhance the recovery of an Illinois fine coal sample[33]. With the assistance of microbubbles, more coal and less ash were recovered. Not only was the combustible recovery significantly improved, but the consumption of reagent and air was reduced as well. Similar effects were found in the flotation of fine and ultrafine chalcopyrite particles[33,55]. The microbubbles generated by hydrodynamic cavitation increased their recovery by 16% - 21% and reduced the consumption of the collector and the frother by 75% and 50% respectively. As reported, compared to fine particles, the enhancement of ultrafine particle recovery was much more effective[42].

2.6 Reference

(1) Von Oertzen, G. U.; Harmer, S. L.; Skinner, W. M. XPS and Ab Initio Calculation of Surface States of Sulfide Minerals: Pyrite, Chalcopyrite and Molybdenite. *Mol. Simul.* **2006**, *32* (15), 1207–1212.

(2) Wenk, H.-R. and Bulakh, A. *Minerals: Their Constitution and Origin*; Cambridge

University Press, 2004.

(3) Wan, H.; Yang, W.; Cao, W.; He, T.; Liu, Y.; Yang, J.; Guo, L.; Peng, Y. The Interaction between Ca^{2+} and Molybdenite Edges and Its Effect on Molybdenum Flotation. *Minerals.* **2017**, *7* (8), 141.

(4) Song, S.; Zhang, X.; Yang, B.; Lopez-Mendoza, A. Flotation of Molybdenite Fines as Hydrophobic Agglomerates. *Sep. Purif. Technol.* **2012**, *98*, 451–455.

(5) Lucay, F.; Cisternas, L. A.; Gálvez, E.; Lopez-Valdivieso, A. Study of the Natural Floatability of Molybdenite Fines in Saline Solutions and Effect of Gypsum Precipitation. *Miner. Metall. Process.* **2015**, *32* (4), 203–208.

(6) Jiangang, F.; Kaida, C.; Hui, W.; Chao, G.; Wei, L. Recovering Molybdenite from Ultrafine Waste Tailings by Oil Agglomerate Flotation. *Miner. Eng.* **2012**, *39*, 133–139.

(7) Zanin, M.; Ametov, I.; Grano, S.; Zhou, L.; Skinner, W. A Study of Mechanisms Affecting Molybdenite Recovery in a Bulk Copper/molybdenum Flotation Circuit. *Int. J. Miner. Process.* **2009**, *93* (3–4), 256–266.

(8) Farrokhpay, S. The Significance of Froth Stability in Mineral Flotation - A Review. *Adv. Colloid Interface Sci.* **2011**, *166* (1–2), 1–7.

(9) Miettinen, T.; Ralston, J.; Fornasiero, D. The Limits of Fine Particle Flotation. *Miner. Eng.* **2010**, *23* (5), 420–437.

(10) Trahar, W. J.; Warren, L. J. The Flotability of Very Fine Particles - A Review. *Int. J. Miner. Process.* **1976**, *3* (2), 103–131.

(11) Ahmed, N.; Jameson, G. J. The Effect of Bubble Size on the Rate of Flotation of Fine Particles. *Int. J. Miner. Process.* **1985**, *14* (3), 195–215.

(12) Yoon, R. H.; Luttrell, G. H. The Effect of Bubble Size on Fine Particle Flotation. *Miner. Process. Extr. Metall. Rev.* **1989**, *5* (1–4), 101–122.

(13) Gaudin, A.M.; Groh, J.O. and Henderson, H.B. Effect of particle size on flotation. *AIME, Tech. Publ.* **1931**, 414, 3–23.

(14) Coleman, D.; Toll, F. N. Agglomeration-Flotation : Hydrophobic Components Fine Tailings Recovery of from Oil Sands. *Fuel.* **1995**, *74* (8), 1156–1161.

(15) Collins, G. L.; Jameson, G. J. Experiments on the Flotation of Fine Particles the Influence of Particle Size and Charge. *Chem. Eng. Sci.* **1976**, *31*, 985–991.

(16) Matis, K. A.; Gallios, G. P.; Kydros, K. A. Separation of Fines by Flotation Techniques. *Sep. Technol.* **1993**, *3* (2), 76–90.

(17) Spiegler, K. S. Diffusion of Gases across Porous Media. *Ind. Eng. Chem. Fundam.* **1966**, *5* (4), 529–532.

(18) Reay, D.; Ratcliff, G. A. Removal of Fine Particles from Water by Dispersed Air Flotation: Effects of Bubble Size and Particle Size on Collection Efficiency. *Can. J. Chem. Eng.* **1973**, *51* (2), 178–185.

(19) Janse, P.; Gomez, C. O.; Finch, J. A. Effect of Pulp Fibres on Gas Holdup in a Flotation Column. *Can. J. Chem. Eng.* **1999**, *77* (1), 22–25.

(20) Ham, N. J. M. V. A. N.; Behie, L. E. O. A.; Svrcek, W. Y. The Effect of Air Distribution on the Induced Air Flotation of Fine Oil in Water Emulsions. **1983**, *61*,

541–547.

(21) Dziensiewicz, J., Pryor, E. J. An Investigation into the Action of Air in Froth Flotation. *Trans. IMM.* **1950**, *59*, 455–491.

(22) Klassen, V.J., Mokrousov, V. A. *An Introduction to the Theory of Flotation*; Butterworths, London, 1963.

(23) Dai, Z.; Fornasiero, D.; Ralston, J. Influence of Dissolved Gas on Bubble-Particle Heterocoagulation. *J. Chem. Soc. - Faraday Trans.* **1998**, *94* (14), 1983–1987.

(24) Sarkar, M. S. K. A.; Evans, G. M.; Donne, S. W. Bubble Size Measurement in Electroflotation. *Miner. Eng.* **2010**, *23* (11–13), 1058–1065.

(25) Gonzales, L. V.; Veneu, D. M.; Torem, M. L. Measurement and Analysis of Micro-Bubbles Produced in Electroflotation. **1934**, *I*, 26–44.

(26) Padilla-Martinez, J. P.; Berrospe-Rodriguez, C.; Aguilar, G.; Ramirez-San-Juan, J. C.; Ramos-Garcia, R. Optic Cavitation with CW Lasers: A Review. *Phys. Fluids.* **2014**, *26* (12).

(27) Vinogradova, O. I.; Bunkin, N. F.; Churaev, N. V.; Kiseleva, O. A.; Lobeyev, A. V.; Ninham, B. W. Submicrocavity Structure of Water between Hydrophobic and Hydrophilic Walls as Revealed by Optical Cavitation. *Journal of Colloid And Interface Science*. 1995, pp 443–447.

(28) Zhao, H. L.; Wang, D. X.; Cai, Y. X.; Zhang, F. C. Removal of Iron from Silica Sand by Surface Cleaning Using Power Ultrasound. *Miner. Eng.* **2007**, *20* (8), 816–818.

(29) Gurpinar, G.; Sonmez, E.; Bozkurt, V. Effect of Ultrasonic Treatment on Flotation of Calcite, Barite and Quartz. *Miner. Process. Extr. Metall. Trans. Inst. Min. Metall. Sect. C.* **2004**, *113* (2), 91–95.

(30) Farmer, a. .; Collings, a. .; Jameson, G. . Effect of Ultrasound on Surface Cleaning of Silica Particles. *Int. J. Miner. Process.* **2000**, *60*, 101–113.

(31) Ozkan, S. G.; Kuyumcu, H. Z. Investigation of Mechanism of Ultrasound on Coal Flotation. *Int. J. Miner. Process.* **2006**, *81* (3), 201–203.

(32) Ozkan, S. G.; Kuyumcu, H. Z. Design of a Flotation Cell Equipped with Ultrasound Transducers to Enhance Coal Flotation. *Ultrason. Sonochem.* **2007**, *14* (5), 639–645.

(33) Sobhy, A.; Tao, D. Nanobubble Column Flotation of Fine Coal Particles and Associated Fundamentals. *Int. J. Miner. Process.* **2013**, *124*, 109–116.

(34) Ozkan, S. G. Effects of Simultaneous Ultrasonic Treatment on Flotation of Hard Coal Slimes. *Fuel.* **2012**, *93*, 576–580.

(35) Ozkan, S. G. Beneficiation of Magnesite Slimes with Ultrasonic Treatment. *Miner. Eng.* **2002**, *15* (1–2), 99–101.

(36) Videla, A. R.; Morales, R.; Saint-Jean, T.; Gaete, L.; Vargas, Y.; Miller, J. D. Ultrasound Treatment on Tailings to Enhance Copper Flotation Recovery. *Miner. Eng.* **2016**, *99*, 89–95.

(37) Gogate, P. R.; Pandit, A. B. A Review and Assessment of Hydrodynamic Cavitation as a Technology for the Future. *Ultrason. Sonochem.* **2005**, *12* (1–2 SPEC. ISS.), 21–27.

(38) Zhou, Z. A.; Xu, Z.; Finch, J. A.; Masliyah, J. H.; Chow, R. S. On the Role of Cavitation in Particle Collection in Flotation - A Critical Review. II. *Miner. Eng.* **2009**, *22* (5), 419–433.

(39) Sun, W.; Hu, Y.; Dai, J.; Liu, R. Observation of Fine Particle Aggregating Behavior Induced by High Intensity Conditioning Using High Speed CCD. *Trans. Nonferrous Met. Soc. China.* **2006**, *16* (1), 198–202.

(40) Wu, C.; Nesset, K.; Masliyah, J.; Xu, Z. Generation and Characterization of Submicron Size Bubbles. *Adv. Colloid Interface Sci.* **2012**, *179–182*, 123–132.

(41) Wu, C.; Wang, L.; Harbottle, D.; Masliyah, J.; Xu, Z. Studying Bubble-Particle Interactions by Zeta Potential Distribution Analysis. *J. Colloid Interface Sci.* **2015**, *449*, 399–408.

(42) Rahman, A.; Darban, K.; Mahmoud, A.; Maoming, F. Nano-Microbubble Flotation of Fine and Ultrafine Chalcopyrite Particles. *Int. J. Min. Sci. Technol.* **2014**, *24* (4), 559–566.

(43) Zhou, W.; Chen, H.; Ou, L.; Shi, Q. Aggregation of Ultra-Fine Scheelite Particles Induced by Hydrodynamic Cavitation. *Int. J. Miner. Process.* **2016**, *157*, 236–240.

(44) Duerkop, M.; Berger, E.; Dürauer, A.; Jungbauer, A. Impact of Cavitation, High Shear Stress and Air/Liquid Interfaces on Protein Aggregation. *Biotechnol. J.* **2018**, *13* (7), 1–9.

(45) Kumar, P. S.; Pandit, A. B. Modeling Hydrodynamic Cavitation. *Chem. Eng. Technol.* **1999**, *22* (12), 1017–1027.

(46) Hu, H.; Finch, J. a.; Zhou, Z.; Xu, Z. Numerical and Experimental Study of a Hydrodynamic Cavitation Tube. *Metall. Mater. Trans. B.* **1998**, *29* (4), 911–917.

(47) Tao, D. Role of Bubble Size in Flotation of Coarse and Fine Particles—A Review. *Sep. Sci. Technol.* **2005**, *39* (4), 741–760.

(48) Moholkar, V. S.; Pandit, A. B. Modeling of Hydrodynamic Cavitation Reactors : A Uniÿed Approach. **2001**, *56*, 6295–6302.

(49) Arrojo, S.; Benito, Y. A Theoretical Study of Hydrodynamic Cavitation. *Ultrason. Sonochem.* **2008**, *15* (3), 203–211.

(50) Soyama, H.; Hoshino, J. Enhancing the Aggressive Intensity of Hydrodynamic Cavitation through a Venturi Tube by Increasing the Pressure in the Region Where the Bubbles Collapse. *AIP Adv.* **2016**, *6* (4).

(51) Zhou, Z. a.; Xu, Z.; Finch, J. a.; Hu, H.; Rao, S. R. Role of Hydrodynamic Cavitation in Fine Particle Flotation. *Int. J. Miner. Process.* **1997**, *51* (1–4), 139–149.

(52) Fan, M.; Tao, D.; Honaker, R.; Luo, Z. Nanobubble Generation and Its Application in Froth Flotation (Part I): Nanobubble Generation and Its Effects on Properties of Microbubble and Millimeter Scale Bubble Solutions. *Min. Sci. Technol.* **2010**, *20* (1), 1–19.

(53) Pourkarimi, Z.; Rezai, B.; Noaparast, M. Effective Parameters on Generation of Nanobubbles by Cavitation Method for Froth Flotation Applications. *Physicochem. Probl. Miner. Process.* **2017**, *53* (2), 920–942.

(54) Li, H.; Afacan, A.; Liu, Q.; Xu, Z. Study Interactions between Fine Particles and

Micron Size Bubbles Generated by Hydrodynamic Cavitation. *Miner. Eng.* **2015**, *84*, 106–115.

(55) Peng, F. F.; Yu, X. Pico-Nano Bubble Column Flotation Using Static Mixer-Venturi Tube for Pittsburgh No. 8 Coal Seam. *Int. J. Min. Sci. Technol.* **2015**, *25* (3), 347–354.

Chapter 3 Material and Experimental Methods

3.1 Materials

The high concentrate molybdenite provided by Teck Highland Valley Copper was used for the entirety of the tests except Zeta potential distribution measurement. It was first placed in the vacuum oven at 50 ℃ for 12 hours to let it dry, and then classified by dry screening into the following four different size ranges: < 37 µm, 37 - 74 µm, 74 - 105 µm, and 105 - 150 µm. To remove the residual organic reagents and collectors absorbed on the surface of the particles, ethanol (Reagent Alcohol, Fisherbrand) was used to wash them three times[1]. After that, the sample was rinsed with an amount of Milli-Q water and dried again in the oven at 50℃ for another 12 hours. FTIR was used to confirm that the organics had been removed and XPS was used to make sure that the sample had been oxidized after treatment. The purity of the treated molybdenite was determined by using X-ray fluorescence (XRF). The ultrafine molybdenum sulfide powder purchased from Sigma–Aldrich with a grade of 99% was only used for ZetaPhoremeter measurement.

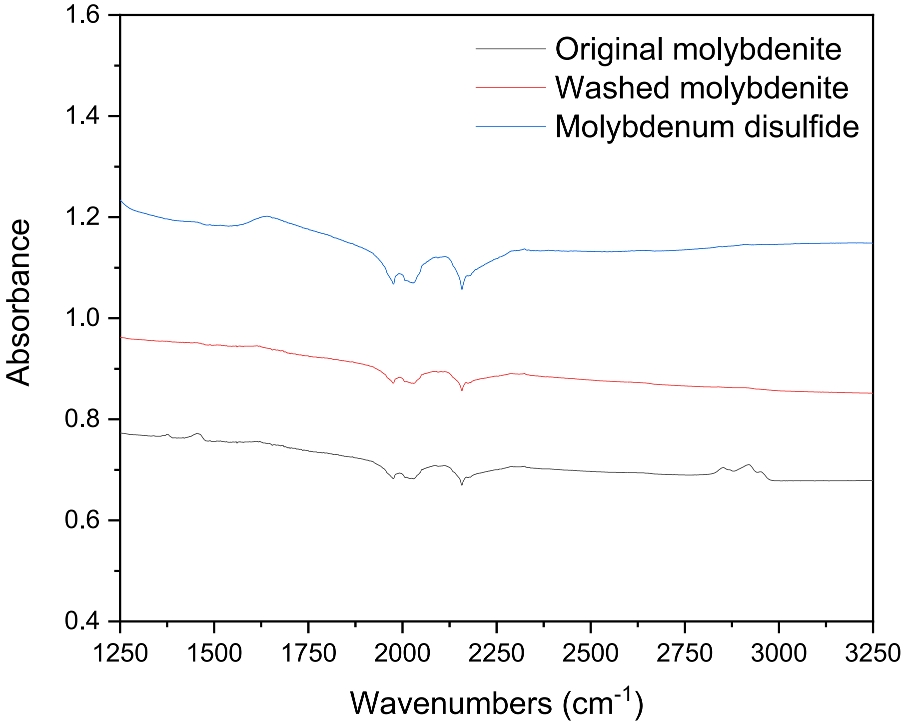

Figure 3-1 FTIR spectra of the molybdenite concentrate before and after washing and ultrafine molybdenum disulfide powder

FTIR spectroscopy has been used to characterize the samples to check if the organics were washed away. The spectra show peaks at the 1250 - 3250 cm^{-1} region, which includes most of the main absorption bands corresponding to organics. As absorbed in Figure 3-1, the signal of the original molybdenite, related to -CH$_2$- (1450, 2847, 2918 cm^{-1}) and -CH$_3$ (1375 cm^{-1}), has been eliminated after being washed, which indicates that the organic collectors absorbed on the molybdenite concentration during industry mineral flotation have been removed by ethanol[1,2]. To further understand the properties of the samples, XRF and XRD were used to analyze their compositions.

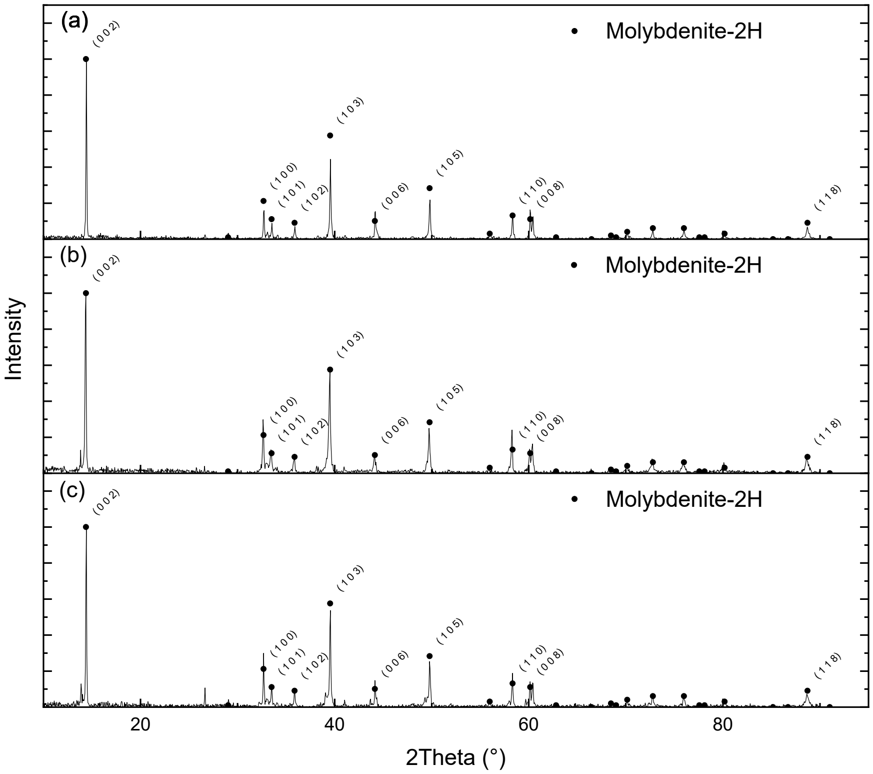

Figure 3-2 XRD patterns of the molybdenite concentrate before (a) and after (b) washing and ultrafine molybdenum disulfide powder (c)

Both molybdenite concentrate and ultrafine molybdenum disulfide powder have been analyzed by the XRD as shown in Figure 3-2. All the samples show very sharp peaks with very high intensity, indicating a good crystallization[3,4]. The strong [002] peak (14.4°) also shows a well-stacked layered structure[5,6]. Almost no extra peak shows in the patterns except molybdenite-2H itself, which indicates a very high phase purity of molybdenite concentrate.

Table 3-1 Summary of XRF test results of the molybdenite concentrate before and after washing and ultrafine molybdenum disulfide powder

Sample	**Si**	**S**	**Fe**	**Mo**
	(wt%)	**(wt%)**	**(wt%)**	**(wt%)**
Original molybdenite	1	35.46	1.83	61.71
Washed molybdenite	0.98	36.29	1.76	60.97
Molybdenum disulfide	0	42.45	0.2	57.35

The XRF data in Table 3-1 shows that the purity of molybdenite is more than 96%, which is suitable for micro-flotation tests with pure fine particles in later tests. The concentration of elements doesn't change after washing. As for the ultrafine molybdenum disulfide particles, the purity almost reaches 100%, which can show us very reliable results in zeta potential distribution measurement since no ion will affect the accuracy of the results.

The elemental ratio of Molybdenum and Sulfur seems strange in Table 3-1, which is due to the detector resolution. In the periodic table of elements, the Kα energy of S is 2.309 keV and the Lα energy of Mo is 2.292 keV. These two values are very close causing overlapping peaks of Mo and S, which cannot be distinguished precisely by the software. However, the total weight percentage of molybdenum and sulfur is accurate. Therefore, XPS was performed to determine the chemical composition of the molybdenite concentration.

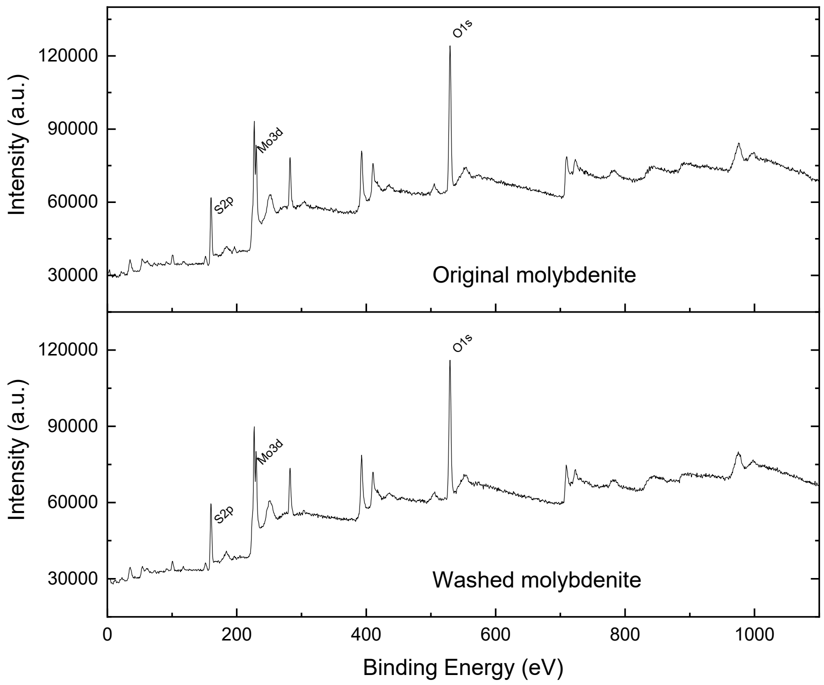

Figure 3-3 Wide-scan XPS spectrums of the molybdenite concentrate before and after washing

Table 3-2 Elements atomic contents of molybdenite concentrate before and after washing

Sample	O (at%)	Fe (at%)	Mo (at%)	S (at%)	Si (at%)
Original molybdenite	45.23	3.77	15.6	27.17	8.23
Washed molybdenite	46.3	5	15.5	25.26	7.93

The XPS spectra of molybdenite (before and after treatment) over a binding energy of 0 - 1200 eV is presented in Figure 3-3. The atomic content of molybdenite (before and after treatment) is listed in Table 3-2. In the calibration of the charge effects, the C 1s photoemission was set at 284.2 eV[7]. No significant differences were observed after the molybdenite was washed, indicating that the Mo (IV) on molybdenite was not oxidized to Mo (VI) during the washing process. It is suitable to use molybdenite as the samples for hydrodynamic cavitation since the molybdenite has been proved with very stable chemical properties.

Milli-Q water with a resistivity of 18.2 MΩ was used in the preparation of all solutions and suspensions. Reagent grade KCl (Fisher Scientific) was used to prepare the background electrolyte in zeta potential measurements and reagent grade HCl (Fisher Scientific) and NaOH (Fisher Scientific) were used to adjust the pH. MIBC (4-Methyl-2-pentanol, Sigma–Aldrich), a kind of surfactant, was used as the frother to promote the generation and stabilization of the microbubbles generated via hydrodynamic cavitation.

3.2 Experimental Techniques

3.2.1 X-ray fluorescence (XRF)

X-ray fluorescence is a non-destructive analytical technique used for elemental composition analysis. It is an accurate and economic analytical method that has been widely used in the investigation of metals, minerals and materials. It can determine the elemental concentrations of a sample by measuring the fluorescent (or secondary) X-ray emitted from a sample when it is excited by a primary X-ray source. When the sample is exposed to X-rays, the atoms inside of it are excited and a vacancy will be formed. The electrons in higher orbitals will fill the vacancy and emit radiation at the same time, which will show energy characteristic of the atoms. Since the characteristic fluorescent X-ray that each element emits is unique, it can be used to determine the content of the elements.

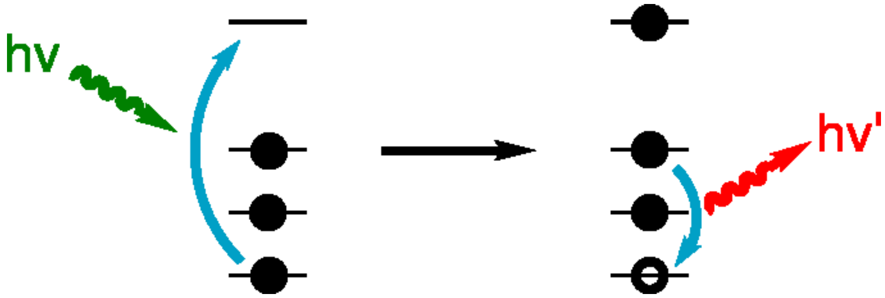

Figure 3-4 Physics of X-ray fluorescence in a schematic representation[8]

In XRF measurement, the pellets of the samples were measured using the Orbis PC Micro-XRF Analyzer. The X-ray was set to a voltage of 40 kV and a current of 200 mA to keep DTM around 30%. The pellets were measured under vacuum conditions for 30 s.

3.2.2 X-ray diffraction (XRD)

XRD (X-ray diffraction) is one of the most basic and important technology used for measuring the crystal structure. The crystal, illuminated with a beam of incident X-rays, will produce diffraction patterns into many specific directions. By measuring the angles and intensities of these diffracted beams, we can deduce the structure of the crystal. This analytical method is also widely used in determining the arrangement of atoms in minerals and metals, especially in the qualitative and quantitative analysis of the minerals.

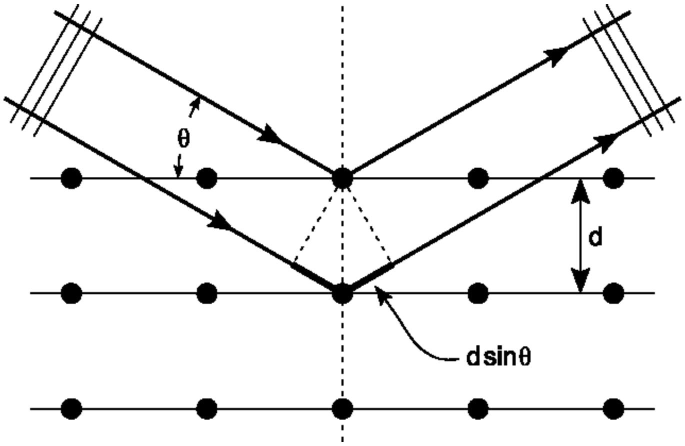

Figure 3-5 Schematic representation of X-Ray diffraction[9]

X-ray diffraction measurements were performed with fine molybdenite particles using the Bruker XRD. The samples were put in a square groove with a flat surface. The scanning rate was 2°/s. The scanning range of 2 Theta angles was from 10° to 90°.

3.2.3 X-ray photoelectron spectroscopy (XPS)

X-ray photoelectron spectroscopy is a commonly used surface-sensitive quantitative spectroscopic technique to measure the elemental composition, chemical state and electron state of the elements in the sample. When the sample is irradiated by X-rays, the inner electrons of atoms and molecules are excited and emitted, which is also known as photoelectric effect. By measuring the binding energy and the number of photoelectrons that escape from the top 0 to 10 nm of the material surface, the analyzer can plot out the XPS spectrum.

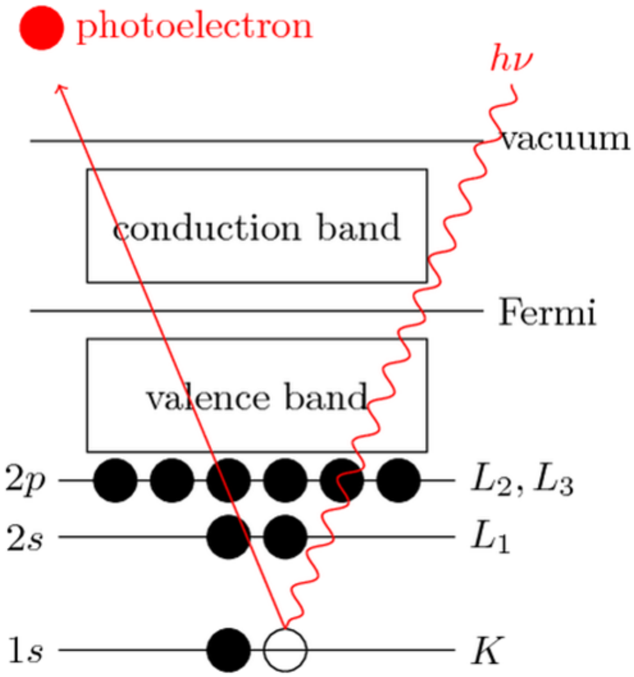

Figure 3-6 Schematic representation of X-ray photoelectron spectroscopy[10]

The spectra and percent atomic concentration of samples were obtained using the Kratos AXIS 165 X-ray photoelectron spectrometer in this research. Survey scans were collected in the range of 0 - 1100 eV (binding energy) and high-resolution scans were obtained for Fe2p, O1s, Mo3d, S2p and Si2p.

3.2.4 Fourier transform infrared spectroscopy (FTIR)

Fourier-transform infrared spectroscopy is an infrared spectroscopy technique used to obtain the absorption spectrum and the emission spectrum of a solid, liquid or gas, which makes use of Fourier transform to convert the raw data into the actual spectrum. It can simultaneously collect high-spectral-resolution data over a wide spectral range.

ATR is an accessory of FTIR, which can analyze surface properties of solid or thin film samples rather than their bulk properties by measuring the changes that occur in an internally reflected IR beam when the beam hits a sample surface. This internal reflectance creates an evanescent wave which extends beyond the surface of the sample with a penetration depth of around 1 μm or 2 μm depending on the sample conditions.

The chamber of the equipment was flushed with dry Nitrogen during measurements. The spectra of samples were obtained using the Nicolet iS50 ATR-FTIR spectrophotometer with the number of scans set to 32, at a resolution of 4 cm^{-1}, and in the range of 400 - 4000 cm^{-1}.

3.2.5 Optical profilometer

The optical profilometer provides a simple way for surface measurements without direct contact. It makes use of the wave properties of light to compare the differences of the surfaces. During the measurement, a light beam with the fixed wavelength is emitted through an optical microscope. Half of it is reflected from the reference mirror, and another half passing through the focal plane of the microscope is reflected by the test material. Both are combined by the sensor to form the interference image, which makes it possible to get the height variations of the surface and calculate the surface roughness.

3.2.6 Optical tensiometer

The optical tensiometer (Biolin Scientific) is an innovative system capable of measuring dynamic contact angle, wettability, 3D surface roughness, surface free energy and surface tension. It consists of the most advanced camera to capture images of the droplet spreading on the surface with the help of a monochromatic, non-heating LED light. It can provide high resolution images for real time measurement of the droplet volume, contact angle, surface tension, etc.

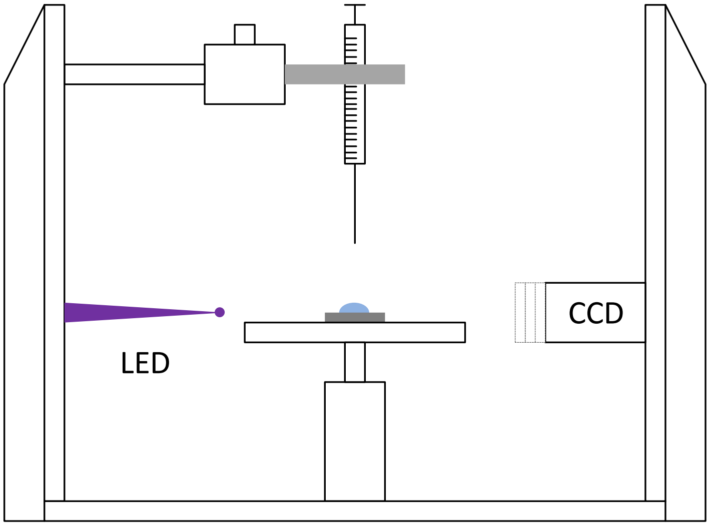

Figure 3-7 Schematic representation of tensiometer for contact angle measurement

To keep a flat and smooth surface for contact angle measurement, the pellets were prepared with fine powders. The sessile drop technique was used in the measurement. A 5 μL water drop precisely controlled by the needle was placed on the surface of the pellets and the real time video was recorded. The water drop images were analyzed by the software based on the sessile drop technique. The initial contact angle was collected as soon as the water drop attach to the pellet surface. Four points were placed on each pellet and their mean value was reported[11].

3.2.7 Mastersizer with Hydro EV

The Mastersizer 3000 (Malvern Instruments, Inc., San Bernadino, CA) is a popular instrument used to measure the size of particles using laser diffraction. It can measure the intensity of light scattered as a laser beam passes through a dispersed particulate sample, which is then used to analyze the size distribution of the particles based on the scattering pattern. The scale of the measured particle size ranges from the nanometer to the millimeter. The size distribution curve is based on number, surface area and volume, which can focus on different parts of the size distribution curve. The Hydro EV is a unique dip-in wet sample dispersion with a centrifugal pump and stirrer, which can not only precisely match the volume of the solution, but also control the stirring speed used for mixing. It can also be used to analyze the real-time particle size changing in the solution.

The particle size of molybdenite particles was measured using alcohol solution to ensure good dispersion. The stirring speed was set at 500 rev/min to agitate the samples. The mean value of a continuous 5 s' measurement was plotted in both number based and volume based. The results in number based were focus on smaller size portion, while the results in volume based preferred the larger particles.

3.2.8 Turbidimeter

Turbidity is the cloudiness or haziness of a fluid caused by suspended particles, which is often used as a general water quality indicator for relative water clarity measurements. It is also used as an indirect way to measure the settling rate of particles. The units of turbidity from a calibrated nephelometer are called Nephelometric Turbidity Unit (NTU). To give an example of scale, the turbidity of Milli-Q water used in the lab is 0.02 NTU.

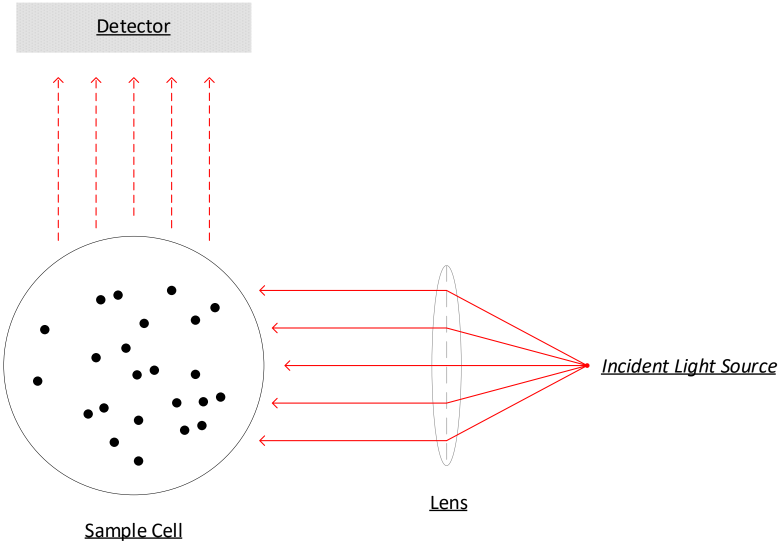

Figure 3-8 Schematic representation of Turbidimeter

Turbidimeter is a simple and convenient instrument used to quickly measure the turbidity of water. When an incident light travels through a volume of water, it is scattered or absorbed by the existence of particles which are suspended within the water. By analyzing the amount of light scattered at 90°, the detector can indicate the turbidity value.

3.2.9 Zetasizer

Zetasizer Nano ZS (Malvern Instruments, Inc., San Bernadino, CA) is a high performance system used for the measurement of the size, electrophoretic mobility, zeta potential of colloids and nanoparticles. While measuring zeta potential, an electric field is applied to a solution or a dispersion of particles. Their moving speed is measured using a patented laser interferometric technique, whose data can be used to calculate electrophoretic mobility and zeta potential.

3.2.10 Zetaphoremeter

ZetaPhoremeter IV (SEPHY-CAD Instrumentations, France) is a well-designed system used for zeta potential distribution measurement by tracking the movement of the particles under an applied electric field (electrophoresis). A laser light is used for illumination to make the nanoparticles in the single horizontal plane that can be observed by the CCD camera. By measuring the electrophoretic mobility, the zeta potential of colloidal suspensions can be calculated[12–14].

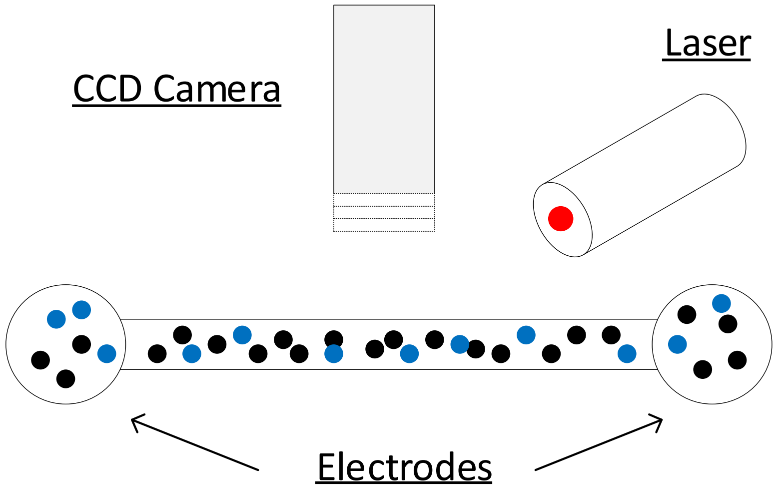

Figure 3-9 Schematic representation of Zetaphoremeter

3.2.11 Optical microscope

The optical microscope (Carl-Zeiss, Axioskop 40) equipped with 10x and 40x lenses was used for floc observation. A 3D-printed cell with two glass slides on the top and bottom was used to contain the cavitated slurry. The digital images were captured with a high speed camera linked to the optical microscope.

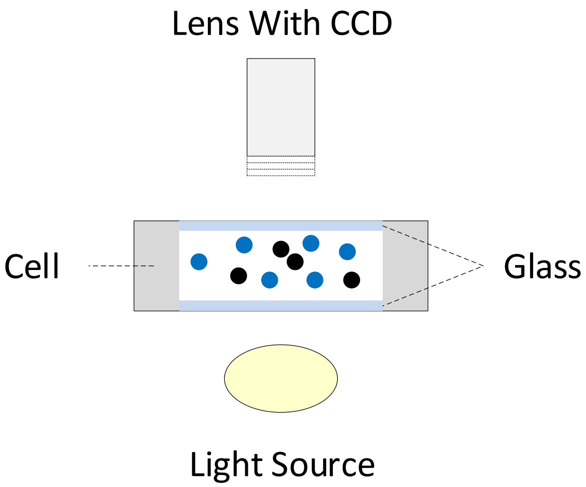

Figure 3-10 Schematic representation of flocs observation

A shutter time of 1/10000 s was used for observation with the 10X lens. When using the 40X lens, the shutter time was increased to 1/1000 s. All the samples were collected immediately after hydrodynamic cavitation.

3.2.12 Hallimond tube

An optimized Hallimond tube designed by Cao and Liu was used to simulate the flotation column in conventional mineral flotation process, which can also be used to study the recovery of mineral particles at the lab scale[15]. In micro-flotation tests, millimeter-size Nitrogen bubbles are generated by the sintered glass frit at the bottom of the tube with a constant rate of Nitrogen gas injection. A magnetic stirring bar for agitating the flotation pulp is used to prevent particle settling. The froth carried by the bubbles is able to pass through the narrow throat and enter the collection bulb. The water level should be kept at the same height as the throat during the micro-flotation test to ensure the froth is easily transported. The flotation recovery can be calculated based on the dry weight ratio of the concentrate and the tailing[1,16]. Additionally, it can minimize the effect of the water recovery to achieve a very low mechanical entrainment.

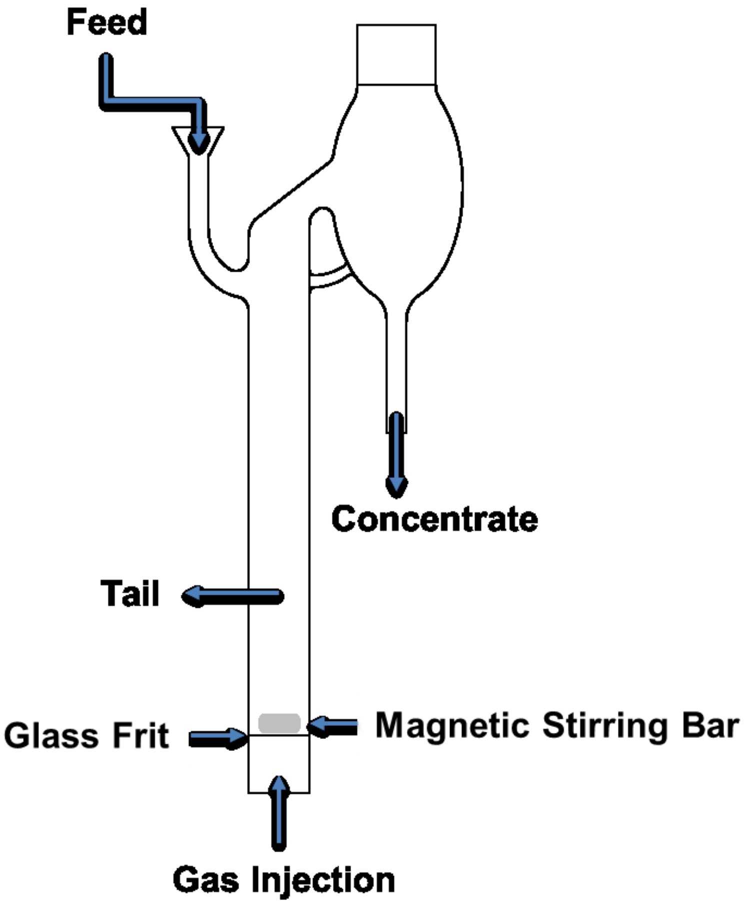

Figure 3-11 Schematic representation of the Hallimond tube

3.3 Experimental Procedures

3.3.1 Hydrodynamic cavitation

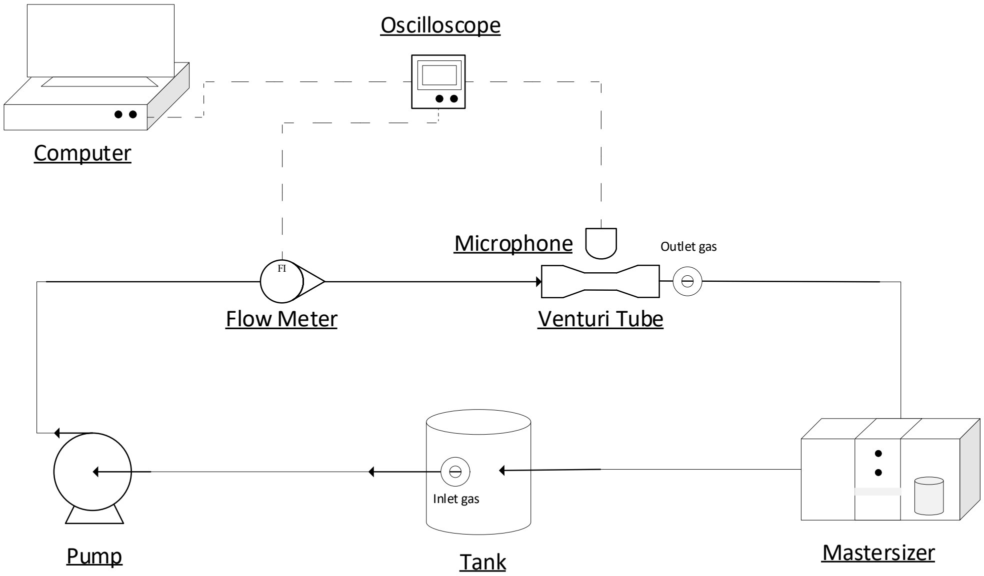

Figure 3-12 Schematic diagram of the cavitation system

All the aqueous solutions were prepared by dissolving the desired chemicals in the Milli-Q water at room temperature. Since the molybdenite particles are relatively hydrophobic and not easy to separate, the stirring plate was set at 800 rev/min and the samples were mixed for 10 min to achieve a suitable dispersion. The particle size of the solutions were measured to check if they were the same as the molybdenite particles in ethanol. This was done to make sure they would not influence the size measurement of flocs. A chosen slurry for analysis was then pumped through the circuit by a peristaltic pump (Masterflex I/P Easy-Load) which was able to provide a flow rate from 0 to 20 m/s (throat velocity)[17]. The flow rate was measured by the flow meter (Omega FLR1001). A high performance microphone was used to measure the frequency of the voice caused by the liquid surface rupture during bubble generation. All the data measured by the flowmeter and microphone was sent to the oscilloscope (Rigol DS1054Z) for analysis. The probability of the cavitation for different flow rates under different gas injection conditions was calculated based on the interaction between the voice frequency and the throat velocity. The mastersizer (Malvern Instruments Mastersizer 3000) was used to measure the particle (bubble) size distribution and analyze the change in particle (bubble) size. Air with 1 to 2 L/min was injected from inlet or outlet of the Venturi tube to investigate the effect of gas content in hydrodynamic cavitation. A concentration of 20 to 40 ppm MIBC was added to study the influence of the frother on cavitated bubble size.

In the hydrodynamic cavitation process, the formation of bubbles in the flow liquid is due to the rupture of liquid-liquid or liquid-solid surfaces. This phenomenon is usually caused by the reduction of local pressure. To study the relation between the liquid flow rate and local pressure, Bernoulli's equation is introduced below[18–20]:

$$P+\frac{1}{2}\rho V^{2}=C\left(constant\right) \tag{3.1}$$

where P is the pressure of the throat, V is the liquid throat velocity and ρ is the liquid density. Under ideal conditions, when V increases sufficiently, P will decrease to the liquid vapor pressure at the operating temperature and cavitated bubbles will form.

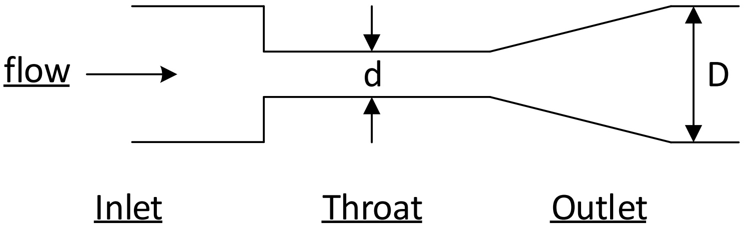

Figure 3-13 Schematic diagram of the optimized cavitation tube

The optimized cavitation tube was printed by a 3D printing system (The Formlabs Form 2) with white standard resin. Its geometry is shown in Figure 3-13. Based on the study of the Venturi tube geometry previously in our research group, the optimized Venturi tube has an inlet diameter of 9 mm, and a 10 mm long throat with a diameter of 2 mm. The inlet angle was set to 90º to decrease the minimum flow rate required for hydrodynamic cavitation. The outlet angle was set to 5º to reduce the impact of the sudden expansion on the bubbles stability.

3.3.2 Pellet preparation

The samples for XRF, contact angle and surface roughness measurements were prepared as pellets (Figure 3-14). Boric acid was used as the bottom support. The sieved fine molybdenite powders were first evenly separated by a micro rotary riffler. The vibration level was adjusted to control a proper feed rate of powders. The powders were accurately divided into eight test tubes and then mixed with boric acid powders[21]. The mixing weight ratio of molybdenite powders to boric acid powders was 1: 1. In the process of pellet preparation, 2 g of boric acid powder was first added into a 25.4 mm diameter die as the bottom layer[11]. Another 4 g of mixed sample powder was then added to fully cover the boric acid, forming the top layer. The whole material was compressed in a manual hydraulic press (Enerpac JH-5) under 40 MPa pressure within 30 s.

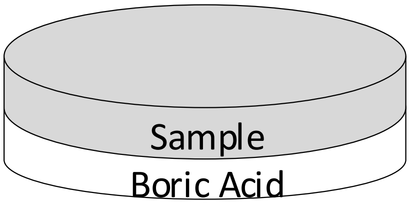

Figure 3-14 Schematic representation of the pellet

3.3.3 Contact angle measurement

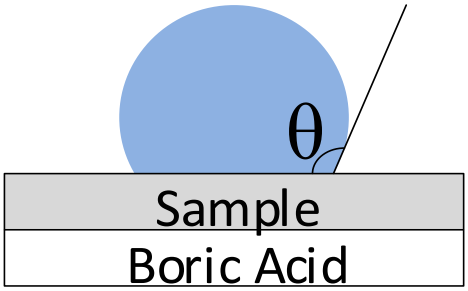

Figure 3-15 Schematic representation of contact angle measurement

Contact angle measurement was performed with a water drop on a solid surface. The relation between the contact angle and interface tensions is determined by the Young–Laplace equation. It is a well-known equation used to describe thermodynamic equilibrium between the three phases[22,23].

$$\gamma_{\mathrm{SG}} = \gamma_{\mathrm{SL}} + \gamma_{\mathrm{LG}} \cos\theta_{\mathrm{C}} \tag{3.2}$$

where γ_{SG} represents solid–gas interfacial tension, γ_{SL} represents solid–liquid interfacial tension, γ_{LG} represents liquid–gas interfacial tension, and θ_{C} is the equilibrium contact angle.

As mentioned before, the pellets for contact angle measurement were compressed with the samples and boric acid together with a mixing weight ratio of 1:1. In other words, the surface for measurement was a composite surface composed of sample and boric acid. In such a homogeneous wetting regime, the composite surfaces had varied effects on the contact angle of the liquids. This means the contact angle we measured was not the true contact angle of the samples.

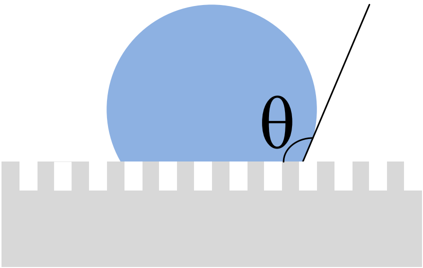

Figure 3-16 Schematic representation of Cassie–Baxter model

Therefore, the Cassie–Baxter (CB) model was introduced to solve this problem[24–27]. The apparent contact angle (θ_{CB}) is given by equation[28]:

$$\cos\theta_{CB} = f_s \cos\theta_c + f_v \cos\theta_v \tag{3.3}$$

where θ_{CB} is apparent contact angle on the textured surface, θ_c is intrinsic contact angle of a liquid droplet on the original smooth surface, θ_v is the contact angle of vapor, and f_s and f_v are the area fractions of the solid and vapor on the surface, respectively.

In this study, Eq. 3.3 can be written as follows:

$$\cos\theta_p = f_s \cos\theta_s + f_b \cos\theta_b \tag{3.4}$$

where θ_p is the apparent contact angle on the surface of pellets, θ_s is the intrinsic contact angle of the sample, θ_b is the intrinsic contact angle of boric acid, and f_s and f_b are the area fractions of the sample and boric acid on the surface, respectively.

During the contact angle measurements, a 5 μL water droplet precisely controlled by the needle was placed on the surface of the pellets and the real time video was recorded. The water drop images were analyzed by software based on the sessile drop technique. The initial contact angle was collected as soon as the water drop attached to the pellet surface. Four sampling points were examined on each pellet and two pellets were tested for each sample. Finally, the mean value of all samplings was reported.

This method only applies when the size of water drop is sufficiently large compared to the surface roughness scale, so all pellets were analyzed using an optical profilometer for surface roughness measurement to make sure they would fulfill the requirements[26].

3.3.4 Particle/bubble size measurement

The solutions for original particle size measurement were prepared by dissolving 0.5 g of sample into 50 mL ethanol and stirring with 800 rev/min for 1 min to make sure the particles disperse well.

For bubble size measurements, Milli-Q water was pumped into the cavitation system for 5 min to stabilize the bubble size. For comparison, Milli-Q water with 50 ppm MIBC was treated with same method to investigate the effect of surfactant on cavitated bubble size. All the measurements were processed during hydrodynamic cavitation.

3.3.5 Zeta potential measurement

To further investigate the interaction between bubbles and particles, SEPHY-CAD ZetaPhoremeter IV was used for zeta potential distribution measurement. This innovative approach designed by Xu and Masliyah was used to characterize the interaction potential between particles in dynamic environments[14,29]. It can measure electrophoretic mobility of particles by tracking the particles' movement in an electric field and calculating the zeta potential distribution. This technique was further developed to study bubble-particle interaction[12].

Ultrafine molybdenum disulfide powders (D90 < 15 μm) were used for the measurements. All suspensions were prepared with 10 mM KCl solutions.

During the preparation of molybdenum disulfide emulsion, 1.5 g powders were added into 750 mL of 10 mM KCl solutions, stirred at 800 rev/min for 5 min and sonicated for 1 min to ensure full particle dispersion. The pH value of the suspensions was about 4.5, measured by pH meter (Accumet CPXL20). The transparent part was collected for zeta potential distribution measurement.

To prepare the bubble suspension, 0.15 g MIBC was added to 750 mL 10 mM KCl solution, and stirred at 800 rev/min for 5 min. The pH value was adjusted with HCl and NaOH. The obtained emulsion was then cavitated for 5 min with 2 L/min of inlet air injection. The cavitated solution with stabilized microbubbles was then used for zeta potential distribution experiments.

During the zeta potential measurements, all the solutions were pumped slowly by a 20 mL syringe into the square measurement cell. Two valves at both ends were closed immediately to prevent liquid reflux, which may interfere with the particle mobility measurements. In mobility measurements, 20 to 50 particles/bubbles were tracked and analyzed using software to calculate their zeta potential values by the Smoluchowski method[30,31]. All the measurements were conducted at ambient temperature of 20 ± 0.5 °C. Each of them was repeated for five times for the same suspension/emulsion and the results were combined together to plot out their zeta potential distribution histograms[12]. In the histograms, it is possible to identify the deposition conditions of the components in a binary suspension system[14]. This method was described as follows.

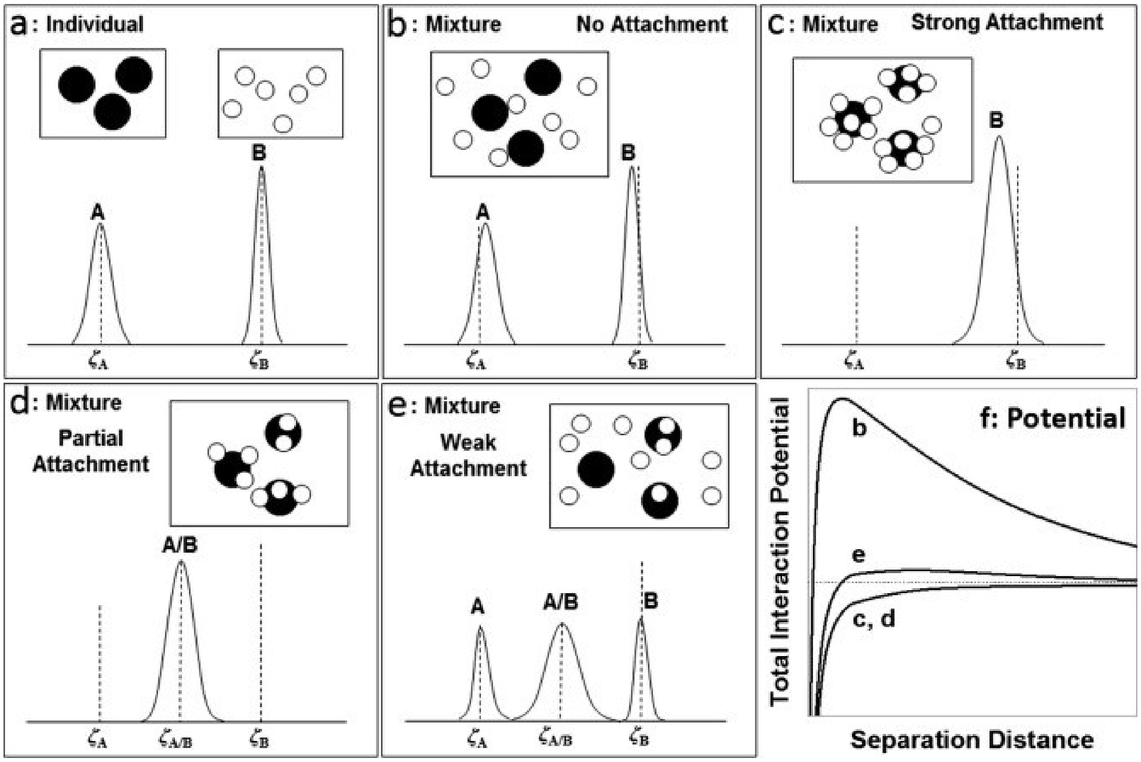

Figure 3-17 Schematic zeta potential distributions for a binary particulate component system[12]

Figure 3-17 shows the possible phenomenon for particle attachment in a binary suspension system based on zeta potential distribution measurement. Figure 3-17a shows us the zeta potential distributions of two different particles (or bubbles), where each of them has a unique peak. This overlaid figure is just for illustrative purposes and would not be shown in reality. Figure 3-17b describes a possible phenomenon whereby components A and B are mixed together without any attachment. Their zeta potential distribution will still show two distinct peaks which are a little bit closer together; this is known as electrophoretic retardation. When the external electric field is applied in the measurement of particle mobility, the hydrodynamic interactions of moving particles tend to bring them closer tougher, which shows a slight shift of ζ_A and ζ_B toward each other. In the case that A and B strongly attach together, the individual distribution peaks of two components merge together to form a new individual distribution peak. If A is completely covered by B as shown in Figure 3-17c, the quantity of B should be much more than A, which makes the new distribution peak tend to B but not very closely. As for another case shown in Figure 3-17d, if A is partially covered by B, the new zeta potential distribution peak will tend to either A or B, depending on the ratio of these two components. Respectively, this phenomenon is mainly caused by the insufficient quantity of one component which has the ability to fully cover the other one. However, for a weak attachment between two components, two or three distribution peaks are likely to be observed as in Figure 3-17e. The position of the new distribution peak will mainly be affected by the strength of attraction between the two components and their ratio.

3.3.6 Micro-flotation test

To investigate the influence of hydrodynamic cavitation in fine particle flotation, a modified Hallimond tube was used for micro-flotation test. As mentioned before, it can simulate the mineral flotation process in the industry.

In this study, 1 g of mineral particles were mixed with 150 mL Milli-Q water in a typical micro-flotation test[1,32]. Specifically, fine molybdenite slurry with 10 g/L concentration in natural pH was used in the hydrodynamic cavitation treatment at different conditions. The slurry was then used to conduct the micro-flotation test. Milli-Q water was used to fill the collection bulb to keep a constant water level. The slurry was floated with high purity nitrogen at a flow rate of 30 SCCM (standard cubic centimeters per minute). Two kinds of flotation tests were carried out, in which one was a single recovery after 5 min of flotation, and another was a kinetic cumulative recovery within 10 min of flotation. The agitation speed of a magnetic bar was controlled at 550 rev/min. In floc durability tests, the slurry after the hydrodynamic cavitation was floated after waiting for 0, 20, 40 and 60 min. As for floc stability measurements, the cavitated slurry was tested after 30 s of stirring treatment at 300 rev/min and 600 rev/min. The experiments with each condition were repeated for a total of 3 times and the average flotation recoveries were presented.

The recovery of molybdenite/silica was calculated with the dry weights of the feed and concentrate as below:

$$R = \frac{m_{conc}}{m_{feed}} = \frac{m_{conc}}{m_{conc} + m_{tail}} \times 100\% \tag{3.5}$$

where R is the flotation recovery, m_{feed} is the weight of feed, m_{conc} is the weight of concentrate, m_{tail} is the weight of the tailing.

In selectivity tests of the molybdenite and silica mixture, the grade of molybdenite is calculated with the formula below:

$$G = \frac{m_{conc,metal}}{m_{conc,ore}} \times 100\% \tag{3.6}$$

where G is the grade of the valuable part in ore, $m_{conc,metal}$ is the weight of valuable part in concentrate, and $m_{conc,ore}$ is the weight of concentrate.

A classical first-order flotation model is used in this study to demonstrate the calculation of the proposed modified rate constant and ultimate recovery[33,34]:

$$R = R_{\infty} \times \left(1 - e^{-k(t+\phi)}\right) \tag{3.7}$$

where R is the recovery at time t, R_{∞} is the ultimate recovery, k is the first-order rate constant, and ϕ is the time correction factor.

3.3.7 Flotation column test

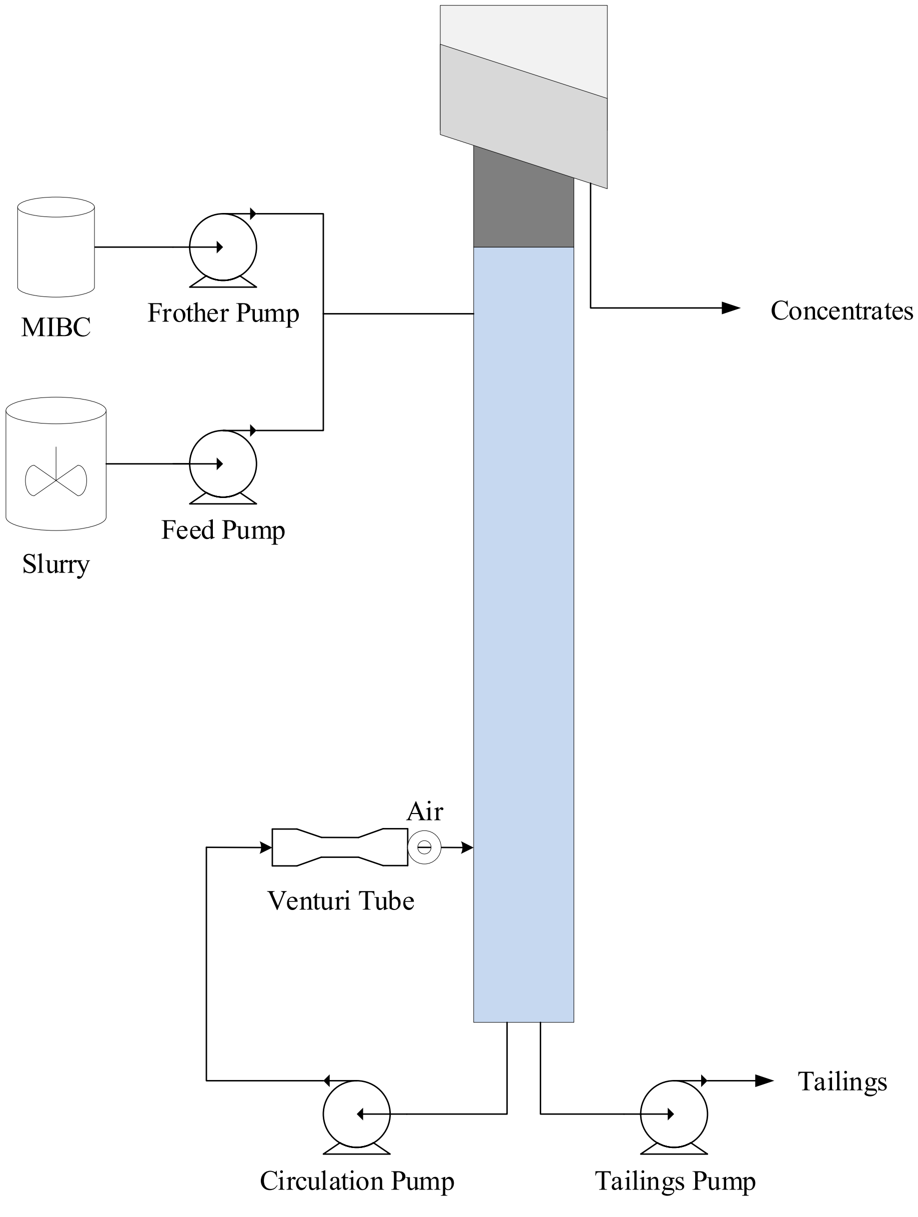

Figure 3-18 Schematic diagram of the flotation column system

To study the influence of hydrodynamic cavitation in real mineral flotation, an optimized flotation column was used for gold flotation tests. Figure 3-18 shows the illustration of the flotation column system.

Table 3-3 Head assay of samples

Sample	TCM	Au	S
	(%)	(g/ton)	(%)
GWK1 (commercial sparger)	0.43	3.14	2.45
GWK2 (U of A sparger)	0.47	3.02	2.3
GWK1 & GWK2 average	0.45	3.08	2.38

The sample was a kind of gold ore. The contents in head assay of sample were shown in Table 3-3. It was considered as double refractory because of sulfides and high carbonaceous matter content in it. The sample was first ground to P80 of about 75 μm by using a pilot rod mill. The Mastersizer 2000 was used to quickly measure the particle size distribution. During the grinding process, the commercial collector (250 g/ton) was added, sodium silicate (1050.3 g/ton) was also added to prevent quartz in ore from floating during flotation process. After grounding, the sample was mixed with water to make a 50 L slurry with 20 wt% solid. The frother (5 g/ton) was added at the same time. An overhead agitator with 400 rev/min rotation speed was used for mixing the slurry.

The slurry was then pumped into the flotation column. The diluted MIBC was also pumped into the column at the same time with a fixed rate related to slurry feed rate. The circulation system would start after the whole column was filled with 4.8 L slurry. The Venturi tube with optimized geometry was set in the circulation system. The throat velocity was set at 15 m/s to keep a strong cavitation condition. Air injection with 6 SLPM (standard liter per minute) flow rate was used during cavitation. Another commercial sparger was used as a comparison. The tailing pump was controlled by the sensor of the column to keep a stable water level in the column.

In the tests, three different conditions of feed rate were studied with two spargers. The specific parameters were shown in Table 3-4.

Table 3-4 Operational paprameters for the tests

Sparger	**Feed rate**	**Residence time**	**Stabilization time**	**Sampling Time**
	(mL/min)	**(min)**	**(min)**	**(min)**
Commercial sparger	480	10	25	10
	960	5	7	6
	1600	3	3	4
U of A sparger	480	10	10	10
	960	5	6	5
	1600	3	3	3

3.4 Reference

(1) Qiu, Z.; Liu, G.; Liu, Q.; Zhong, H. Understanding the Roles of High Salinity in Inhibiting the Molybdenite Flotation. *Colloids Surfaces A Physicochem. Eng. Asp.* **2016**, *509*, 123–129.

(2) Reyes-Bozo, L.; Escudey, M.; Vyhmeister, E.; Higueras, P.; Godoy-Faúndez, A.; Salazar, J. L.; Valdés-González, H.; Wolf-Sepúlveda, G.; Herrera-Urbina, R. Adsorption of Biosolids and Their Main Components on Chalcopyrite, Molybdenite and Pyrite: Zeta Potential and FTIR Spectroscopy Studies. *Miner. Eng.* **2015**, *78*, 128–135.

(3) Zhang, H.; Lu, S. B.; Zheng, J.; Du, J.; Wen, S. C.; Tang, D. Y.; Loh, K. P. Molybdenum Disulfide (MoS_2) as a Broadband Saturable Absorber for Ultra-Fast Photonics. *Opt. Express*. **2014**, *22* (6), 7249–7260.

(4) Tian, Y.; He, Y.; Zhu, Y. Low Temperature Synthesis and Characterization of Molybdenum Disulfide Nanotubes and Nanorods. *Mater. Chem. Phys.* **2004**, *87* (1), 87–90.

(5) Du, G.; Guo, Z.; Wang, S.; Zeng, R.; Chen, Z.; Liu, H. Superior Stability and High Capacity of Restacked Molybdenum Disulfide as Anode Material for Lithium Ion Batteries. *Chem. Commun.* **2010**, *46* (7), 1106–1108.

(6) Feng, C.; Ma, J.; Li, H.; Zeng, R.; Guo, Z.; Liu, H. Synthesis of Molybdenum Disulfide (MoS2) for Lithium Ion Battery Applications. *Mater. Res. Bull.* **2009**, *44* (9), 1811–1815.

(7) Hou, Z.; Yokota, O.; Tanaka, T.; Yashima, T. Characterization of Ca-Promoted Ni/α-Al2O3catalyst for CH4reforming with CO2. *Appl. Catal. A Gen.* **2003**, *253* (2), 381–387.

(8) Calvero. X-ray fluorescence https://en.wikipedia.org/wiki/X-ray_fluorescence (accessed Sep 26, 2018).

(9) Hydrargyrum. X-ray crystallography https://en.wikipedia.org/wiki/X-ray_crystallography (accessed Sep 26, 2018).

(10) Laurin, M. Principle of X-ray photoelectron spectroscopy (XPS) | TikZ example http://www.texample.net/tikz/examples/principle-of-x-ray-photoelectron-

spectroscopy-xps/ (accessed Sep 26, 2018).

(11) Dang-Vu, T.; Jha, R.; Wu, S. Y.; Tannant, D. D.; Masliyah, J.; Xu, Z. Wettability Determination of Solids Isolated from Oil Sands. *Colloids Surfaces A Physicochem. Eng. Asp.* **2009**, *337* (1–3), 80–90.

(12) Wu, C.; Wang, L.; Harbottle, D.; Masliyah, J.; Xu, Z. Studying Bubble-Particle Interactions by Zeta Potential Distribution Analysis. *J. Colloid Interface Sci.* **2015**, *449*, 399–408.

(13) Zhao, H.; Long, J.; Masliyah, J. H.; Xu, Z. Effect of Divalent Cations and Surfactants on Silica-Bitumen Interactions. *Ind. Eng. Chem. Res.* **2006**, *45* (22), 7482–7490.

(14) Liu, J.; Zhou, Z.; Xu, Z.; Masliyah, J. Bitumen-Clay Interactions in Aqueous Media Studied by Zeta Potential Distribution Measurement. *J. Colloid Interface Sci.* **2002**, *252* (2), 409–418.

(15) Cao, M.; Liu, Q. Reexamining the Functions of Zinc Sulfate as a Selective Depressant in Differential Sulfide Flotation-The Role of Coagulation. *J. Colloid Interface Sci.* **2006**, *301* (2), 523–531.

(16) Qiu, Z.; Liu, G.; Liu, Q.; Zhong, H.; Zhang, M. Separation of Pyrite from Chalcopyrite and Molybdenite by Using Selective Collector of N-Isopropoxypropyl-N’-ethoxycarbonyl Thiourea in High Salinity Water. *Miner. Eng.* **2017**, *100*, 93–98.

(17) Li, M. Influence of Venturi Tube Geometry and Particle Properties on the

Hydrodynamic Cavitation for Fine Particle Flotation. Master's thesis, University of Alberta, **2017**.

(18) Kumar, P. S.; Pandit, A. B. Modeling Hydrodynamic Cavitation. *Chem. Eng. Technol.* **1999**, *22* (12), 1017–1027.

(19) He, L.; Ruiz, F. Effect of Cavitation on Flow and Turbulence in Plain Orifices for High-Speed Atomization. *Atomization and Sprays*. **1995**, pp 569–584.

(20) Kinnas, S. A.; Fine, N. E. A Numerical Non-Linear Analysis of the Fow around Two and Three Dimensional Partially Cavitating Hydrofoils. *J. Fluid Mech.* **1993**, *254*, 151–181.

(21) Parus, J.; Kierzek, J.; Mało, B. Determination of the Carbon Content in Coal and Ash by XRF. *X-Ray Spectrom.* **2000**, *29* (November 1999), 192–195.

(22) Kwok, D. Y.; Neumann, a. W. *Contact Angle Measurement and Contact Angle Interpretation*. **1999**; *81(3)*, 167–249.

(23) Zhao, T.; Jiang, L. Contact Angle Measurement of Natural Materials. *Colloids Surfaces B Biointerfaces.* **2018**, *161*, 324–330.

(24) Murakami, D.; Jinnai, H.; Takahara, A. Wetting Transition from the Cassie-Baxter State to the Wenzel State on Textured Polymer Surfaces. *Langmuir.* **2014**, *30* (8), 2061–2067.

(25) Choi, W.; Tuteja, A.; Mabry, J. M.; Cohen, R. E.; McKinley, G. H. A Modified Cassie-Baxter Relationship to Explain Contact Angle Hysteresis and Anisotropy on Non-Wetting Textured Surfaces. *J. Colloid Interface Sci.* **2009**, *339* (1), 208–216.

(26) Marmur, A. Wetting on Hydrophobic Rough Surfaces: To Be Heterogeneous or Not to Be? *Langmuir.* **2003**, *19* (20), 8343–8348.

(27) Giacomello, A.; Meloni, S.; Chinappi, M.; Casciola, C. M. Cassie-Baxter and Wenzel States on a Nanostructured Surface: Phase Diagram, Metastabilities, and Transition Mechanism by Atomistic Free Energy Calculations. *Langmuir.* **2012**, *28* (29), 10764–10772.

(28) Cassie, B. Y. A. B. D.; Baxter, S. Wettability of Porous Surfaces. *Physics (College. Park. Md).* **1944**, No. 5, 546–551.

(29) Liu, J.; Xu, Z.; Masliyah, J. Studies on Bitumen-Silica Interaction in Aqueous Solutions by Atomic Force Microscopy. *Langmuir.* **2003**, *19* (9), 3911–3920.

(30) Delgado, A, Gonzalez-Caballero, F, Bruque, J. On the Zeta Potential and Surface Charge Density of Montmorillonite in Aqueous Electrolyte Solutions. *J. Colloid Interface Sci.* **1986**, *113* (1), 203–211.

(31) Sze, A.; Erickson, D.; Ren, L.; Li, D. Zeta-Potential Measurement Using the Smoluchowski Equation and the Slope of the Current-Time Relationship in Electroosmotic Flow. *J. Colloid Interface Sci.* **2003**, *261* (2), 402–410.

(32) Zhang, M. Investigation of Chalcopyrite and Pyrite Flotation in High Salinity Water. Master's thesis, University of Alberta, **2015**.

(33) Xu, M. Modified Flotation Rate Constant and Selectivity Index. *Miner. Eng.* **1998**, *11* (3), 271–278.

(34) Uçurum, M. Influences of Jameson Flotation Operation Variables on the Kinetics

and Recovery of Unburned Carbon. *Powder Technol.* **2009**, *191* (3), 240–246.

Chapter 4 Flocs Formation by Hydrodynamic Cavitation

4.1 Surface Roughness

The surface roughness of pellets was measured to demonstrate the feasibility of the proposed method for contact angle measurements. The results obtained by optical profilometer are shown in Table 4-1.

Table 4-1 Roughness parameters of pellet surfaces

Surface	R_a	R_q	R_t
	(μm)	**(μm)**	**(μm)**
Boric acid	0.45	0.579	3.457
Boric acid and molybdenite	1.275	1.734	9.886
Boric acid and silica	1.517	1.906	7.525

R_a is the arithmetical mean deviation, which expresses the arithmetical mean of the absolute values of Z(x) in a sampling length. R_q is the root mean square deviation, expressing the root mean square of Z(x) in a sampling length. R_t is the maximum peak-to-valley height, an absolute value between the highest and lowest peaks.

In order to get an accurate apparent contact angle of the pellets, the water drop should be significantly large enough compared to the surface roughness. The volume of each water drop is about 5.00 ± 0.05 μm. The maximum diameter of the droplet is about 2285.39 μm according to the calculation, which is about three orders of magnitude larger than the maximum peak-to-valley height (R_t). In other words, the ratio between the diameter of water droplet and surface roughness parameters is sufficiently large for the sessile drop method[1,2]. This approach demonstrated the credibility of the pellets in contact angle measurements.

4.2 Contact Angle Measurement

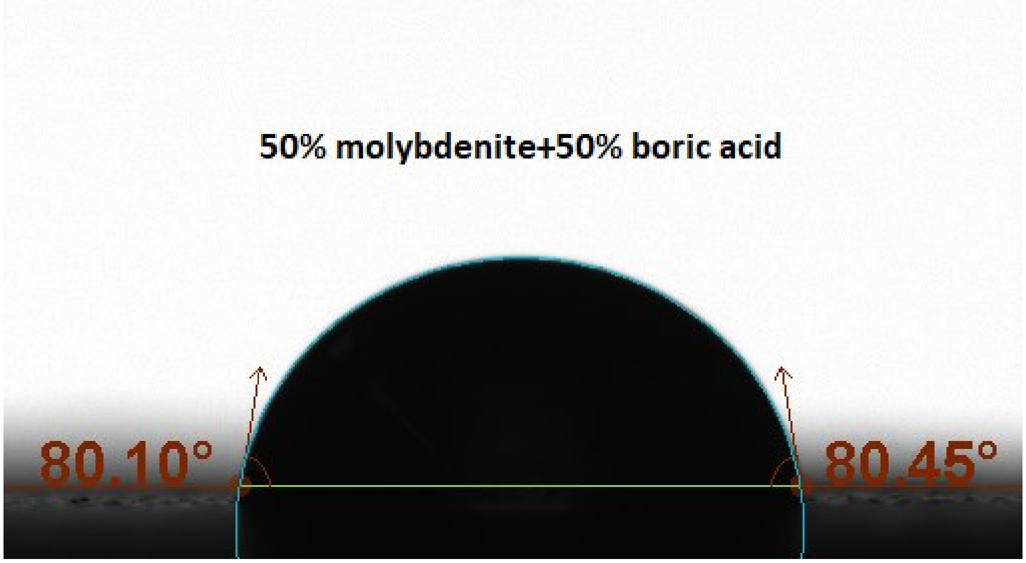

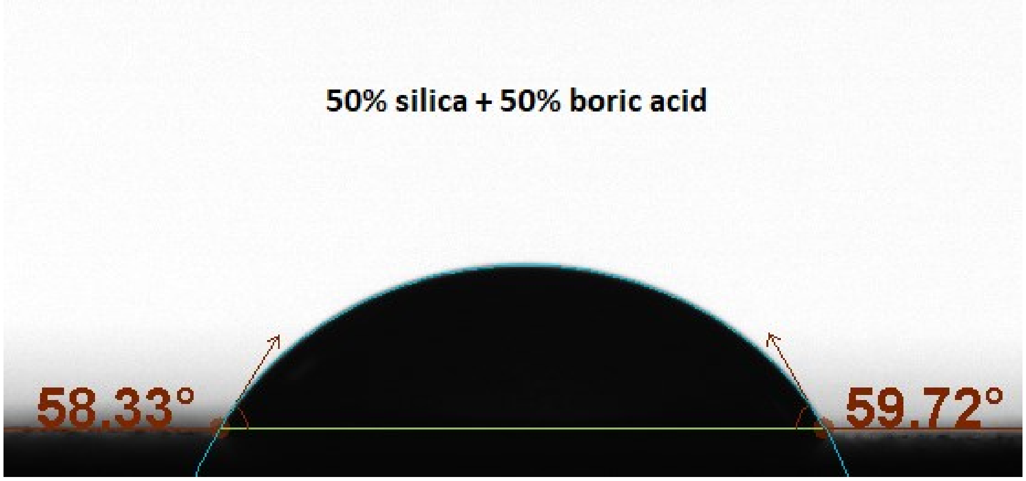

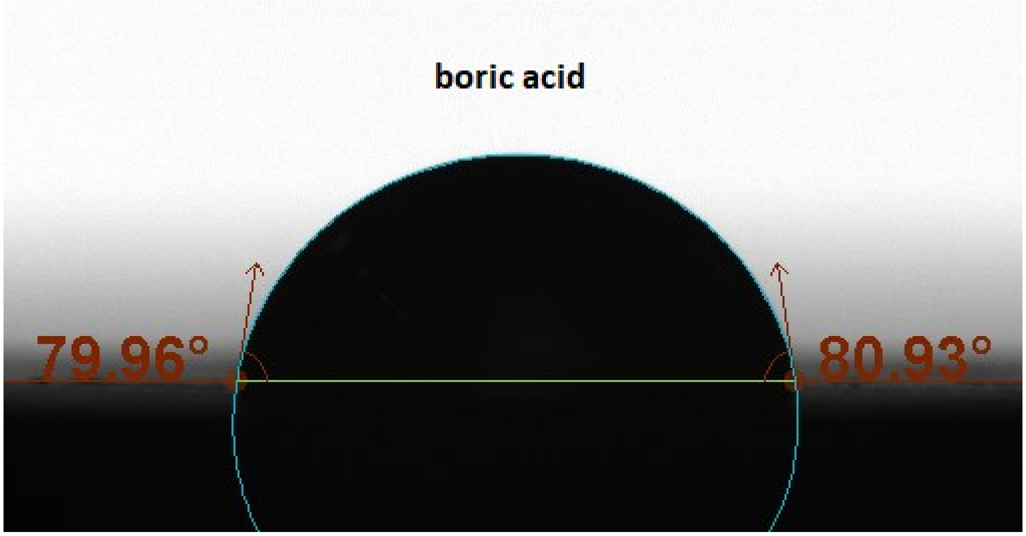

Figure 4-1 Apparent contact angle of the pellets

Table 4-2 Apparent contact angle of pellets, θ_{ap}, apparent contact angle of boric acid, θ_b, and intrinsic contact angle of the sample, θ_c

Sample	θ_{ap} (°)	θ_b (°)	θ_c (°)
Molybdenite	78.074	79.704	74.267
Silica	60.257	79.704	38.861

The initial contact angle of water drop on the surface of pellets images are shown in Figure 4-1. The results with the intrinsic contact angle of molybdenite and silica calculated based on the Cassie–Baxter model are shown in Table 4-2. The contact angle of molybdenite is 74.267°, while silica has a contact angle of just 38.861°. These results indicate that molybdenite is much more hydrophobic than silica. They also display the natural flotability of molybdenite, which is good for pure mineral flotation investigations without the addition of any collector or frother.

4.3 Cavitation Probability Measurement

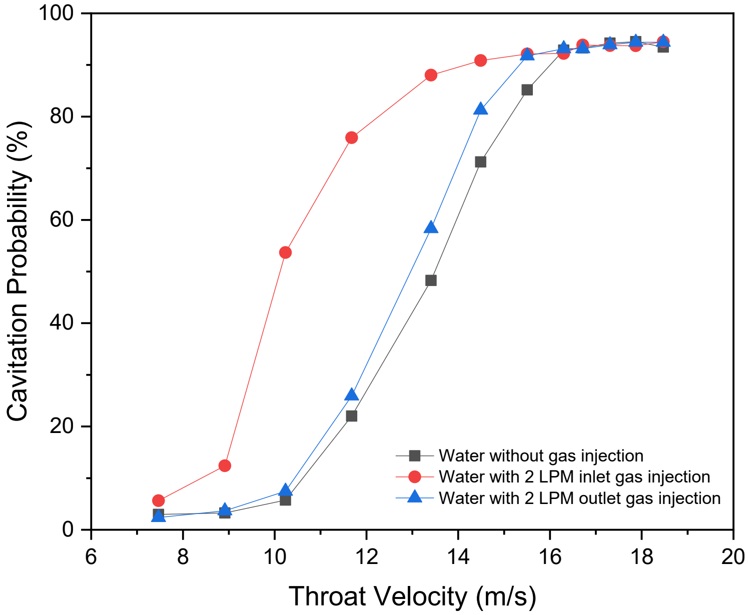

Figure 4-2 Cavitation probability vs. throat velocity with and without gas injection

Figure 4-2 shows the relation of cavitation probability in terms of throat velocity. The cavitation probability is a value which shows the probability of cavitation instead of the intensity of cavitation. It was calculated by the time that throat pressure lower than the vapor pressure based on the voice frequency collected from microphone. When hydrodynamic cavitation happens, bubbles in the liquids break, causing a very high frequency voice. The velocity of liquids showed in Figure 4-2 was calculated based on the liquids flow rate in the pipe and the ratio of the tube to pipe diameter. When liquid passes through a nozzle, its velocity significantly increases. In the condition without gas injection, the cavitation probability was very low initially, which meant that no cavitation had occurred yet. As the throat velocity increased to 14 m/s in our system, a sharp increase in cavitation probability of 48% was achieved. In other words, the local pressure at that speed partially decreased below vapor pressure. As the throat velocity increased to 16 m/s or higher, the cavitation probability reached 90% and became much more stable. In the presence of gas injection, the minimum throat velocity for hydrodynamic cavitation decreased, which indicated that the undissolved gas bubbles in water significantly decreased the threshold of hydrodynamic cavitation[3]. In addition, the dissolved gas in water results in the inception of cavitation at pressures much higher than the vapor pressure. Further, the existence of gas nuclei acts as a weak spot in water, making it easier to generate bubbles at a higher local pressure with a lower pressure drop needed and less energy consumed[4]. The ideal throat velocity has been investigated, but the quantity of bubbles generated in different flow rates remains unclear. Therefore, the turbidity of water after cavitation was studied to measure the concentration of cavitated bubbles in water.

4.4 Turbidity Measurement

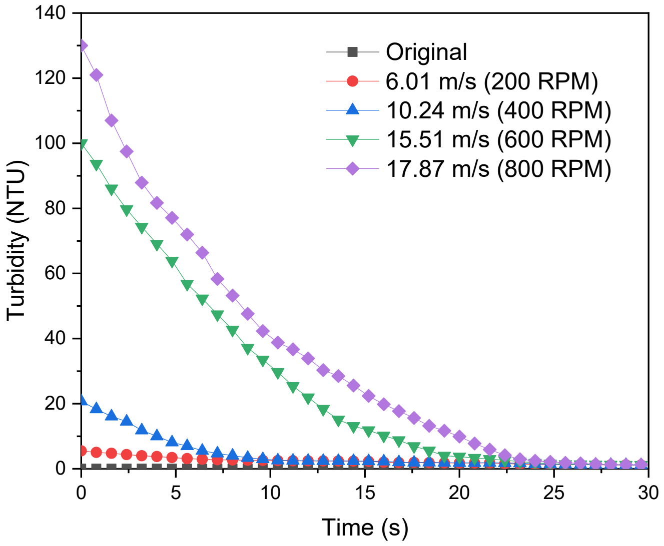

Figure 4-3 Turbidity values of cavitated bubbles as a function of time in different throat velocity

Many researchers have used turbidity measurement to describe the effect of hydrodynamic cavitation$^{5–9}$. Figure 4-3 shows the turbidity of cavitated water in different throat velocity. The cavitated water with a higher throat velocity has a higher initial turbidity. This increase indicates a higher concentration of bubbles in water. The throat velocity at 6.01 m/s does not reach the minimum rate needed for cavitation, so its turbidity is almost the same as pure water. In addition, turbidity increases as the throat velocity increases, indicating that much more cavitation bubbles are generated due to the higher cavitation intensity.

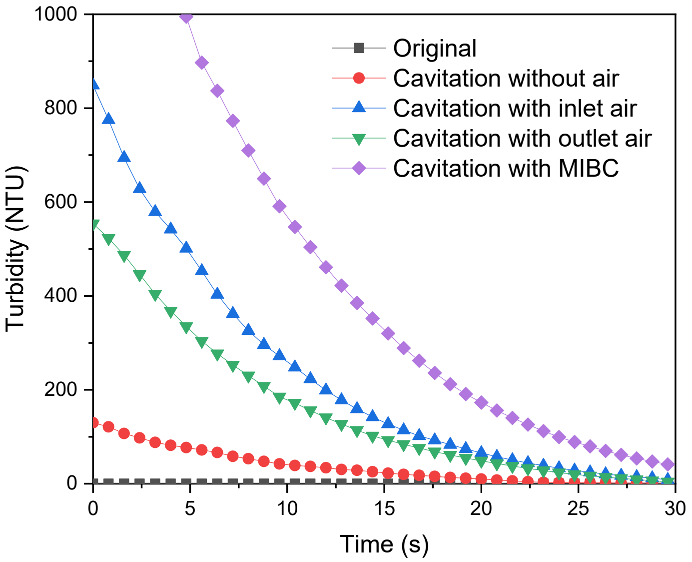

Figure 4-4 Turbidity values of cavitated bubbles as a function of time in different cavitation conditions

Figure 4-4 describes the influence of gas content and surfactant on bubble generation by hydrodynamic cavitation. The hydrodynamic cavitation with air injection showes a much higher initial turbidity as compared to the one without gas injection. This indicates that the existence of gas nuclei is beneficial to hydrodynamic since a lower energy barrier needed to be overcome for microbubbles generation; this is consistent with the cavitation probability results mentioned previously. Since the solubility of air in water is proportional to the pressure, the air is easily separated and formed microbubbles[10,11]. As well, the highest turbidity is achieved by hydrodynamic cavitation with MIBC. Its initial value is even larger the limit of 1000 NTU. This is because MIBC frother, as a kind of surfactant, can deter bubbles from coalescing and increase their stability by forming a film on their surfaces.

This method is also used in zeta potential distribution measurements to get sufficiently tiny and stable bubbles.

4.5 Particle/Bubble Size Measurement

The particle size of the samples is shown in Figure 4-5. In the description of particle size distribution, D-Values (D10, D50 & D90) are the most commonly used, which are the intercepts for 10%, 50% and 90% of the cumulative mass.

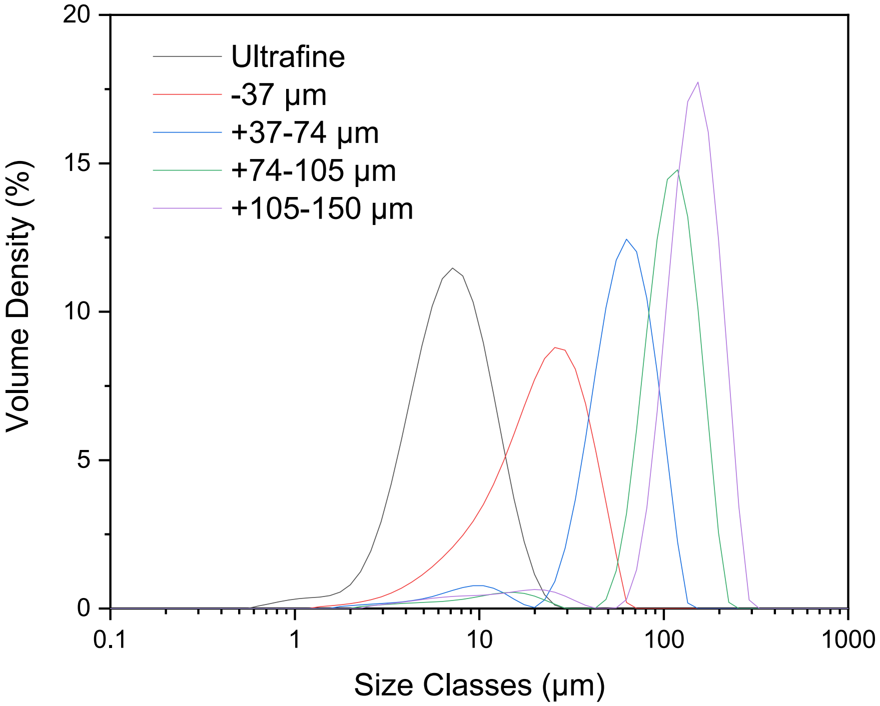

Figure 4-5 Volume based particle size distribution of the sieved molybdenite concentrate and ultrafine molybdenum disulfide powder

From Figure 4-5, it is very clear that ethanol works well to disperse molybdenite particles since the all the distributions are very clear and identical. These curves were used as original data for later tests and analysis.

Table 4-3 Particle size distribution of the sieved molybdenite concentrate and ultrafine molybdenum disulfide powder

Sample	**Dx (10) (µm)**	**Dx (50) (µm)**	**Dx (90) (µm)**
Ultrafine	3.36	6.95	13.2
< 37 µm	7.75	21.8	40.9
37 - 74 µm	30.8	59.2	93.9
74 - 105 µm	69.7	106	158
105 - 150 µm	82.6	142	209

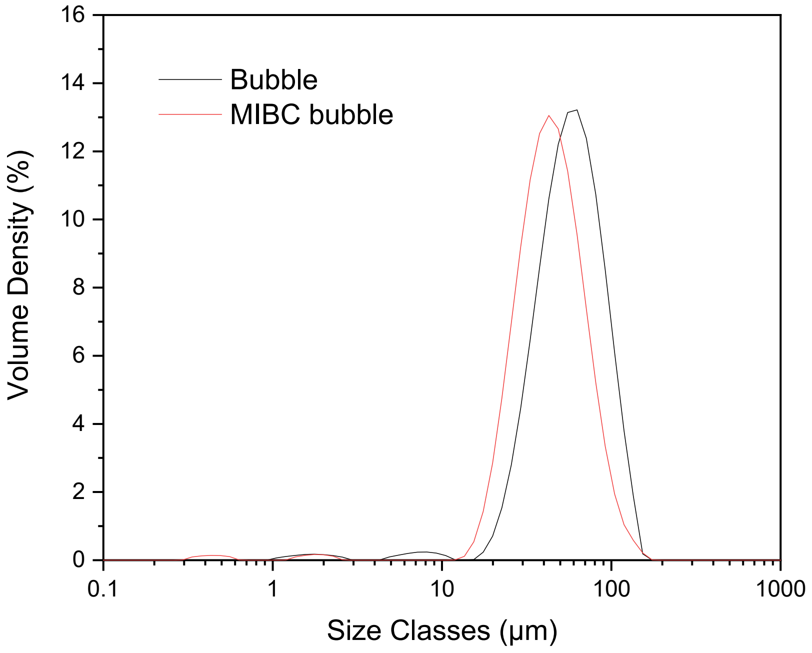

Figure 4-6 Volume based particle size distribution of caivtated bubbles with and without MIBC

Table 4-4 Particle size distribution of cavitated bubbles with and without MIBC

Sample	Dx (10) (µm)	Dx (50) (µm)	Dx (90) (µm)
Bubble	31.1	57.1	97.8
Bubble with MIBC	24.8	43.4	81.1

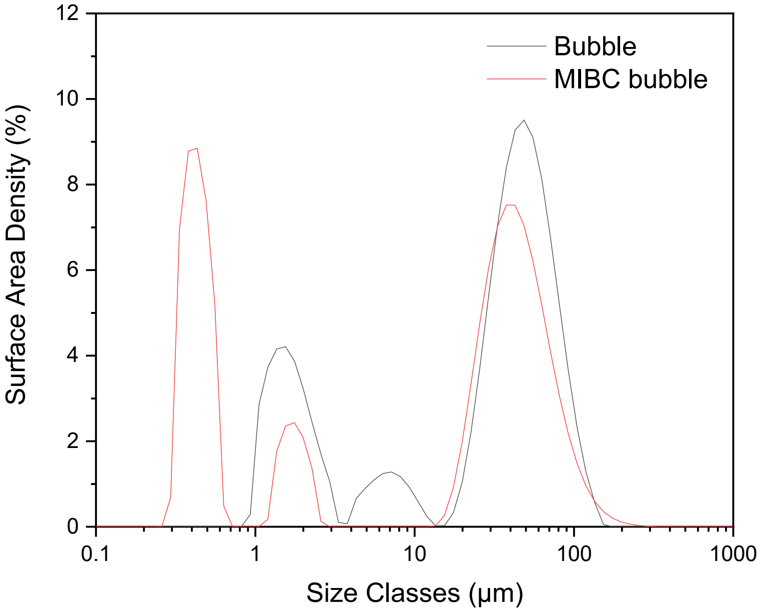

Figure 4-7 Surface area based particle size distribution of caivtated bubbles with and without MIBC

Table 4-5 Particle size distribution of caivtated bubbles with and without MIBC

Sample	**Dx (10)**	**Dx (50)**	**Dx (90)**
	(μm)	**(μm)**	**(μm)**
Bubble	1.05	1.34	2.07
Bubble with MIBC	0.327	0.393	0.519

The bubbles were generated by hydrodynamic cavitation with the Venturi tube. Figure 4-6 and Figure 4-7 show the size distribution of cavitated bubbles measured at 10 min after the final generation from air naturally dissolved in water. The results based on the volume of bubbles emphasize the lager part, while the surface area based results focus on the smaller size range. Each distribution curve consists of three individual peaks in the nano and micron size. The size of cavitated nanobubbles is smaller than 1 μm, which is expected as the ideal size for fine particle flotation. The size of cavitated bubbles with MIBC is much smaller than original shown in Figure 4-7. In Table 4-5, the Dx (50) of normal cavitated bubbles is 1.34 μm. As for the bubbles with MIBC, it decreases to 0.393 μm. This is because MIBC significantly reduces the surface tension of bubbles. The bubbles with MIBC were only used for zeta potential measurement since tiny bubbles were easily captured by CCD camera.

4.6 Floc Size Measurement

We have discussed the quantity of bubbles generated with hydrodynamic cavitation under different conditions in the turbidity measurement. In order to further understand the effect of cavitated microbubbles in fine particle flotation, particle size after hydrodynamic cavitation was measured. This can also be representative of the extent of floc formation. In floc size measurements, Dx (90) is used to describe the real-time particle size during hydrodynamic cavitation. Particle size may change as the cavitation time increases, indicating the status of floc formation in hydrodynamic cavitation process.

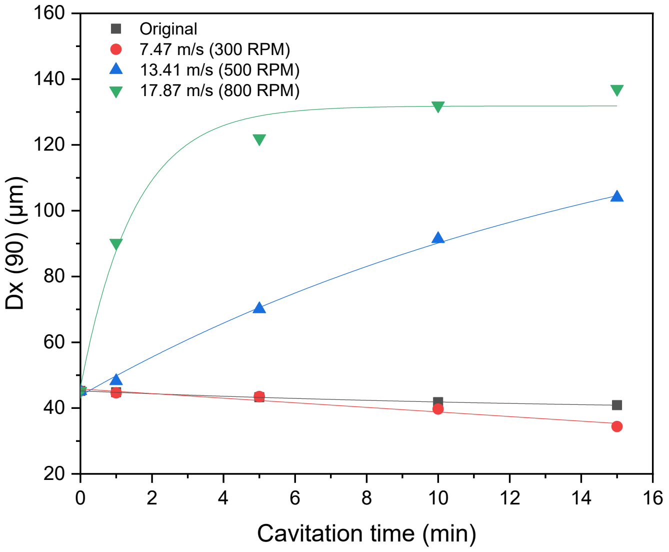

Figure 4-8 Particle size change as a function of time in different throat velocity

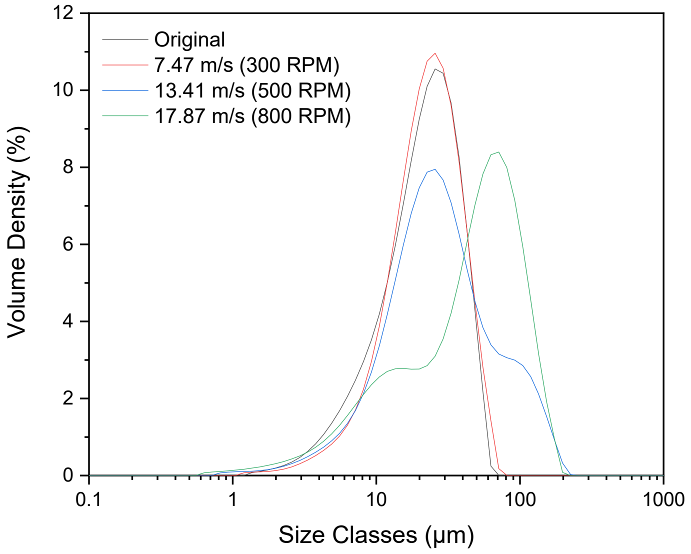

Figure 4-9 Comparison of particle size after 10 min cavitation in different throat velocity

Figure 4-8 and Figure 4-9 show the particle size data as a function of cavitation time at different throat velocity values. At a lower throat velocity where the cavitation did not occur, the particle size curve showed a decreasing trend, which means the Venturi tube acted as a disperser instead of an enabler hydrodynamic cavitation. As the throat velocity reaches 13.41 m/s above the minimum, there was a significant increase of particle size which increased to 103 μm after being treated for 15 min. As the throat velocity further increased, a huge increase of particle size from 42 μm to 121 μm was observed within a 5 min hydrodynamic cavitation, indicating a high cavitation intensity at 17.87 m/s. Based on the turbidity results, the quantity of the microbubbles generated in weak hydrodynamic cavitation was still much lower than during full hydrodynamic cavitation conditions, which could not provide sufficient bubbles in the process of bubble and particle collision and attachment. As a result, the rate of floc generation under weak cavitation conditions was much slower than under full cavitation conditions.

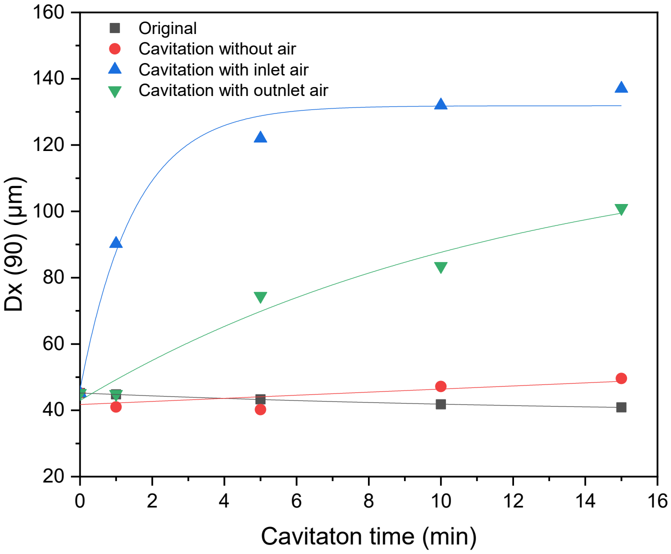

Figure 4-10 Particle size change as a function of time in different air injection conditions

Figure 4-10 showed the rate of floc formation at different air injection conditions. The rate of floc formation was much slower in cavitation without air injection as compared to the other two conditions, which illustrated that the microbubbles generated in this condition were not enough for fine particles to aggregate. With outlet air injection, floc formation became much quicker, because dissolved gas content could provide enough gas nuclei for the microbubble generation process in hydrodynamic cavitation. Furthermore, the normal air bubbles injected from inlet would be easily crushed into microbubbles by hydrodynamic cavitation. This result was consistent with the turbidity result mentioned above.

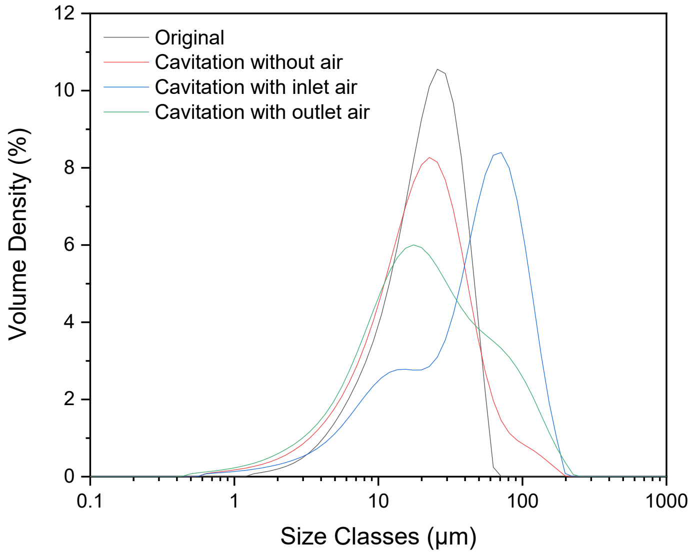

Figure 4-11 Comparison of particle size after 10 min cavitation in different air injection conditions

In Figure 4-11, the particle size distribution after cavitation shifts to the right, which means the cavitation did have an effect with a larger floc formation. After air injection, the particle size distribution changed quite a lot, especially for the inlet air injection condition. A new peak is generated, which means that a larger number of bigger flocs were formed. Also, with the same air injection rate, the floc generated with inlet air injection seems much more efficient. The results indicated that the flocs were mainly formed in the tube portion, which created many microbubbles by cavitation. At the same region, high shear forces could provide enough energy to overcome the energy barrier of collision, which could make microbubbles and particles with the same surface charge easily attach. In comparison, with the same air injection rate, the air injected from inlet showed a much higher efficiency. The air bubbles growing at the throat of the Venturi tube under the negative pressure might easily break into tiny bubbles, which greatly increased the number of cavitated microbubbles as shown in Figure 4-4. As a result, a large number of microbubbles significantly enhanced the efficiency of floc formation.

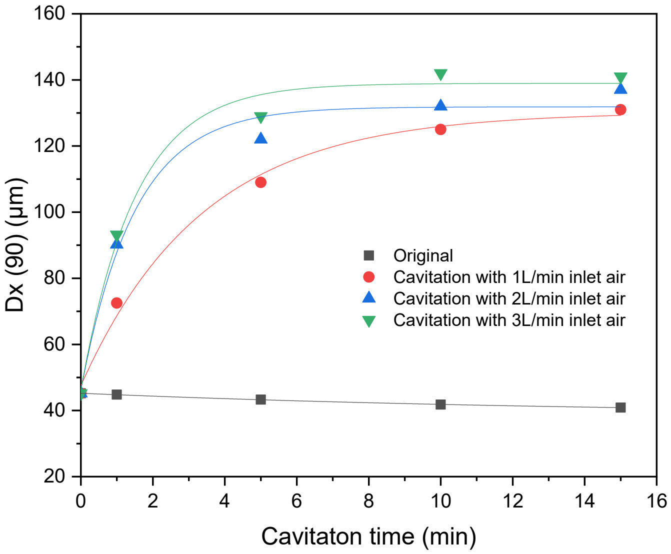

Figure 4-12 Particle size change as a function of time in different air injection rate

As illustrated before, the air injection from inlet was beneficial to bubble generation and floc formation[12]. To deeply investigate the effect of air injection rate in hydrodynamic cavitation, three different rates of air injection were chosen in this measurement. In Figure 4-12, some differences in different air injection rates could still be observed within 5 or 10 min of hydrodynamic cavitation, but as the rate increased even higher, the curve seemed very similar as the floc sizes all exist in the range of 120 μm and 140 μm. In other words, the rate of floc formation reached the maximum value at 2 L/min of air injection rate after 10 min of cavitation.

4.7 Flocs Images

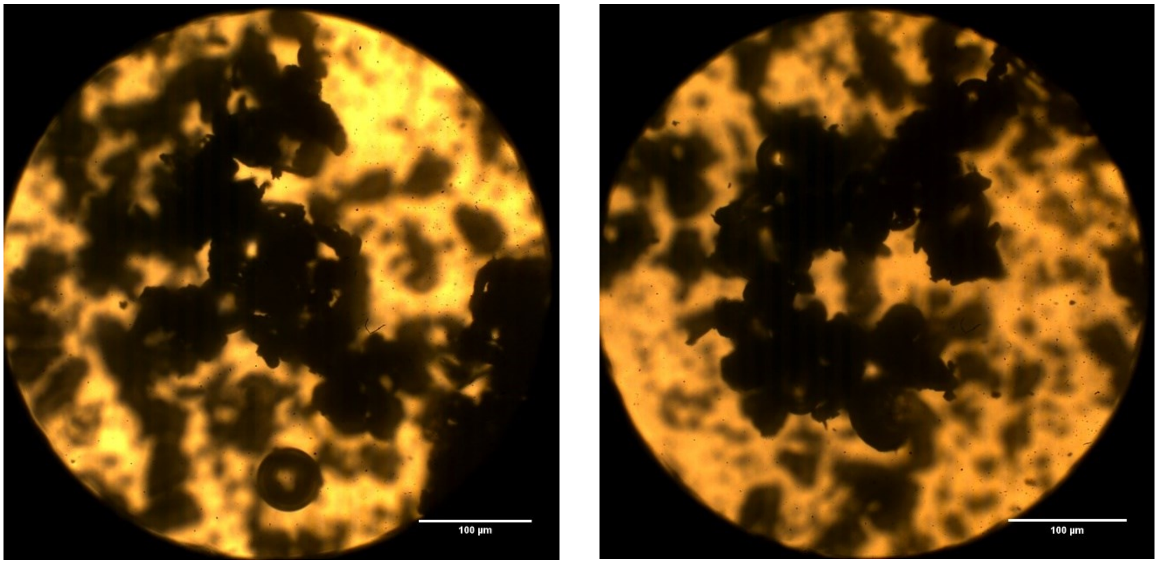

Figure 4-13 Microscope images of cavitated floc of fine molybdenite particles at 40X lens

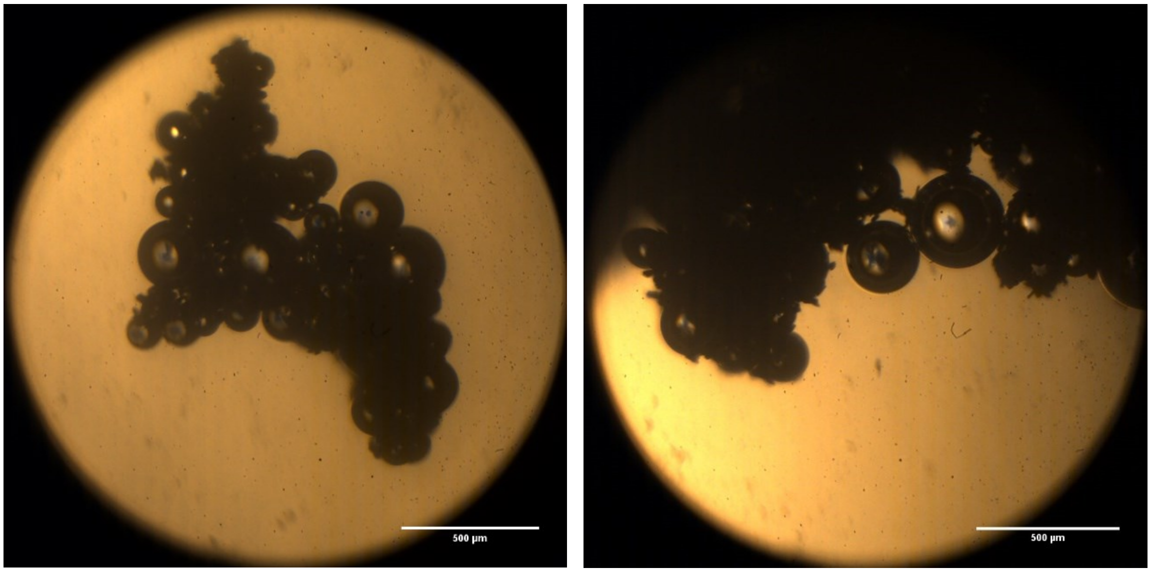

Figure 4-14 Microscope images of cavitated floc of fine molybdenite particles at 10X lens

It was observed from Figure 4-13 that the floc was structured with plenty of microbubbles with diameters ranging from about 10 µm to 20 µm. No microbubble coalescence was observed in this floc structure, which showed a high stability and durability. This is mainly due to the hydrophobic interactions between microbubbles and particle-bubble[7,13]. It was also illustrated that the nanobubbles would generate on the surface of hydrophobic particles during hydrodynamic cavitation, which made these particles frosted with nanobubbles become easily to attach to microbubbles[3,14]. Figure 4-14 shows a floc with diameter of about 1 mm. It obviously consisted of the smaller flocs shown above and bigger microbubbles with diameter about 100 µm, which worked as the bubble bridge between the smaller flocs. The presence of these large microbubbles were mainly due to the enhancement of air injection[15]. Not only would the air injection provide sufficient gas nuclei for hydrodynamic cavitation, but also could make the microbubbles grow larger. It was also believed that this kind of flocs would have a higher up-rising rate in flotation column, providing a higher floatability[16].

4.8 Zeta Potential Distribution Measurement

The current study clearly showed the influence of hydrodynamic cavitation in floc formation. To prove the existence of nanobubbles and investigate the interaction of nanobubbles and particles in the process of flocs formation, the zeta potential results were used[17–20].

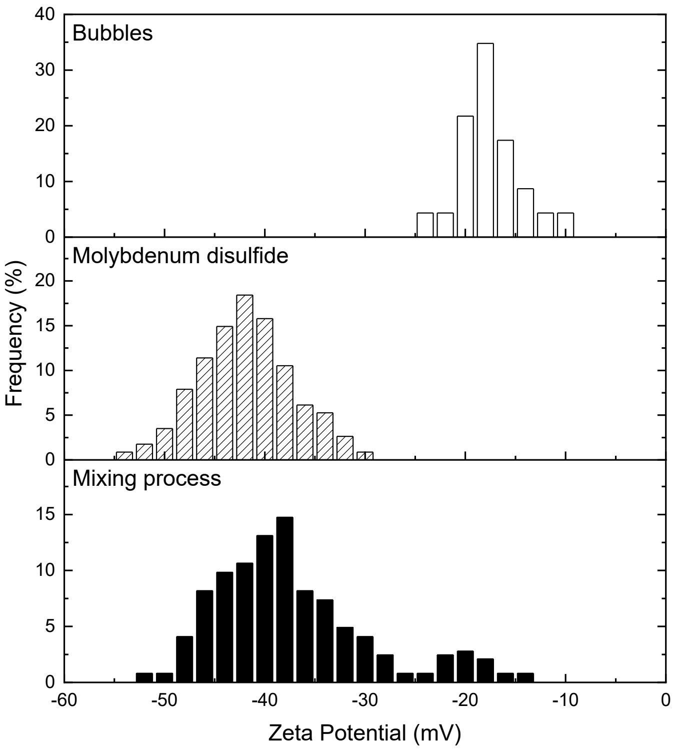

Figure 4-15 Zeta potential distribution of ultrafine molybdenum disulfide particle suspension, gas bubbles and their mixture

For illustrative purpose, all the measurements were processed at pH 5.0, which was also the natural pH for ultrafine molybdenum disulfide particle suspension. The zeta potential of molybdenum disulfide suspension measured via Zetasizer was -43.5 mV, which could be used as a reference to check the reliability of ZetaPhoremeter measurements.

For the individual components, the results in Figure 4-15 shows unique peaks for molybdenum disulfide and bubbles. It exhibited a negative zeta potential of molybdenum disulfide with the distribution centered at -42 mV, which was very close to the results obtained via Zetasizer. In the zeta potential measurement of cavitated microbubbles, HCl was used to adjust the pH, and MIBC was used as to keep the bubbles stable. MIBC is a non-polar chemical compound used primarily as a frother in mineral flotation, which does not change the bubble’s surface charge. The peak of the bubbles was located at -18 mV. Similar results were shown in others work[21].

As presented in Figure 4-15, when the ultrafine molybdenum disulfide suspension and cavitated bubbles were mixed together, the mixture showed two distinct distribution peaks at -40 mV and -22 mV. However, it was noticed the peaks were a little closer to each other as compared with the value of particles and bubbles measured independently, which might be due to electrophoretic retardation[22]. It could also be considered as a very weak attachment. This result illustrated that molybdenum disulfide particles and bubbles would not attach to each other spontaneously due to the electrostatic repulsive force among the negatively charged particles and bubbles.

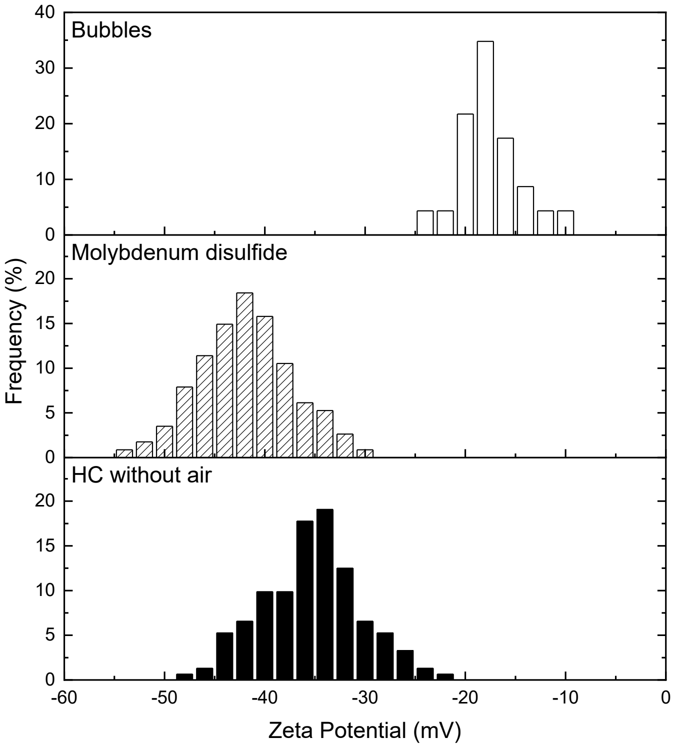

Figure 4-16 Zeta potential distribution of ultrafine molybdenum disulfide particle suspension, gas bubbles and suspension cavitated without air

After hydrodynamic cavitation treatment without air injection, a significant change is shown in Figure 4-16. The zeta potential distribution of cavitated ultrafine molybdenum disulfide suspension was a broad but clear single peak, located at -36 mV. This is characteristic of two individual component distributions merging to form a single distribution; the peak being positioned closer to the distribution peak of molybdenum disulfide indicates a strong attachment of bubbles to particles. It was believed that during hydrodynamic cavitation, the high shear force and energy could overcome the energy barrier between particle and bubble and make them easily collide with each other. At a short enough distance, the Van der Waals force and hydrophobic effect would take a lead to finally accomplish strong attachment. During the mixing process, long-range forces such as the electrostatic repulsive force (Coulomb force) were dominant without opposite forces from the outside, so the attachment of bubble to particle was difficult.

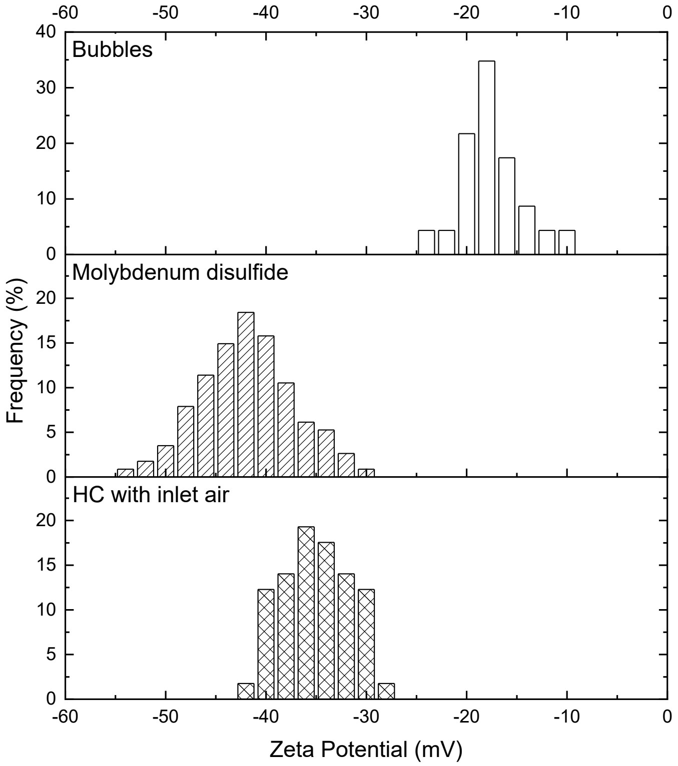

Figure 4-17 Zeta potential distribution of ultrafine molybdenum disulfide particle suspension, gas bubbles and suspension cavitated with inlet air

The ultrafine molybdenum disulfide suspension treated by hydrodynamic cavitation with inlet air injection showed a similar but much more uniform zeta potential distribution in Figure 4-17. The peak of the bubbles is shown in the first measurement right after cavitation but disappeared very soon after since bubbles without MIBC or any other surfactant were easily merged or collapsed, making them difficult to be captured by the ZetaPhoremeter. As discussed before, sufficient air injection would be beneficial to larger floc formation. However, due to the limitations of experimental conditions, large flocs are not easily suspended in the liquid. In order words, this technique is only used to demonstrate the attachment of microbubbles and ultrafine particles in this study.

4.9 Reference

(1) Dang-Vu, T.; Jha, R.; Wu, S. Y.; Tannant, D. D.; Masliyah, J.; Xu, Z. Wettability Determination of Solids Isolated from Oil Sands. *Colloids Surfaces A Physicochem. Eng. Asp.* **2009**, *337* (1–3), 80–90.

(2) Meiron, T. S.; Marmur, A.; Saguy, I. S. Contact Angle Measurement on Rough Surfaces. *J. Colloid Interface Sci.* **2004**, *274* (2), 637–644.

(3) Zhou, Z. a.; Xu, Z.; Finch, J. a.; Hu, H.; Rao, S. R. Role of Hydrodynamic Cavitation in Fine Particle Flotation. *Int. J. Miner. Process.* **1997**, *51* (1–4), 139–149.

(4) Fan, M.; Tao, D.; Honaker, R.; Luo, Z. Nanobubble Generation and Its Application in Froth Flotation (Part I): Nanobubble Generation and Its Effects on Properties of Microbubble and Millimeter Scale Bubble Solutions. *Min. Sci. Technol.* **2010**, *20* (1), 1–19.

(5) Li, S.; Liao, Y.; Li, G.; Li, Z.; Cao, Y. Flocculating and Dewatering Performance of Hydrophobic and Hydrophilic Solids Using a Thermal-Sensitive Copolymer. *Water Sci. Technol.* **2017**, *76* (3), 694–704.

(6) Calgaroto, S.; Azevedo, A.; Rubio, J. Separation of Amine-Insoluble Species by Flotation with Nano and Microbubbles. *Miner. Eng.* **2016**, *89*, 24–29.

(7) Oliveira, C.; Rodrigues, R. T.; Rubio, J. A New Technique for Characterizing Aerated Flocs in a Flocculation- Microbubble Flotation System. *Int. J. Miner. Process.* **2010**, *96* (1–4), 36–44.

(8) Yang, B.; Song, S.; Lopez-Valdivieso, A. Kinetics of Hydrophobic Agglomeration of Molybdenite Fines in Aqueous Suspensions. *Physicochem. Probl. Miner. Process.* **2015**, *51* (1), 181–189.

(9) Zhou, W.; Chen, H.; Ou, L.; Shi, Q. Aggregation of Ultra-Fine Scheelite Particles Induced by Hydrodynamic Cavitation. *Int. J. Miner. Process.* **2016**, *157*, 236–240.

(10) Kawamura, T.; Kakugawa, A.; Kodama, Y. Controlling the Size of Microbubbles for Drag Reduction. *3rd Symp. Smart Control Turbul.* **2002**.

(11) Fujiwara, A.; Takagi, S.; Watanabe, K.; Matsumoto, Y. Experimental Study on the New Micro-Bubble Generator and Its Application to Water Purification System. *SME/JSME 2003 4th Jt. Fluids Summer Eng. Conf.* **2003**, 469–473.

(12) Ozkan, F.; Ozturk, M.; Baylar, A. Experimental Investigations of Air and Liquid Injection by Venturi Tubes. *Water Environ. J.* **2006**, *20* (3), 114–122.

(13) Hu, Y.; Qiu, G.; Miller, J. D. Hydrodynamic Interactions between Particles in Aggregation and Flotation. *Int. J. Miner. Process.* **2003**, *70* (1–4), 157–170.

(14) Oliveira, C.; Rubio, J. A Short Overview of the Formation of Aerated Flocs and Their Applications in Solid/Liquid Separation by Flotation. *Miner. Eng.* **2012**, *39*, 124–132.

(15) Carissimi, E.; Rubio, J. The Floes Generator Reactor-FGR: A New Basis for

Flocculation and Solid-Liquid Separation. *Int. J. Miner. Process.* **2005**, *75* (3–4), 237–247.

(16) Song, S.; Zhang, X.; Yang, B.; Lopez-Mendoza, A. Flotation of Molybdenite Fines as Hydrophobic Agglomerates. *Sep. Purif. Technol.* **2012**, *98*, 451–455.

(17) Zhao, H.; Long, J.; Masliyah, J. H.; Xu, Z. Effect of Divalent Cations and Surfactants on Silica-Bitumen Interactions. *Ind. Eng. Chem. Res.* **2006**, *45* (22), 7482–7490.

(18) Liu, J.; Xu, Z.; Masliyah, J. Studies on Bitumen-Silica Interaction in Aqueous Solutions by Atomic Force Microscopy. *Langmuir.* **2003**, *19* (9), 3911–3920.

(19) Wu, C.; Wang, L.; Harbottle, D.; Masliyah, J.; Xu, Z. Studying Bubble-Particle Interactions by Zeta Potential Distribution Analysis. *J. Colloid Interface Sci.* **2015**, *449*, 399–408.

(20) Liu, J.; Zhou, Z.; Xu, Z.; Masliyah, J. Bitumen-Clay Interactions in Aqueous Media Studied by Zeta Potential Distribution Measurement. *J. Colloid Interface Sci.* **2002**, *252* (2), 409–418.

(21) Yang, C.; Dabros, T.; Li, D.; Czarnecki, J.; Masliyah, J. H. Measurement of the Zeta Potential of Gas Bubbles in Aqueous Solutions by Microelectrophoresis Method. *J. Colloid Interface Sci.* **2001**, *243* (1), 128–135.

(22) Wu, C. A Fundamental Study of Bubble-Particle Interactions through Zeta-Potential Distribution Analysis. Master's thesis, University of Alberta, **2011**.

Chapter 5 Application of Hydrodynamic Cavitation in Fine Particle Flotation

5.1 Molybdenite Micro-flotation

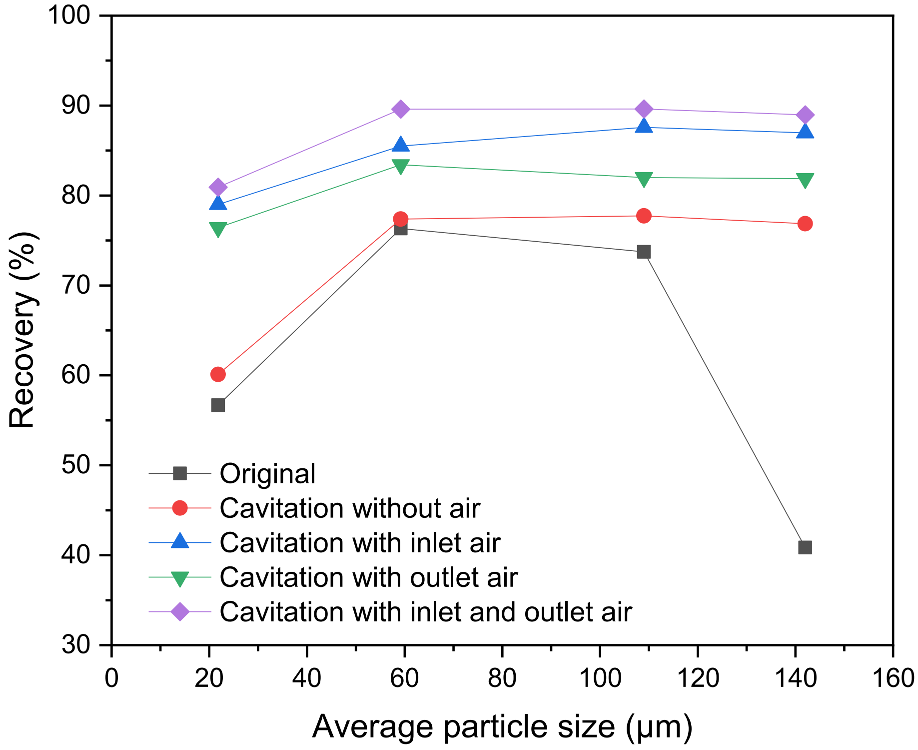

Figure 5-1 Flotation recovery of Molybdenite with different particle sizes in different hydrodynamic cavitation conditions

Figure 5-1 shows a significant increase in flotation recovery of molybdenite after hydrodynamic dynamic treatment. Overall, the hydrodynamic cavitation with inlet and outlet gas injection provides the maximum flotation recovery of molybdenite in all particle size ranges. It achieved a 26% increase of recovery in fine molybdenite particle flotation tests. Comparing with the original micro-flotation test, just a little enhancement of the fine molybdenite particle recovery is observed in the case of hydrodynamic cavitation without gas injection. This is due to the insufficient gas content for generating cavitation bubbles. In the presence of air injection, there was a great enhancement in the recovery of not only the fine molybdenite particles (< 37 μm) but also the coarse particles (> 105 μm). These results are consistent with the floc size results discussed in chapter 4, which also showed a large increase in floc size generated by hydrodynamic cavitation treatment with gas injection. It is obvious that the formation of the flocs strongly increases the possibility of particle and bubble collisions, making them much more likely to attach together[1–4]. Several hypothesizes have been proposed in literature to explain this phenomenon[5–7]. Based on the study in chapter 4, the gas nuclei or microbubbles on the surface of particles acted as a bridge in floc formation as shown in Figure 4-10 and Figure 4-11, resulting in an increase of the apparent particle size. In other words, microbubbles, presented as the role of collector, increase the possibility of bubble and particle collision and attachment. Hence, the recovery of fine molybdenite particles dramatically increases.

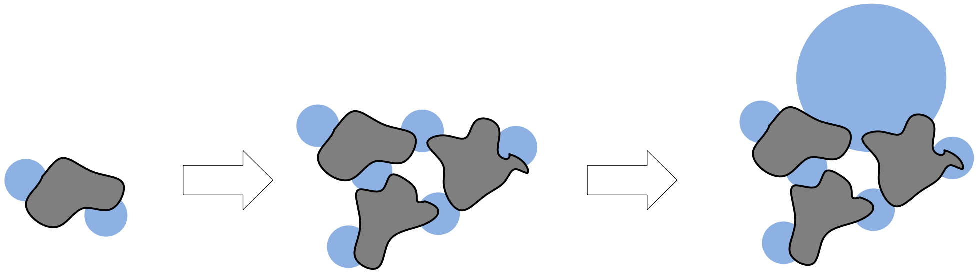

Figure 5-2 Illustration of floc formation in hydrodynamic cavitation

As for the coarse particles, results of the micro-flotation tests reveal that the hydrodynamic cavitation also takes effect in coarse mineral flotation recovery with an increase of 49%. To study the floc formation with coarse particles, the slurry was measured using the mastersizer.

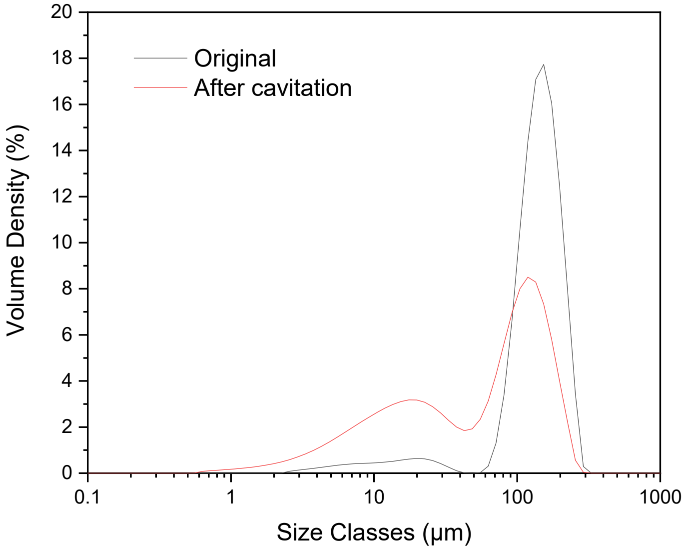

Figure 5-3 Particle size distribution of coarse molybdenite particles before and after cavitation

It is clearly noticed that the size of coarse particles became smaller after hydrodynamic cavitation in Figure 5-3. As mentioned before, the Venturi tube operated as a disperser under some conditions, which may easily break down the coarse molybdenite particles[8,9]. Because of the layered structure, the bond between layers are easily broken under an external force, forming new parallel surfaces. As the molybdenite slurry is pumped through the Venturi tube, coarse particles break into smaller particles due to a high shear force at the tube throat. At the same time, the cavitation-nucleated microbubbles by hydrodynamic cavitation bridge with broken particles to form the flocs as shown in Figure 5-4. These flocs surrounded by microbubbles promote attachment with Nitrogen bubbles in the micro-flotation tests since the attachment between microbubbles and larger bubbles is more favored by the hydrophobic attraction.

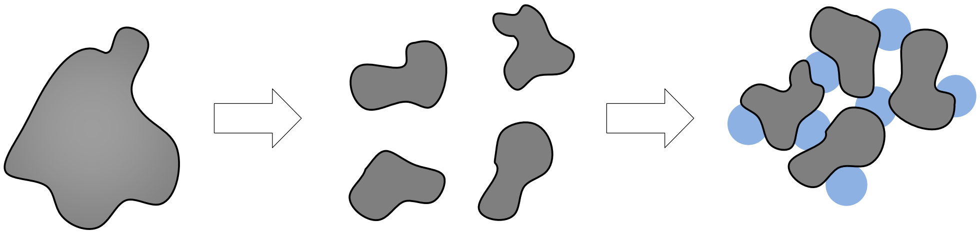

Figure 5-4 Illustration of coarse particles in the hydrodynamic cavitation

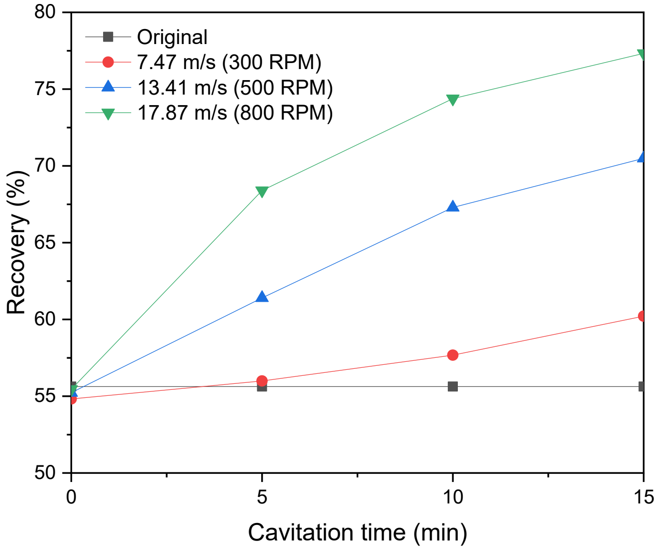

Figure 5-5 Flotation recovery of fine molybdenite particles under different cavitation time in different hydrodynamic cavitation throat velocity

A significant increase of fine particle recovery at the appropriate throat velocity can be observed in Figure 5-5. At a low throat velocity of 7.47 m/s, the recovery of fine molybdenite particles is not significantly improved. This is because the flow rate in the test is lower than the minimum speed required for the Venturi tube to generate microbubbles. It would not show any improvement theoretically, and such a little improvement may be due to the gas injection from inlet as increasing the gas content in water is beneficial to mineral flotation. A higher increase of recovery is observed when the throat velocity reached 13.41 m/s, which is demonstrated by a weak hydrodynamic cavitation illustrated before. As the throat velocity increased to 17.87 m/s, the highest recovery of 78% is achieved in 15 min of cavitation due to strong hydrodynamic cavitation with thousands of microbubbles generated.

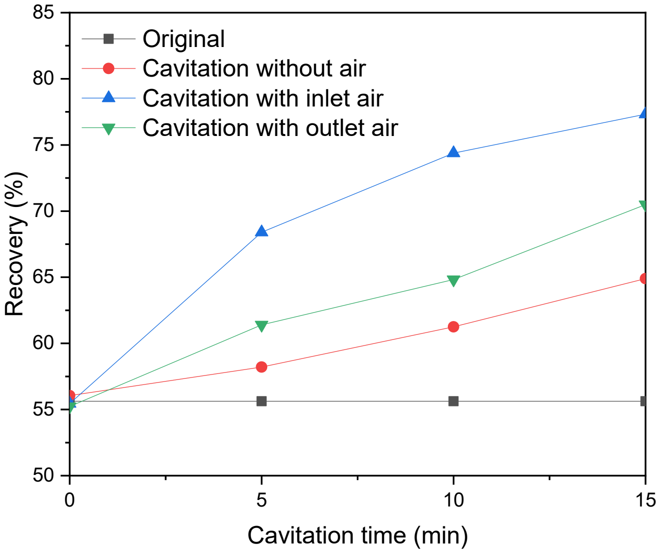

Figure 5-6 Flotation recovery of fine molybdenite particles under different cavitation time in different hydrodynamic cavitation condition

It is described in Figure 5-6 that with the continuous circulation of hydrodynamic cavitation, and the longer the cavitation time, the higher the recovery of fine particles. This finding can be explained by of the change of floc size as a function of cavitation time discussed before. The longer cavitation time with sufficient gas concentration in water can increase the rate of floc formation, which enhances the probability of particle and bubble attachment. As shown in Figure 5-6, sufficient gas provided by the inlet gas injection increases cavitation intensity. Thus, more microbubbles are formed in the Venturi tube, which is beneficial to flocs generation.

As discussed before, the cavitated microbubbles act as bridges between fine particles in floc formation, which highly increases the possibility of bubble and particle attachment. However, the detachment of flocculation has also been observed by other researchers. Micro-flotation was used to study the durability and stability of the flocs by simulating some conditions used in industry. The durability tests were focused on the residence time of the flocs without any external force influence. The stability tests were used to explain floc stability under external force.

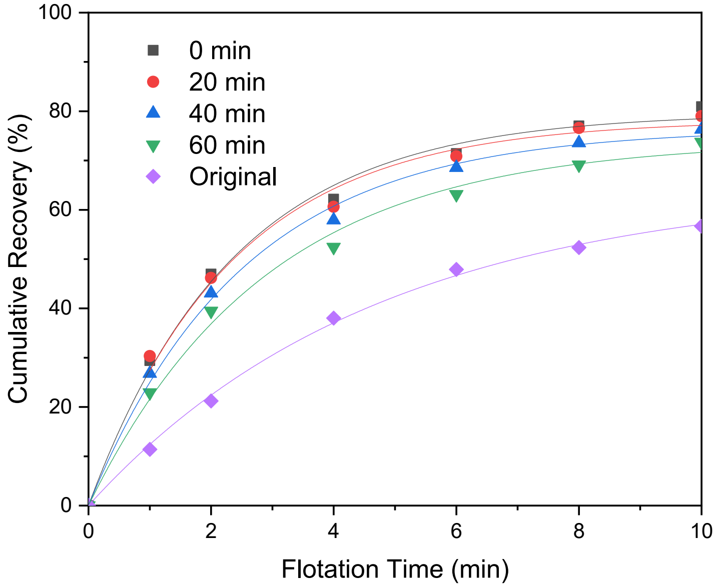

Figure 5-7 Kinetic cumulative flotation recovery of fine molybdenite particles with different residence times

Table 5-1 Model parameters obtained from the model fit to data in Figure 5-7

Value	**Original**	**0 min**	**20min**	**40min**	**60min**
R_∞	64.845	79.631	78.185	76.443	73.998
k	0.212	0.423	0.431	0.396	0.345

It is observed in Figure 5-7 that the residence time has little effect in cumulative recovery. In comparison with the results shown in Table 5-1, the ultimate recovery of molybdnite increased significantly from 64.8% to 79.6% right after cavitation and decreased slowly within 60 mins of residence time. The first-order rate constant k, describing the rate of mineral flotation, shows a similar trend. It has a sharp increase right after hydrodynamic cavitation and is still higher than the original rate after standing for 60 min. The steady ultimate recovery and first-order rate constant represent a very stable status of floc after the hydrodynamic cavitation. This finding reveals a low detachment possibility of bubbles and flocs under the condition without any external force.

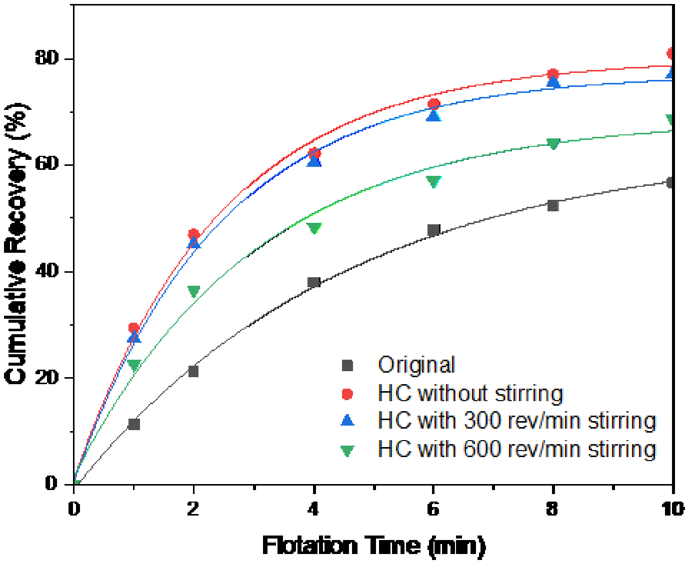

Figure 5-8 Kinetic cumulative flotation recovery of fine molybdenite particles with different stirring speed

Table 5-2 Model parameters obtained from the model fit to data in Figure 5-8

Value	**Original**	**HC without stirring**	**HC with 300 rev/min stirring**	**HC with 600 rev/min stirring**
R_∞	64.845	79.631	76.989	68.171
k	0.212	0.423	0.420	0.349

To better understand the effect of external forces on the cavitated flocs, different stirring speeds were studied in order to introduce different levels of shear force into the tests. From

Figure 5-8, it is interesting to note that the cumulative recovery after stirring at 300 rev/min does not show an obvious difference as compared to no pretreatment. A small change in their ultimate recovery and first-order rate constants is noted in Table 5-2. However, the cumulative recovery significantly decreases with a decrease of the stirring speed to 600 rev/min. Notably, it can be observed that the ultimate recovery at a stir speed of 600 rev/min is very close to the condition without cavitation treatment. It has been known that the external force here is predominantly centrifugal force. Under 600 rev/min, the centrifugal force provided was four times larger than the one of 300 rev/min. In other words, the floc structure can overcome a limited external force. If the external force is over that limit, the bubble bridges between particles would be fragile, causing the floc structure break down easily.

5.2 Silica Micro-flotation

To further investigate the effect of hydrodynamic cavitation to fine particles flotation, fine silica particles, with similar size as fine molybdenite particles, were used as a comparison in this study.

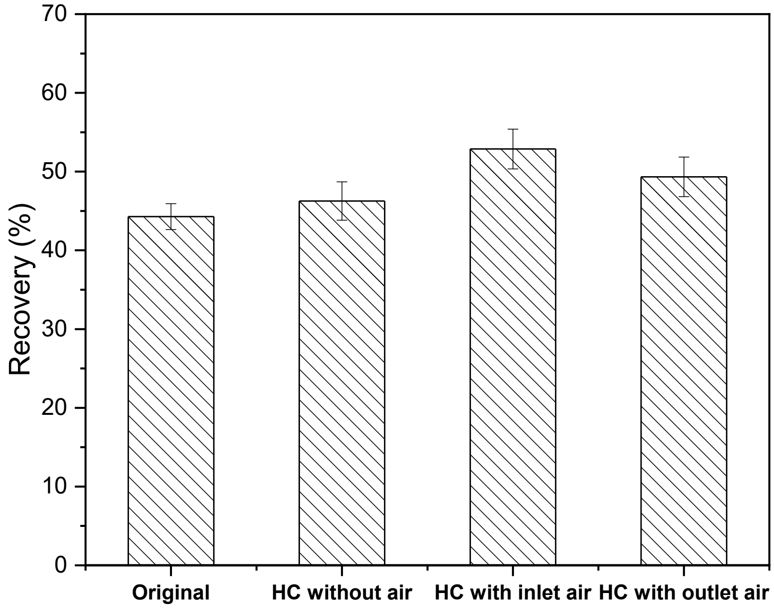

Figure 5-9 Recovery of fine silica particles with and without hydrodynamic cavitation treatment at different conditions

The effect of fine silica recovery after hydrodynamic cavitation treatment is shown in Figure 5-9. With hydrodynamic cavitation and inlet gas injection, the fine silica recovery increased from 45% to 52%. As discussed early, the recovery of fine particles is consistent with their flocs formation in hydrodynamic cavitation. In other words, the flocs of fine silica may be fewer and smaller than molybdenite. As measured before, the contact angle of molybdenite is 75°, while silica contact angle is only 39°. Particles with greater contact angles have a higher attachment efficiency with bubbles[10]. Also, the structure of the flocs could be much stable due to low detachment probability. It was reported in the literature that the microbubbles would easily generate on hydrophobic surfaces due to the presence of more cavities as compared to the hydrophilic surface[11,12]. Also, the gas content within the cavities determines the size of cavities. During hydrodynamic cavitation, the cavities grow larger and quicker with smaller surface tension due to the pressure drop, forming microbubbles on the surface. The microbubbles generated by the rupture of the water's surface prefer to attach to the hydrophobic surface surrounded by the bubbles[13].

5.3 Micro-flotation Selectivity

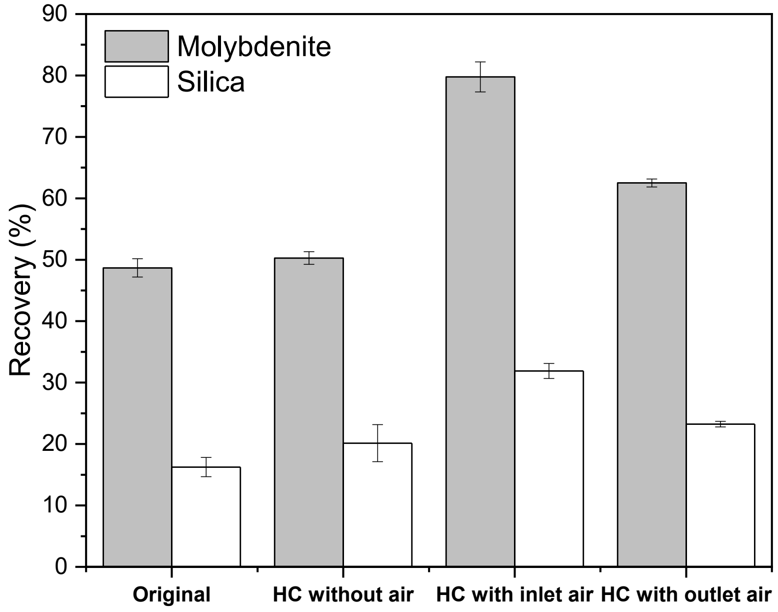

Figure 5-10 Recovery of fine molybdenite and silica mixture after hydrodynamic cavitation treatment with different conditions

A significant improvement of flotation selectivity is shown in Figure 5-10. As discussed before, the hydrodynamic cavitation without air injection does not provide enough gas for microbubble generation. Further, the Venturi tube also acts as a disperser to separate and crack particles. These two facts are not beneficial to the floc formation of fine molybdenite particles, thus hydrodynamic cavitation without air injection has nearly no effect on flotation selectivity of molybdenite. After air injection, the recovery of molybdenite increases by more than 30%, while silica recovery increases by less than just 15%. In other words, hydrodynamic cavitation with enough air can make the hydrophobic particles float much more easily than hydrophilic particles, which can be regarded beneficial not only in fine particle flotation, but also in valuable mineral particle selectivity.

5.4 Reference

(1) Peng, F. F.; Yu, X. Pico-Nano Bubble Column Flotation Using Static Mixer-Venturi Tube for Pittsburgh No. 8 Coal Seam. *Int. J. Min. Sci. Technol.* **2015**, *25* (3), 347–354.

(2) Pourkarimi, Z.; Rezai, B.; Noaparast, M. Effective Parameters on Generation of Nanobubbles by Cavitation Method for Froth Flotation Applications. *Physicochem. Probl. Miner. Process.* **2017**, *53* (2), 920–942.

(3) Zhang, H.; Liu, J.; Wang, Y.; Cao, Y.; Ma, Z.; Li, X. Cyclonic-Static Micro-Bubble Flotation Column. *Miner. Eng.* **2013**, *45*, 1–3.

(4) Zhou, W.; Chen, H.; Ou, L.; Shi, Q. Aggregation of Ultra-Fine Scheelite Particles Induced by Hydrodynamic Cavitation. *Int. J. Miner. Process.* **2016**, *157*, 236–240.

(5) Tao, D. Role of Bubble Size in Flotation of Coarse and Fine Particles—A Review. *Sep. Sci. Technol.* **2005**, *39* (4), 741–760.

(6) Zhou, Z. a.; Xu, Z.; Finch, J. a.; Hu, H.; Rao, S. R. Role of Hydrodynamic Cavitation in Fine Particle Flotation. *Int. J. Miner. Process.* **1997**, *51* (1–4), 139–149.

(7) Zhou, Z. A.; Xu, Z.; Finch, J. A.; Masliyah, J. H.; Chow, R. S. On the Role of Cavitation in Particle Collection in Flotation - A Critical Review. II. *Miner. Eng.* **2009**, *22* (5), 419–433.

(8) Cramers, P. H. M. R.; Beenackers, A. A. C. M.; van Dierendonck, L. L. Hydrodynamics and Mass Transfer Characteristics of a Loop-Venturi Reactor with a Downflow Liquid Jet Ejector. *Chem. Eng. Sci.* **1992**, *47* (13–14), 3557–3564.

(9) Simon, M.; Bart, H. J. Experimental Studies of Coalescence in Liquid/Liquid Systems. *Chem. Eng. Technol.* **2002**, *25* (5), 481–484.

(10) Belova, V.; Gorin, D. A.; Shchukin, D. G.; Möhwald, H. Controlled Effect of Ultrasonic Cavitation on Hydrophobic/ Hydrophilic Surfaces. *ACS Appl. Mater. Interfaces.* **2011**, *3* (2), 417–425.

(11) Fell, M.; Murphy, S. M. The Nucleation and Growth of Gas Bubbles in Irradiated Metals. **1990**, *172*.

(12) Khurana, A. K.; Chen, H.; Wall, C. G. Nucleation of Gas Bubbles in Surface Irregularities. *Chem. Eng. Commun.* **1998**, *165*, 199–215.

(13) Bunkin, N. F.; Kiseleva, O. A.; Lobeyev, A. V.; Movchan, T. G.; Ninham, B. W.; Vinogradova, O. I. Effect of Salts and Dissolved Gas on Optical Cavitation near Hydrophobic and Hydrophilic Surfaces. *Langmuir.* **1997**, *13* (11), 3024–3028.

Chapter 6 Effects of the Optimized Venturi Tube on Fine Particle Flotation

6.1. Column Flotation Results of TCM, Gold and Sulfides

Carbonaceous matters in sulfide minerals may affect the gold recovery during cyanide process, which can adsorb or preg-rob gold[1,2]. These tests were the pretreatments before gold cyanidation, which aim to remove carbonaceous matters in minerals as much as possible. The flotation column set-up was shown in Figure 6-1.

Figure 6-1 Flotation column set-up

Table 6-1 Grade and recovery of TCM, gold and sulfides in the samples

Sparger	Pump feed rate	Residence time	Product	TCM		Au		S	
	(mL/min)	**(min)**		**Gra. (%)**	**Rec. (%)**	**Gra. (g/t)**	**Rec. (%)**	**Gra. (%)**	**Rec. (%)**
Commercial sparger	480	10	Concentrate	7.97	45.67	3.33	5.73	1.86	3.73
			Tail	0.31	54.33	1.79	94.27	1.57	96.27
			Calc. Head	**0.55**	100.00	**1.84**	100.00	**1.58**	100.00
			Assay Head	**0.43**		**3.14**		**2.45**	
Commercial sparger	960	5	Concentrate	5.36	46.39	2.97	7.06	1.72	5.00
			Tail	0.29	53.61	1.83	92.94	1.53	95.00
			Calc. Head	**0.52**	100.00	**1.88**	100.00	**1.54**	100.00
			Assay Head	**0.43**		**3.14**		**2.45**	
Commercial sparger	1,600	3	Concentrate	2.02	55.00	2.02	14.61	1.20	11.15
			Tail	0.28	45.00	2.00	85.39	1.62	88.85
			Calc. Head	**0.53**	100.00	**2.00**	100.00	**1.56**	100.00
			Assay Head	**0.43**		**3.14**		**2.45**	
U of A sparger	480	10	Concentrate	10.20	47.53	2.91	3.75	1.68	2.63
			Tail	0.33	52.47	2.19	96.25	1.82	97.37
			Calc. Head	**0.61**	100.00	**2.21**	100.00	**1.82**	100.00
			Assay Head	**0.47**		**3.02**		**2.30**	
U of A sparger	960	5	Concentrate	6.27	49.19	3.07	4.68	1.78	3.48
			Tail	0.26	50.81	2.51	95.32	1.98	96.52
			Calc. Head	**0.49**	100.00	**2.53**	100.00	**1.97**	100.00
			Assay Head	**0.47**		**3.02**		**2.30**	
U of A sparger	1,600	3	Concentrate	2.05	50.85	2.33	12.58	1.43	10.16
			Tail	0.29	49.15	2.37	87.42	1.85	89.84
			Calc. Head	**0.51**	100.00	**2.36**	100.00	**1.80**	100.00
			Assay Head	**0.47**		**3.02**		**2.30**	

In Table 6-1, we can find the grade and recovery of TCM, gold and sulfides in the samples after treated with commercial sparger and U of A sparger.

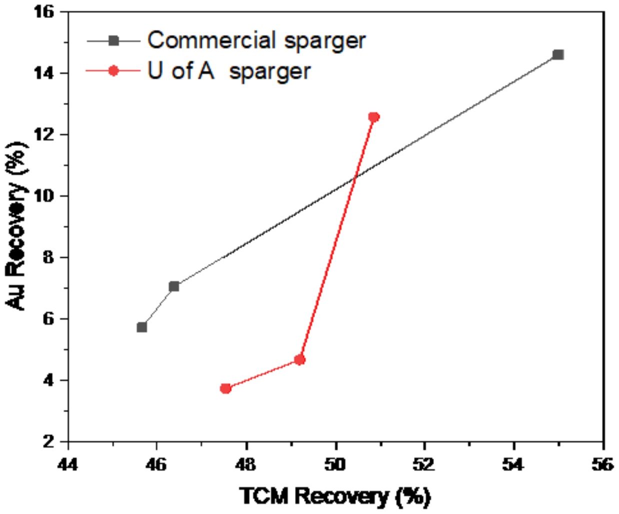

Figure 6-2 Gold recovery in terms of TCM recovery in concentrates

In Figure 6-2, it can be noticed that U of A sparger has a better effect. With 50% of TCM being eliminated, the loss of gold in the concentrate is about 7.8 % with U of A sparger, while it is about 10.2 % of gold lose with commercial sparger. As discussed before, the microbubbles tend to attach to the surface of hydrophobic particles instead of hydrophilic particles. It is known that the carbonaceous matters are much more hydrophobic than gold, which proved the role of microbubbles in flotation selectivity.

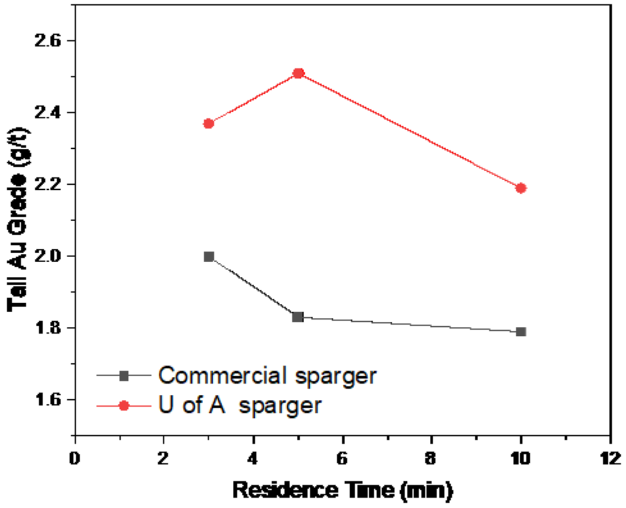

Figure 6-3 Gold grade in tailings under different residence time

As shown in Figure 6-3, the grade of gold in tailings is higher with U of A sparger. 0.6 g/t increase of gold grade was achieved under 5 min residence time, which is about 33% increase. In other words, more gold was maintained in the tailings and more TCM was eliminated at the same time.

Based on these results, it is easy to find that with the help of cavitated microbubbles, the active carbonaceous matters could be better eliminated. In addition, the Venturi tube with optimized geometry could achieve better effect in gold mineral flotation to remove carbonaceous matters in minerals.

6.2. Reference

(1) Rees, K. L.; Van Deventer, J. S. J. Preg-Robbing Phenomena in the Cyanidation of Sulphide Gold Ores. *Hydrometallurgy.* **2000**, *58* (1), 61–80.

(2) Dimov, S. S.; Hart, B. R. Speciation and Quantification of Surface Gold in Carbonaceous Matter by TOF-SIMS: A New Approach in Characterizing Losses during the Gold Recovery Process. *Surf. Interface Anal.* **2011**, *43* (1–2), 446–448.

Chapter 7 Conclusions

In this study, the main contribution is the investigation on the mechanism of floc formation by hydrodynamic cavitation. An optimized Venturi tube was used in the hydrodynamic cavitation system for microbubbles generation. The throat velocity in the tube was first studied to get the relation between cavitation probability and floc formation efficiency. The role of gas behavior in hydrodynamic cavitation and flocs generation was also investigated. The structure of the flocs was confirmed with microscope images. Zeta potential distribution was measured to further understand the interaction of bubbles and particles. Further, hydrodynamic cavitation was applied to the study of micro-flotation of fine molybdenite, simulating the flotation process in industry. Silica and a mixture of molybdenite and silica were used to study the selectivity of microbubbles as a comparison. The major conclusions of this thesis research are summarized as follows:

1. The throat velocity in the tube was first studied to get the relation between cavitation probability and floc formation efficiency, indicating that in our studied system, the minimum throat velocity should be 10 m/s for cavitation to occur. To keep a stable cavitation, a throat velocity of 16 m/s was suggested.
2. The relation of gas content in water and cavitation efficiency was also investigated with air injection in a hydrodynamic cavitation system. The dissolved gas in water increased the threshold pressure for cavitation as compared to the vapor pressure. The existence of gas nuclei acts as a weak spot in water, making it easier to generate bubbles in higher local pressure with a lower pressure drop needed and lower energy consumption.

3. The quantity of bubbles generated in hydrodynamic cavitation was also investigated to show the cavitation efficiency. It is related to gas concentration in the liquid and the liquid flow rate. Higher gas concentration and flow rate will generate more bubbles. However, as the gas concentration reaches an ideal value and the flow rate can achieve continuous cavitation, the number of bubbles will stabilize. This is the same for flocs formation.
4. The floc was structured with plenty of microbubbles, which built a bridge between particles. This kind of structure was very stable without external force and could also overcome limited external forces. Its stability relates to the characteristics of its surface, with more hydrophobic surfaces resulting in a more stable floc.
5. With the help of hydrodynamic cavitation, high shear force and energy could overcome the energy barrier between fine particles and bubbles and make them easily collide with each other.
6. Due to the flocs formation of molybdenite fine particles by hydrodynamic cavitation in the presence of inlet air injection, the recovery of fine molybdenite particles was greatly enhanced as compared to the conventional flotation without hydrodynamic cavitation. For instance, the recovery of fine molybdenite d < 37 μm increased from 58% in the conventional flotation to 80% in the modified flotation with hydrodynamic cavitation and air injection.
7. The generation of flocs was demonstrated to be more favorable with molybdenite hydrophobic particles than with silica particles according to the results of the silica micro flotation study and the selectivity test of a mixture of molybdenite and silica. The result of the silica micro flotation study showed a recovery of about 45% to

52%, which is clearly less than in the study of molybdenite fine particles. In addition, the selectivity test indicated that more molybenite fine particles were collected in the froth than silica particles.

This thesis study is expected to provide a better understanding of the fundamental mechanism of flocs generation by hydrodynamic cavitation, which will support the flotation of fine mineral particles. Hence, this significant problem in the mining and mineral processing industry can be promisingly solved.

Chapter 8 Future Work

There are many related aspects which could not be covered in this study. To further understand the hydrodynamic effect on different particles and the specific structure of the flocs, some suggestions are listed:

1. Some researchers believe the presence of tiny gas nuclei in crevices on hydrophobic rough surfaces assists the hydrodynamic cavitation as a result of the expansion of these gas nuclei under the negative pressure. It is also regarded as the main reason behind hydrodynamic cavitation selectivity. Particles with the same contact angle but different roughness can be used in this study.
2. The structure of the flocs was observed under microscope and the nanobubbles on the surface of particle was demonstrated using the zeta potential distribution in this study. To directly see the specific structure of the flocs and prove the existence of nanobubbles, cryo-SEM can be used in future research.

Bibliography

Ahmed, N. and Jameson, G. J. (1985) ‘The effect of bubble size on the rate of flotation of fine particles’, *International Journal of Mineral Processing*, 14(3), pp. 195–215. doi: 10.1016/0301-7516(85)90003-1.

Arrojo, S. and Benito, Y. (2008) ‘A theoretical study of hydrodynamic cavitation’, *Ultrasonics Sonochemistry*, 15(3), pp. 203–211. doi: 10.1016/j.ultsonch.2007.03.007.

Belova, V., Gorin, D. A., Shchukin, D. G. and Möhwald, H. (2011) ‘Controlled effect of ultrasonic cavitation on hydrophobic/ hydrophilic surfaces’, *ACS Applied Materials and Interfaces*, 3(2), pp. 417–425. doi: 10.1021/am101006x.

Bunkin, N. F., Kiseleva, O. A., Lobeyev, A. V., Movchan, T. G., Ninham, B. W. and Vinogradova, O. I. (1997) ‘Effect of Salts and Dissolved Gas on Optical Cavitation near Hydrophobic and Hydrophilic Surfaces’, *Langmuir*, 13(11), pp. 3024–3028. doi: 10.1021/la960265k.

Calgaroto, S., Azevedo, A. and Rubio, J. (2015) ‘Flotation of quartz particles assisted by nanobubbles’, *International Journal of Mineral Processing*. Elsevier B.V., 137, pp. 64–70. doi: 10.1016/j.minpro.2015.02.010.

Calgaroto, S., Azevedo, A. and Rubio, J. (2016) ‘Separation of amine-insoluble species by flotation with nano and microbubbles’, *Minerals Engineering*. Elsevier Ltd, 89, pp. 24–29. doi: 10.1016/j.mineng.2016.01.006.

Calvero (2006) *X-ray fluorescence - Wikipedia*. Available at: https://en.wikipedia.org/wiki/X-ray_fluorescence.

Cao, M. and Liu, Q. (2006) ‘Reexamining the functions of zinc sulfate as a selective depressant in differential sulfide flotation-The role of coagulation’, *Journal of Colloid and Interface Science*, 301(2), pp. 523–531. doi: 10.1016/j.jcis.2006.05.036.

Carissimi, E. and Rubio, J. (2005) ‘The floes generator reactor-FGR: A new basis for flocculation and solid-liquid separation’, *International Journal of Mineral Processing*, 75(3–4), pp. 237–247. doi: 10.1016/j.minpro.2004.08.021.

Cassell, E. A., Kaufman, K. M. and Matuevic, E. (1975) ‘The effects of bubble size on microflotation’, *Water Research*, 9(12), pp. 1017–1024. doi: 10.1016/0043-1354(75)90095-0.

Cassie, B. Y. A. B. D. and Baxter, S. (1944) ‘Wettability of Porous Surfaces’, *Physics*, (5), pp. 546–551. doi: 10.1039/tf9444000546.

Choi, W., Tuteja, A., Mabry, J. M., Cohen, R. E. and McKinley, G. H. (2009) ‘A modified Cassie-Baxter relationship to explain contact angle hysteresis and anisotropy on non-wetting textured surfaces’, *Journal of Colloid and Interface Science*. Elsevier Inc., 339(1), pp. 208–216. doi: 10.1016/j.jcis.2009.07.027.

Coleman, D. and Toll, F. N. (1995) ‘Agglomeration-flotation : hydrophobic components fine tailings recovery of from oil sands’, *Fuel*, 74(8), pp. 1156–1161.

Collins, G. L. and Jameson, G. J. (1976) ‘Experiments on the Flotation of Fine Particles the Influence of Particle Size and Charge’, *Chemical Engineer Science*, 31, pp. 985–991. doi: http://dx.doi.org/10.1016/0009-2509(76)87019-4.

Cramers, P. H. M. R., Beenackers, A. A. C. M. and van Dierendonck, L. L. (1992)

‘Hydrodynamics and mass transfer characteristics of a loop-venturi reactor with a downflow liquid jet ejector’, *Chemical Engineering Science*, 47(13–14), pp. 3557–3564. doi: 10.1016/0009-2509(92)85070-R.

Dai, Z., Fornasiero, D. and Ralston, J. (1998) ‘Influence of dissolved gas on bubble-particle heterocoagulation’, *Journal of the Chemical Society - Faraday Transactions*, 94(14), pp. 1983–1987. doi: 10.1039/a801144c.

Dai, Z., Fornasiero, D. and Ralston, J. (2000) ‘Particle-bubble collision models--a review’, *Advances in colloid and interface science*, 85(2–3), pp. 231–56. doi: 10.1016/S0001-8686(99)00030-5.

Dang-Vu, T., Jha, R., Wu, S. Y., Tannant, D. D., Masliyah, J. and Xu, Z. (2009) ‘Wettability determination of solids isolated from oil sands’, *Colloids and Surfaces A: Physicochemical and Engineering Aspects*, 337(1–3), pp. 80–90. doi: 10.1016/j.colsurfa.2008.11.055.

Delgado, A, Gonzalez-Caballero, F, Bruque, J. (1986) ‘On the Zeta Potential and Surface Charge Density of Montmorillonite in Aqueous Electrolyte Solutions’, *Journal of Colloid and Interface Science*, 113(1), pp. 203–211.

Derjaguin, B. V. and Dukhin, S. S. (1993) ‘Theory of flotation of small and medium-size particles’, *Progress in Surface Science*, 43(1–4), pp. 241–266. doi: 10.1016/0079-6816(93)90034-S.

Dimov, S. S. and Hart, B. R. (2011) ‘Speciation and quantification of surface gold in carbonaceous matter by TOF-SIMS: A new approach in characterizing losses during the gold recovery process’, *Surface and Interface Analysis*, 43(1–2), pp. 446–448. doi:

10.1002/sia.3448.

Du, G., Guo, Z., Wang, S., Zeng, R., Chen, Z. and Liu, H. (2010) ‘Superior stability and high capacity of restacked molybdenum disulfide as anode material for lithium ion batteries’, *Chemical Communications*, 46(7), pp. 1106–1108. doi: 10.1039/b920277c.

Duerkop, M., Berger, E., Dürauer, A. and Jungbauer, A. (2018) ‘Impact of Cavitation, High Shear Stress and Air/Liquid Interfaces on Protein Aggregation’, *Biotechnology Journal*, 13(7), pp. 1–9. doi: 10.1002/biot.201800062.

Dziensiewicz, J., Pryor, E. J. (1950) ‘An investigation into the action of air in froth flotation’, *Trans. IMM*, 59, pp. 455–491.

Fan, M., Tao, D., Honaker, R. and Luo, Z. (2010) ‘Nanobubble generation and its application in froth flotation (part I): nanobubble generation and its effects on properties of microbubble and millimeter scale bubble solutions’, *Mining Science and Technology*. China University of Mining and Technology, 20(1), pp. 1–19. doi: 10.1016/S1674-5264(09)60154-X.

Farmer, a., Collings, a. and Jameson, G. (2000) ‘Effect of ultrasound on surface cleaning of silica particles’, *International Journal of Mineral Processing*, 60, pp. 101–113. doi: 10.1016/S0301-7516(00)00009-0.

Farrokhpay, S. (2011) ‘The significance of froth stability in mineral flotation - A review’, *Advances in Colloid and Interface Science*. Elsevier B.V., 166(1–2), pp. 1–7. doi: 10.1016/j.cis.2011.03.001.

Fell, M. and Murphy, S. M. (1990) ‘the Nucleation and Growth of Gas Bubbles in

Irradiated Metals', 172.

Feng, C., Ma, J., Li, H., Zeng, R., Guo, Z. and Liu, H. (2009) 'Synthesis of molybdenum disulfide (MoS2) for lithium ion battery applications', *Materials Research Bulletin*, 44(9), pp. 1811–1815. doi: 10.1016/j.materresbull.2009.05.018.

Fujiwara, A., Takagi, S., Watanabe, K. and Matsumoto, Y. (2003) 'Experimental study on the new micro-bubble generator and its application to water purification system', *SME/JSME 2003 4th Joint Fluids Summer Engineering Conference*, pp. 469–473.

Giacomello, A., Meloni, S., Chinappi, M. and Casciola, C. M. (2012) 'Cassie-baxter and wenzel states on a nanostructured surface: Phase diagram, metastabilities, and transition mechanism by atomistic free energy calculations', *Langmuir*, 28(29), pp. 10764–10772. doi: 10.1021/la3018453.

Gogate, P. R. and Pandit, A. B. (2005) 'A review and assessment of hydrodynamic cavitation as a technology for the future', *Ultrasonics Sonochemistry*, 12(1–2 SPEC. ISS.), pp. 21–27. doi: 10.1016/j.ultsonch.2004.03.007.

Gonzales, L. V., Veneu, D. M. and Torem, M. L. (1934) 'Measurement and analysis of micro-bubbles produced in electroflotation', I, pp. 26–44.

Gurpinar, G., Sonmez, E. and Bozkurt, V. (2004) 'Effect of ultrasonic treatment on flotation of calcite, barite and quartz', *Mineral Processing and Extractive Metallurgy: Transactions of the Institute of Mining and Metallurgy, Section C*, 113(2), pp. 91–95. doi: 10.1179/037195504225005796.

Ham, N. J. M. V. A. N., Behie, L. E. O. A. and Svrcek, W. Y. (1983) 'The Effect of Air

Distribution on the Induced Air Flotation of Fine Oil in Water Emulsions', 61(August).

Han, M., Kim, T. Il and Kim, J. (2007) 'Effects of floc and bubble size on the efficiency of the dissolved air flotation (DAF) process', *Water Science and Technology*, 56(10), pp. 109–115. doi: 10.2166/wst.2007.779.

He, L. and Ruiz, F. (1995) 'Effect of Cavitation on Flow and Turbulence in Plain Orifices for High-Speed Atomization', *Atomization and Sprays*, pp. 569–584. doi: 10.1615/AtomizSpr.v5.i6.30.

Hou, Z., Yokota, O., Tanaka, T. and Yashima, T. (2003) 'Characterization of Ca-promoted Ni/α-Al2O3catalyst for CH4reforming with CO2', *Applied Catalysis A: General*, 253(2), pp. 381–387. doi: 10.1016/S0926-860X(03)00543-X.

Hu, H., Finch, J. a., Zhou, Z. and Xu, Z. (1998) 'Numerical and experimental study of a hydrodynamic cavitation tube', *Metallurgical and Materials Transactions B*, 29(4), pp. 911–917. doi: 10.1007/s11663-998-0150-7.

Hu, Y., Qiu, G. and Miller, J. D. (2003) 'Hydrodynamic interactions between particles in aggregation and flotation', *International Journal of Mineral Processing*, 70(1–4), pp. 157–170. doi: 10.1016/S0301-7516(03)00023-1.

Hydrargyrum (2011) *X-ray crystallography - Wikipedia*. Available at: https://en.wikipedia.org/wiki/X-ray_crystallography.

Janse, P., Gomez, C. O. and Finch, J. A. (1999) 'Effect of pulp fibres on gas holdup in a flotation column', *Canadian Journal of Chemical Engineering*, 77(1), pp. 22–25. doi: 10.1002/cjce.5450770105.

Jiangang, F., Kaida, C., Hui, W., Chao, G. and Wei, L. (2012) ‘Recovering molybdenite from ultrafine waste tailings by oil agglomerate flotation’, *Minerals Engineering*. Elsevier Ltd, 39, pp. 133–139. doi: 10.1016/j.mineng.2012.07.006.

Kawamura, T., Kakugawa, A. and Kodama, Y. (2002) ‘Controlling the size of microbubbles for drag reduction’, *3rd Symposium on Smart Control of Turbulence*. Available at: http://www.nmri.go.jp/turbulence/PDF/symposium/FY2001/Kawamura.pdf.

Khurana, A. K., Chen, H. and Wall, C. G. (1998) ‘Nucleation of gas bubbles in surface irregularities’, *Chemical Engineering Communications*, 165, pp. 199–215. doi: 10.1080/00986449808912376.

Kinnas, S. A. and Fine, N. E. (1993) ‘A numerical non-linear analysis of the fow around two and three dimensional partially cavitating hydrofoils’, *Journal of Fluid Mechanics*, 254, pp. 151–181.

Kitchener, J. A. and Gochin, R. J. (1981) ‘The mechanism of dissolved air flotation for potable water: basic analysis and a proposal’, *Water Research*, 15(5), pp. 585–590. doi: 10.1016/0043-1354(81)90021-X.

Klassen, V.J., Mokrousov, V. A. (1963) *An Introduction to the Theory of Flotation*. Butterworths, London.

Kumar, P. S. and Pandit, A. B. (1999) ‘Modeling hydrodynamic cavitation’, *Chemical Engineering and Technology*, 22(12), pp. 1017–1027. doi: 10.1002/(SICI)1521-4125(199912)22:12<1017::AID-CEAT1017>3.0.CO;2-L.

Kwok, D. Y. and Neumann, a. W. (1999) *Contact angle measurement and contact angle* *interpretation*, *Advances in Colloid and Interface Science*. doi: 10.1016/S0001-8686(98)00087-6.

Kyzas, G. Z. and Matis, K. A. (2016) ‘Electroflotation process: A review’, *Journal of Molecular Liquids*, 220, pp. 657–664. doi: 10.1016/j.molliq.2016.04.128.

Laurin, M. (2009) *Example: Principle of X-ray photoelectron spectroscopy (XPS)*. Available at: http://www.texample.net/tikz/examples/principle-of-x-ray-photoelectron-spectroscopy-xps/.

Li, H., Afacan, A., Liu, Q. and Xu, Z. (2015) ‘Study interactions between fine particles and micron size bubbles generated by hydrodynamic cavitation’, *Minerals Engineering*. Elsevier Ltd, 84, pp. 106–115. doi: 10.1016/j.mineng.2015.09.023.

Li, M. (2017). *Influence of Venturi Tube Geometry and Particle Properties on the Hydrodynamic Cavitation for Fine Particle Flotation.* Master's thesis. University of Alberta.

Li, S., Liao, Y., Li, G., Li, Z. and Cao, Y. (2017) ‘Flocculating and dewatering performance of hydrophobic and hydrophilic solids using a thermal-sensitive copolymer’, *Water Science and Technology*, 76(3), pp. 694–704. doi: 10.2166/wst.2017.260.

Liu, J., Xu, Z. and Masliyah, J. (2003) ‘Studies on bitumen-silica interaction in aqueous solutions by atomic force microscopy’, *Langmuir*, 19(9), pp. 3911–3920. doi: 10.1021/la0268092.

Liu, J., Zhou, Z., Xu, Z. and Masliyah, J. (2002) ‘Bitumen-clay interactions in aqueous media studied by zeta potential distribution measurement’, *Journal of Colloid and*

Interface Science, 252(2), pp. 409–418. doi: 10.1006/jcis.2002.8471.

Lucay, F., Cisternas, L. A., Gálvez, E. and Lopez-Valdivieso, A. (2015) ‘Study of the natural floatability of molybdenite fines in saline solutions and effect of gypsum precipitation’, *Minerals & Metallurgical Processing*, 32(4), pp. 203–208.

Marmur, A. (2003) ‘Wetting on hydrophobic rough surfaces: To be heterogeneous or not to be?’, *Langmuir*, 19(20), pp. 8343–8348. doi: 10.1021/la0344682.

Matis, K. A., Gallios, G. P. and Kydros, K. A. (1993) ‘Separation of fines by flotation techniques’, *Separations Technology*, 3(2), pp. 76–90. doi: 10.1016/0956-9618(93)80007-E.

Meiron, T. S., Marmur, A. and Saguy, I. S. (2004) ‘Contact angle measurement on rough surfaces’, *Journal of Colloid and Interface Science*, 274(2), pp. 637–644. doi: 10.1016/j.jcis.2004.02.036.

Miettinen, T., Ralston, J. and Fornasiero, D. (2010) ‘The limits of fine particle flotation’, *Minerals Engineering*. Elsevier Ltd, 23(5), pp. 420–437. doi: 10.1016/j.mineng.2009.12.006.

Mishchuk, N., Ralston, J. and Fornasiero, D. (2002) ‘Influence of Dissolved Gas on van der Waals Forces between Bubbles and Particles’, *The Journal of Physical Chemistry A*, 106(4), pp. 689–696. doi: 10.1021/jp0118221.

Moholkar, V. S. and Pandit, A. B. (2001) ‘Modeling of hydrodynamic cavitation reactors : a uniÿed approach’, 56, pp. 6295–6302.

Murakami, D., Jinnai, H. and Takahara, A. (2014) ‘Wetting transition from the cassie-baxter state to the wenzel state on textured polymer surfaces', *Langmuir*, 30(8), pp. 2061–2067. doi: 10.1021/la4049067.

Nguyen, A. V., George, P. and Jameson, G. J. (2006) 'Demonstration of a minimum in the recovery of nanoparticles by flotation: Theory and experiment', *Chemical Engineering Science*, 61(8), pp. 2494–2509. doi: 10.1016/j.ces.2005.11.025.

Nguyen Van, A. and Kmet', S. (1992) 'Collision efficiency for fine mineral particles with single bubble in a countercurrent flow regime', *International Journal of Mineral Processing*, 35(3–4), pp. 205–223. doi: 10.1016/0301-7516(92)90034-T.

Von Oertzen, G. U., Harmer, S. L. and Skinner, W. M. (2006) 'XPS and ab initio calculation of surface states of sulfide minerals: Pyrite, chalcopyrite and molybdenite', *Molecular Simulation*, 32(15), pp. 1207–1212. doi: 10.1080/08927020601081616.

Oliveira, C., Rodrigues, R. T. and Rubio, J. (2010) 'A new technique for characterizing aerated flocs in a flocculation- microbubble flotation system', *International Journal of Mineral Processing*. Elsevier B.V., 96(1–4), pp. 36–44. doi: 10.1016/j.minpro.2010.07.001.

Oliveira, C. and Rubio, J. (2012) 'A short overview of the formation of aerated flocs and their applications in solid/liquid separation by flotation', *Minerals Engineering*. Elsevier Ltd, 39, pp. 124–132. doi: 10.1016/j.mineng.2012.05.024.

De Oliveira Da Mota, I., De Castro, J. A., De Góes Casqueira, R. and De Oliveira Junior, A. G. (2015) 'Study of electroflotation method for treatment of wastewater from washing soil contaminated by heavy metals', *Journal of Materials Research and Technology*. Korea Institute of Oriental Medicine, 4(2), pp. 109–113. doi: 10.1016/j.jmrt.2014.11.004.

Ozkan, F., Ozturk, M. and Baylar, A. (2006) 'Experimental investigations of air and liquid injection by venturi tubes', *Water and Environment Journal*, 20(3), pp. 114–122. doi: 10.1111/j.1747-6593.2005.00003.x.

Ozkan, S. G. (2002) 'Beneficiation of magnesite slimes with ultrasonic treatment', *Minerals Engineering*, 15(1–2), pp. 99–101. doi: 10.1016/S0892-6875(01)00205-9.

Ozkan, S. G. (2012) 'Effects of simultaneous ultrasonic treatment on flotation of hard coal slimes', *Fuel*. Elsevier Ltd, 93, pp. 576–580. doi: 10.1016/j.fuel.2011.10.032.

Ozkan, S. G. and Kuyumcu, H. Z. (2006) 'Investigation of mechanism of ultrasound on coal flotation', *International Journal of Mineral Processing*, 81(3), pp. 201–203. doi: 10.1016/j.minpro.2006.07.011.

Özkan, Ş. G. and Kuyumcu, H. Z. (2007) 'Design of a flotation cell equipped with ultrasound transducers to enhance coal flotation', *Ultrasonics Sonochemistry*, 14(5), pp. 639–645. doi: 10.1016/j.ultsonch.2006.10.001.

Padilla-Martinez, J. P., Berrospe-Rodriguez, C., Aguilar, G., Ramirez-San-Juan, J. C. and Ramos-Garcia, R. (2014) 'Optic cavitation with CW lasers: A review', *Physics of Fluids*, 26(12). doi: 10.1063/1.4904718.

Parus, J., Kierzek, J. and Mało, B. (2000) 'Determination of the carbon content in coal and ash by XRF', *X-Ray Spectrometry*, 29(November 1999), pp. 192–195.

Peng, F. F. and Yu, X. (2015) 'Pico-nano bubble column flotation using static mixer-venturi tube for Pittsburgh No. 8 coal seam', *International Journal of Mining Science and Technology*. China University of Mining & Technology, 25(3), pp. 347–354. doi:

10.1016/j.ijmst.2015.03.004.

Pourkarimi, Z., Rezai, B. and Noaparast, M. (2017) 'Effective parameters on generation of nanobubbles by cavitation method for froth flotation applications', *Physicochemical Problems of Mineral Processing*, 53(2), pp. 920–942. doi: 10.5277/ppmp170220.

Qiu, Z., Liu, G., Liu, Q. and Zhong, H. (2016) 'Understanding the roles of high salinity in inhibiting the molybdenite flotation', *Colloids and Surfaces A: Physicochemical and Engineering Aspects*. Elsevier B.V., 509, pp. 123–129. doi: 10.1016/j.colsurfa.2016.08.059.

Qiu, Z., Liu, G., Liu, Q., Zhong, H. and Zhang, M. (2017) 'Separation of pyrite from chalcopyrite and molybdenite by using selective collector of N-isopropoxypropyl-N'-ethoxycarbonyl thiourea in high salinity water', *Minerals Engineering*. Elsevier Ltd, 100, pp. 93–98. doi: 10.1016/j.mineng.2016.10.010.

Rahman, A., Darban, K., Mahmoud, A. and Maoming, F. (2014) 'Nano-microbubble flotation of fine and ultrafine chalcopyrite particles', *International Journal of Mining Science and Technology*. China University of Mining & Technology, 24(4), pp. 559–566. doi: 10.1016/j.ijmst.2014.05.021.

Reay, D. and Ratcliff, G. A. (1973) 'Removal of fine particles from water by dispersed air flotation: Effects of bubble size and particle size on collection efficiency', *The Canadian Journal of Chemical Engineering*, 51(2), pp. 178–185. doi: 10.1002/cjce.5450510207.

Rees, K. L. and Van Deventer, J. S. J. (2000) 'Preg-robbing phenomena in the cyanidation of sulphide gold ores', *Hydrometallurgy*, 58(1), pp. 61–80. doi: 10.1016/S0304-386X(00)00131-6.

Reyes-Bozo, L., Escudey, M., Vyhmeister, E., Higueras, P., Godoy-Faúndez, A., Salazar, J. L., Valdés-González, H., Wolf-Sepúlveda, G. and Herrera-Urbina, R. (2015) 'Adsorption of biosolids and their main components on chalcopyrite, molybdenite and pyrite: Zeta potential and FTIR spectroscopy studies', *Minerals Engineering*. Elsevier Ltd, 78, pp. 128–135. doi: 10.1016/j.mineng.2015.04.021.

Sarkar, M. S. K. A., Evans, G. M. and Donne, S. W. (2010) 'Bubble size measurement in electroflotation', *Minerals Engineering*. Elsevier Ltd, 23(11–13), pp. 1058–1065. doi: 10.1016/j.mineng.2010.08.015.

Simon, M. and Bart, H. J. (2002) 'Experimental studies of coalescence in liquid/liquid systems', *Chemical Engineering and Technology*, 25(5), pp. 481–484. doi: 10.1002/1521-4125(200205)25:5<481::AID-CEAT481>3.0.CO;2-T.

Sobhy, A. and Tao, D. (2013) 'Nanobubble column flotation of fine coal particles and associated fundamentals', *International Journal of Mineral Processing*. Elsevier B.V., 124, pp. 109–116. doi: 10.1016/j.minpro.2013.04.016.

Song, S., Zhang, X., Yang, B. and Lopez-Mendoza, A. (2012) 'Flotation of molybdenite fines as hydrophobic agglomerates', *Separation and Purification Technology*. Elsevier B.V., 98, pp. 451–455. doi: 10.1016/j.seppur.2012.06.016.

Soyama, H. and Hoshino, J. (2016) 'Enhancing the aggressive intensity of hydrodynamic cavitation through a Venturi tube by increasing the pressure in the region where the bubbles collapse', *AIP Advances*, 6(4). doi: 10.1063/1.4947572.

Spiegler, K. S. (1966) 'Diffusion of gases across porous media', *Industrial and Engineering Chemistry Fundamentals*, 5(4), pp. 529–532. doi: 10.1021/i160020a017.

Sun, W., Hu, Y., Dai, J. and Liu, R. (2006) ‘Observation of fine particle aggregating behavior induced by high intensity conditioning using high speed CCD’, *Transactions of Nonferrous Metals Society of China*, 16(1), pp. 198–202. doi: 10.1016/S1003-6326(06)60035-6.

Sutherland, K. L. (1948) ‘Physical chemistry of flotation. XI: Kinetics of the flotation process’, *Journal of Physical and Colloid Chemistry*, 52(2), pp. 394–425. doi: 10.1021/j150458a013.

Sze, A., Erickson, D., Ren, L. and Li, D. (2003) ‘Zeta-potential measurement using the Smoluchowski equation and the slope of the current-time relationship in electroosmotic flow’, *Journal of Colloid and Interface Science*, 261(2), pp. 402–410. doi: 10.1016/S0021-9797(03)00142-5.

Gaudin, A.M., Groh, J.O. and Henderson, H.B. (1931) ‘Effect of particle size on flotation’, *AIME, Tech. Publ.,* 414, pp. 3–23.

Tao, D. (2005) ‘Role of Bubble Size in Flotation of Coarse and Fine Particles—A Review’, *Separation Science and Technology*, 39(4), pp. 741–760. doi: 10.1081/SS-120028444.

Teixeira, M. R. and Rosa, M. J. (2006) ‘Integration of dissolved gas flotation and nanofiltration for M. aeruginosa and associated microcystins removal’, *Water Research*, 40(19), pp. 3612–3620. doi: 10.1016/j.watres.2006.06.006.

Tian, Y., He, Y. and Zhu, Y. (2004) ‘Low temperature synthesis and characterization of molybdenum disulfide nanotubes and nanorods’, *Materials Chemistry and Physics*, 87(1), pp. 87–90. doi: 10.1016/j.matchemphys.2004.05.010.

Trahar, W. J. and Warren, L. J. (1976) ‘The flotability of very fine particles - A review’, *International Journal of Mineral Processing*, 3(2), pp. 103–131. doi: 10.1016/0301-7516(76)90029-6.

Uçurum, M. (2009) ‘Influences of Jameson flotation operation variables on the kinetics and recovery of unburned carbon’, *Powder Technology*. Elsevier B.V., 191(3), pp. 240–246. doi: 10.1016/j.powtec.2008.10.014.

Videla, A. R., Morales, R., Saint-Jean, T., Gaete, L., Vargas, Y. and Miller, J. D. (2016) ‘Ultrasound treatment on tailings to enhance copper flotation recovery’, *Minerals Engineering*. Elsevier Ltd, 99, pp. 89–95. doi: 10.1016/j.mineng.2016.09.019.

Vinogradova, O. I., Bunkin, N. F., Churaev, N. V., Kiseleva, O. A., Lobeyev, A. V. and Ninham, B. W. (1995) ‘Submicrocavity Structure of Water between Hydrophobic and Hydrophilic Walls as Revealed by Optical Cavitation’, *Journal of Colloid And Interface Science*, pp. 443–447. doi: 10.1006/jcis.1995.1345.

Wan, H., Yang, W., Cao, W., He, T., Liu, Y., Yang, J., Guo, L. and Peng, Y. (2017) ‘The Interaction between Ca^{2+} and Molybdenite Edges and Its Effect on Molybdenum Flotation’, *Minerals*, 7(8), p. 141. doi: 10.3390/min7080141.

Wenk, H.-R. and Bulakh, A. (2004) *Minerals: Their Constitution and Origin*. Cambridge University Press.

Wu, C. (2011). *A Fundamental Study of Bubble-Particle Interactions through Zeta-Potential Distribution Analysis.* Master's thesis. University of Alberta.

Wu, C., Nesset, K., Masliyah, J. and Xu, Z. (2012) ‘Generation and characterization of submicron size bubbles', *Advances in Colloid and Interface Science*. Elsevier B.V., 179–182, pp. 123–132. doi: 10.1016/j.cis.2012.06.012.

Wu, C., Wang, L., Harbottle, D., Masliyah, J. and Xu, Z. (2015) 'Studying bubble-particle interactions by zeta potential distribution analysis', *Journal of Colloid and Interface Science*. Elsevier Inc., 449, pp. 399–408. doi: 10.1016/j.jcis.2015.01.040.

Xu, M. (1998) 'Modified flotation rate constant and selectivity index', *Minerals Engineering*, 11(3), pp. 271–278. doi: 10.1016/S0892-6875(98)00005-3.

Yang, B., Song, S. and Lopez-Valdivieso, A. (2015) 'Kinetics of hydrophobic agglomeration of molybdenite fines in aqueous suspensions', *Physicochemical Problems of Mineral Processing*, 51(1), pp. 181–189. doi: 10.5277/ppmp150117.

Yang, C., Dabros, T., Li, D., Czarnecki, J. and Masliyah, J. H. (2001) 'Measurement of the zeta potential of gas bubbles in aqueous solutions by microelectrophoresis method', *Journal of Colloid and Interface Science*, 243(1), pp. 128–135. doi: 10.1006/jcis.2001.7842.

Yoon, R. H. (1993) 'Microbubble flotation', *Minerals Engineering*, 6(6), pp. 619–630. doi: 10.1016/0892-6875(93)90116-5.

Yoon, R. H. and Luttrell, G. H. (1989) 'The Effect of Bubble Size on Fine Particle Flotation', *Mineral Processing and Extractive Metallurgy Review*, 5(1–4), pp. 101–122. doi: 10.1080/08827508908952646.

Zanin, M., Ametov, I., Grano, S., Zhou, L. and Skinner, W. (2009) 'A study of mechanisms affecting molybdenite recovery in a bulk copper/molybdenum flotation circuit', *International Journal of Mineral Processing*. Elsevier B.V., 93(3–4), pp. 256–266. doi: 10.1016/j.minpro.2009.10.001.

Zhang, H., Liu, J., Wang, Y., Cao, Y., Ma, Z. and Li, X. (2013) 'Cyclonic-static micro-bubble flotation column', *Minerals Engineering*. Elsevier Ltd, 45, pp. 1–3. doi: 10.1016/j.mineng.2013.01.006.

Zhang, H., Lu, S. B., Zheng, J., Du, J., Wen, S. C., Tang, D. Y. and Loh, K. P. (2014) 'Molybdenum disulfide (MoS_2) as a broadband saturable absorber for ultra-fast photonics', *Optics Express*, 22(6), p. 7249. doi: 10.1364/OE.22.007249.

Zhang, M. (2015) *Investigation of Chalcopyrite and Pyrite Flotation in High Salinity Water*. Master's thesis. University of Alberta.

Zhao, H. L., Wang, D. X., Cai, Y. X. and Zhang, F. C. (2007) 'Removal of iron from silica sand by surface cleaning using power ultrasound', *Minerals Engineering*, 20(8), pp. 816–818. doi: 10.1016/j.mineng.2006.10.005.

Zhao, H., Long, J., Masliyah, J. H. and Xu, Z. (2006) 'Effect of divalent cations and surfactants on silica-bitumen interactions', *Industrial and Engineering Chemistry Research*, 45(22), pp. 7482–7490. doi: 10.1021/ie060348o.

Zhao, T. and Jiang, L. (2018) 'Contact angle measurement of natural materials', *Colloids and Surfaces B: Biointerfaces*. Elsevier B.V., 161, pp. 324–330. doi: 10.1016/j.colsurfb.2017.10.056.

Zhou, W., Chen, H., Ou, L. and Shi, Q. (2016) 'Aggregation of ultra-fine scheelite particles induced by hydrodynamic cavitation', *International Journal of Mineral Processing*.

Elsevier B.V., 157, pp. 236–240. doi: 10.1016/j.minpro.2016.11.003.

Zhou, Z. a., Xu, Z., Finch, J. a., Hu, H. and Rao, S. R. (1997) ‘Role of hydrodynamic cavitation in fine particle flotation’, *International Journal of Mineral Processing*, 51(1–4), pp. 139–149. doi: 10.1016/S0301-7516(97)00026-4.

Zhou, Z. A., Xu, Z., Finch, J. A., Masliyah, J. H. and Chow, R. S. (2009) ‘On the role of cavitation in particle collection in flotation - A critical review. II’, *Minerals Engineering*. Elsevier Ltd, 22(5), pp. 419–433. doi: 10.1016/j.mineng.2008.12.010.